Sensitive and selective ammonia gas sensor based on molecularly functionalized tin dioxide working at room temperature

Mohamad Hijazi

N°d'ordre NNT : 2017LYSEM030

THESE de DOCTORAT DE L'UNIVERSITE DE LYON
opérée au sein de
l'Ecole des Mines de Saint-Etienne

Ecole Doctorale N° 488
Sciences, Ingénierie, Santé

Spécialité de doctorat : Génie des procédés

Soutenue publiquement le 20/10/2017, par :
Mohamad Hijazi

Capteur de gaz SnO_2 fonctionnalisé fonctionnant à température ambiante, sensible et sélectif pour la détection d'ammoniac

---

Devant le jury composé de :

Menini, Philippe	Professeur LAAS-CNRS	Président
Chaix, Carole	Directrice de recherche CNRS-ISA	Rapporteur
Di Natale, Corrado	Professeur Université de Roma Tor Vergata	Rapporteur
Viricelle, Jean-Paul	Directeur de recherche ENSM-SE	Directeur de thèse
Stambouli, Valérie	Chargée de recherche CNRS/INP-Grenoble	Co-directrice de thèse
Rieu, Mathilde	Chargée de recherche ENSM-SE	Co-encadrante
Pijolat, Christophe	Professeur ENSM-SE	Invité

Spécialités doctorales	Responsables :	Spécialités doctorales	Responsables
SCIENCES ET GENIE DES MATERIAUX	K. Wolski Directeur de recherche	MATHEMATIQUES APPLIQUEES	O. Roustant, Maître-assistant
MECANIQUE ET INGENIERIE	S. Drapier, professeur	INFORMATIQUE	O. Boissier, Professeur
GENIE DES PROCEDES	F. Gruy, Maître de recherche	SCIENCES DES IMAGES ET DES FORMES	JC. Pinoli, Professeur
SCIENCES DE LA TERRE	B. Guy, Directeur de recherche	GENIE INDUSTRIEL	X. Delorme, Maître assistant
SCIENCES ET GENIE DE L'ENVIRONNEMENT	D. Graillot, Directeur de recherche	MICROELECTRONIQUE	Ph. Lalevée, Professeur

EMSE : Enseignants-chercheurs et chercheurs autorisés à diriger des thèses de doctorat (titulaires d'un doctorat d'Etat ou d'une HDR)

ABSI	Nabil	CR	Génie industriel	CMP
AUGUSTO	Vincent	CR	Image, Vision, Signal	CIS
AVRIL	Stéphane	PR2	Mécanique et ingénierie	CIS
BADEL	Pierre	MA(MDC)	Mécanique et ingénierie	CIS
BALBO	Flavien	PR2	Informatique	FAYOL
BASSEREAU	Jean-François	PR	Sciences et génie des matériaux	SMS
BATTON-HUBERT	Mireille	PR2	Sciences et génie de l'environnement	FAYOL
BEIGBEDER	Michel	MA(MDC)	Informatique	FAYOL
BLAYAC	Sylvain	MA(MDC)	Microélectronique	CMP
BOISSIER	Olivier	PR1	Informatique	FAYOL
BONNEFOY	Olivier	MA(MDC)	Génie des Procédés	SPIN
BORBELY	Andras	MR(DR2)	Sciences et génie des matériaux	SMS
BOUCHER	Xavier	PR2	Génie Industriel	FAYOL
BRODHAG	Christian	DR	Sciences et génie de l'environnement	FAYOL
BRUCHON	Julien	MA(MDC)	Mécanique et ingénierie	SMS
CAMEIRAO	Ana	MA(MDC)	Génie des Procédés	SPIN
CHRISTIEN	Frédéric	PR	Science et génie des matériaux	SMS
DAUZERE-PERES	Stéphane	PR1	Génie Industriel	CMP
DEBAYLE	Johan	MR	Sciences des Images et des Formes	SPIN
DEGEORGE	Jean-Michel	MA(MDC)	Génie industriel	Fayol
DELAFOSSE	David	PR0	Sciences et génie des matériaux	SMS
DELORME	Xavier	MA(MDC)	Génie industriel	FAYOL
DESRAYAUD	Christophe	PR1	Mécanique et ingénierie	SMS
DJENIZIAN	Thierry	PR	Science et génie des matériaux	CMP
DOUCE	Sandrine	PR2	Sciences de gestion	FAYOL
DRAPIER	Sylvain	PR1	Mécanique et ingénierie	SMS
FAUCHEU	Jenny	MA(MDC)	Sciences et génie des matériaux	SMS
FAVERGEON	Loïc	CR	Génie des Procédés	SPIN
FEILLET	Dominique	PR1	Génie Industriel	CMP
FOREST	Valérie	MA(MDC)	Génie des Procédés	CIS
FRACZKIEWICZ	Anna	DR	Sciences et génie des matériaux	SMS
GARCIA	Daniel	MR(DR2)	Sciences de la Terre	SPIN
GAVET	Yann	MA(MDC)	Sciences des Images et des Formes	SPIN
GERINGER	Jean	MA(MDC)	Sciences et génie des matériaux	CIS
GOEURIOT	Dominique	DR	Sciences et génie des matériaux	SMS
GONDRAN	Natacha	MA(MDC)	Sciences et génie de l'environnement	FAYOL
GONZALEZ FELIU	Jesus	MA(MDC)	Sciences économiques	FAYOL
GRAILLOT	Didier	DR	Sciences et génie de l'environnement	SPIN
GROSSEAU	Philippe	DR	Génie des Procédés	SPIN
GRUY	Frédéric	PR1	Génie des Procédés	SPIN
GUY	Bernard	DR	Sciences de la Terre	SPIN
HAN	Woo-Suck	MR	Mécanique et ingénierie	SMS
HERRI	Jean Michel	PR1	Génie des Procédés	SPIN
KERMOUCHE	Guillaume	PR2	Mécanique et Ingénierie	SMS
KLOCKER	Helmut	DR	Sciences et génie des matériaux	SMS
LAFOREST	Valérie	MR(DR2)	Sciences et génie de l'environnement	FAYOL
LERICHE	Rodolphe	CR	Mécanique et ingénierie	FAYOL
MALLIARAS	Georges	PR1	Microélectronique	CMP
MOLIMARD	Jérôme	PR2	Mécanique et ingénierie	CIS
MOUTTE	Jacques	CR	Génie des Procédés	SPIN
NEUBERT	Gilles			FAYOL
NIKOLOVSKI	Jean-Pierre	Ingénieur de recherche	Mécanique et ingénierie	CMP
NORTIER	Patrice	PR1	Génie des Procédés	SPIN
O CONNOR	Rodney Philip	MA(MDC)	Microélectronique	CMP
OWENS	Rosin	MA(MDC)	Microélectronique	CMP
PERES	Véronique	MR	Génie des Procédés	SPIN
PICARD	Gauthier	MA(MDC)	Informatique	FAYOL
PIJOLAT	Christophe	PR0	Génie des Procédés	SPIN
PINOLI	Jean Charles	PR0	Sciences des Images et des Formes	SPIN
POURCHEZ	Jérémy	MR	Génie des Procédés	CIS
ROUSSY	Agnès	MA(MDC)	Microélectronique	CMP
ROUSTANT	Olivier	MA(MDC)	Mathématiques appliquées	FAYOL
SANAUR	Sébastien	MA(MDC)	Microélectronique	CMP
STOLARZ	Jacques	CR	Sciences et génie des matériaux	SMS
TRIA	Assia	Ingénieur de recherche	Microélectronique	CMP
VALDIVIESO	François	PR2	Sciences et génie des matériaux	SMS
VIRICELLE	Jean Paul	DR	Génie des Procédés	SPIN
WOLSKI	Krzystof	DR	Sciences et génie des matériaux	SMS
XIE	Xiaolan	PR1	Génie industriel	CIS
YUGMA	Gallian	CR	Génie industriel	CMP

Mise à jour : 03/02/2017

N°d'ordre NNT : 2017LYSEM030

THESE de DOCTORAT DE L'UNIVERSITE DE LYON
opérée au sein de
l'Ecole des Mines de Saint-Etienne

Ecole Doctorale N° 488
Sciences, Ingénierie, Santé

Spécialité de doctorat : Génie des procédés

Soutenue publiquement le 20/10/2017, par :
Mohamad Hijazi

Capteur de gaz SnO_2 fonctionnalisé fonctionnant à température ambiante, sensible et sélectif pour la détection d'ammoniac

---

Devant le jury composé de :

Menini, Philippe	Professeur LAAS-CNRS	Président
Chaix, Carole	Directrice de recherche CNRS-ISA	Rapporteur
Di Natale, Corrado	Professeur Université de Roma Tor Vergata	Rapporteur
Viricelle, Jean-Paul	Directeur de recherche ENSM-SE	Directeur de thèse
Stambouli, Valérie	Chargée de recherche CNRS/INP-Grenoble	Co-directrice de thèse
Rieu, Mathilde	Chargée de recherche ENSM-SE	Co-encadrante
Pijolat, Christophe	Professeur ENSM-SE	Invité

Remerciements

Cette thèse a été effectuée au sein du laboratoire de Procédés de Transformations des Solides et Instrumentation (PTSI), à l'Ecole des Mines de Saint Etienne, en collaboration avec LMGP laboratoire de Grenoble. Je remercie tout le personnel qui m'a permis, de près ou de loin, de mener à bien ce travail dans de bonnes conditions matérielles et humaines.

Je voudrais remercier vivement tous les membres du jury, Mr Philippe Menini, Mme Carole Chaix et Mr Corrado Di Natale d'avoir accepté de rapporter et examiner ce travail.

Je tiens à remercier infiniment mes directeurs de thèse Jean-Paul Viricelle, Christophe Pijolat, Valérie Stambouli et Mathilde Rieu qui m'ont accueilli dans leur équipe pour faire cette thèse. Je voudrais les remercier également de m'avoir épaulé et d'avoir enrichi mes connaissances scientifiques et expérimentales, sans oublier la confiance qu'ils m'ont accordée, et le temps consacré pour discuter les résultats et avancer la rédaction des articles et du rapport de thèse.

Je ne sais pas où dois-je commencer pour exprimer mes remerciements et mes appréciations concernant mon directeur de thèse. Tout d'abord je dois te remercier pour m'avoir donné l'opportunité de travailler avec toi, de découvrir un nouveau domaine en génie des procédée. Grâce à ton humanité, ta sympathie et ta gentillesse permanente, tu m'as permis de construire une grande passion pour le domaine des capteurs. Je suis très heureux d'avoir eu la chance de bénéficier au niveau scientifique, humain et social de ton immense expérience. Je souhaite vivement remercier Jean-Paul Viricelle pour son amitié et lui exprimer ma plus profonde gratitude. Je te remercier aussi pour m'avoir donné l'opportunité de participer dans plusieurs conférence surtout l'IMCS à Juju (je n'oublie pas les poissons qui bouge dans l'assiette).

Maintenant je me déplace vers mon encadrante chère Mathilde Rieu (La chef). Tu étais toujours présente pour remédier aux problèmes que j'ai rencontrés durant la thèse. Aussi, tu acceptais et améliorais toujours mes suggestions et idées lors de nos nombreuses discussions dans ton bureau. Tu m'as fait preuve d'une totale confiance, et tu étais toujours à l'écoute et en

mode actif. Avec ton sens de l'apprentissage, tu m'as motivé encore plus, et je suis devenu prêt à m'engager dans n'importe quelle idée sans avoir le moindre doute et sans avoir peur. Sans toi la thèse n'avait pas la même gueule.

Il ne faut pas aussi oublié de remercier Christophe Pijolat, qui est un dictionnaire et une encyclopédie de capteur de gaz. Il m'a beaucoup aidé à résoudre les principaux problèmes dans cette thèse. Il était toujours à l'écoute et prêt à offrir et partager ses expériences avec moi, que ce soit dans le domaine des capteurs. Christophe je te remercie infiniment pour ton immense aide et ton savoir scientifique illimité. Je n'oublie pas de remercier sa femme Michèle Pijolat pour les discussions riches sur le capteur et de m'encourager de faire les présentations en français.

Je passe en ce moment vers mon encadrante à Grenoble: Valérie Stambouli. Je te remercie vivement pour nombreuses discussions que nous avons eues et faites. Tu m'as bien formé dans le domaine de fonctionnalisation et pour ça je te dois une gratitude infinie.

Je remercie Guy Tournier pour son aide concernant le concept de capteur du gaz surtout le capteur SnO_2 (putain de capteur). Merci pour les discussions riches sur le capteur conductimétrique et pour le cours de français (niveau expert). Il m'a appris beaucoup des expressions qui tombent très bien dans le domaine de capteur, on ne va pas faire un fromage et raconter tout là, comme c'est beaucoup. On a fait ensemble pas mal des manipes qui sont du pipeau mais des fois il cartonne le capteur lorsqu'on met le gaz sur la courge. Il a proposé de laisser tomber le NO_x parce que le capteur va comprendre son bonheur et ça va être « dauber ». On n'oublie pas le capteur qui « grigritte pas mal », et la conclusion a été : « ça marchera jamais ».

Je remercie également mon chèr ami Maxime Minot pour son aide concernant fabrication des capteurs SnO_2 et montage de banc de test et je n'oublie pas son aide de corriger mon français surtout dans les mails. Merci pour les pauses thé qu'on a faite dans son bureau, et de me supporter pendant ces trois ans toujours avec sa bonne humeur. Merci d'avoir partagé avec moi son bureau. Et je lui dis ne mange pas trop « lhalouf ». Merci de me donner ton prénom.

Je remercie Philippe Breuil pour m'aider à monter le banc de test sous gaz surtout dans les parties électronique et informatique (Labview) et les discussions riches en informations scientifiques que nous avons partagées.

Je remercier Laetitia Vieille de m'avoir formé à utiliser l'infrarouge et pour sa bonne humeur. Pareil je remercie Vincent Barnier pour tous les tests XPS et la modèle que on a fait. Et je n'oublie pas de remercier Olivier Valfort pour l'analyse RDX.

Je remercie Rabih Mezher pour son aide dans les grandes équations (cos(teta)) et de me soutenir dans la dernière ligne droite de ma thèse.

Je n'oublie pas les personnes avec lesquelles j'ai travaillé et qui m'ont permis de manipuler dans les meilleures conditions expérimentales : Marie-Claude, Jean-Pierre, Richard, Fabien, Nathalie, Didier, Mariana, Gita, Thomas (corrections des mails), Adrien, Saheb, Kien, Juan-Carlos et Riadh …

Je souhaite adresser des remerciements à tous mes amis, pour leurs encouragements et leur soutien pendant mes années de thèse, et pour les bons moments qu'on a partagés. Je cite en particulier : Mes frères Hussein, houssam et khalil, aussi Omar Kassim, Hussein Hammoud (Fidèle), Ahmad Al-Saabi (Alexandre), Reda kassir et sa famille, Ali …

Je n'oublie pas mon chèr ami Mohamad Abd El-Sater qui m'a accueilli à mon arrivée à Saint Etienne.

Finalement, je remercie mes parents, mes frères et mes sœurs qui m'ont soutenu et encouragé pour continuer mes études supérieures en France (Merci la France), et qui sont restés en contact avec moi, toute cette période. Je ne termine pas mes remerciements sans reconnaître que cette thèse va me permettre de réaliser un rêve … !!!

Table of contents

General introduction

The current concern in the disease diagnosis focuses on the early detection of diseases by a simple and non-invasive way. At the moment, the diagnosis of diseases is based on the analysis of the external symptoms appeared on the patient. This means that the patient is already in advanced stages of the disease which complicates the disease containment in the most cases. Precisely, in some cases, the infection by some diseases can increase the concentration of some species in the blood. Liver or kidney diseases are associated with the increase of ammonia concentration in the blood. In a normal case, the excess of ammonia in the body is transformed into urea by the liver as presented in Figure 1a. The capacity of liver to remove ammonia, formed from the degraded amino acids, may be reduced because of cirrhosis or massive liver necrosis. The blood bypasses the liver through the portal-systemic anastomoses in case of cirrhotic problem with portal hypertension which causes further inability to remove ammonia by the body. In the case of portal hypertension-related esophageal varices rupture and in presence of a massive bleed, the swallowed blood develops even another source of ammonia. Blood is rich in proteins which degrades in the intestines and transforms into amino acids and further into ammonia. Excess of ammonia in the blood, resulting from any of these problems, has a potentially toxic effect on the brain. The concentration of ammonia increases in the brain as shown in Figure 1b. It is considered to play an important nosogenesis role in hepatic encephalopathy disease [1].

The detection of ammonia excess in the blood faces many problems such as the invasiveness and the difficulties in measurements. Such analysis to detect ammonia in the blood is complicated and cannot be available for everybody. Because ammonia has high vapor pressure, it is emitted outside the blood throughout the exhaled breath. Thus, the concentration of ammonia gas in the exhaled breath increases in the case of liver problems. The detection of ammonia in the breath is offering a simple and noninvasive method for the diagnosis of liver diseases. For the diagnosis of liver disease by breath analysis, the first requested thing is to have a selective detection of ammonia because human breath contains a huge amount of volatile organic compounds (VOCs) in addition to nitrogen, oxygen, water vapor and carbon dioxide and so on. Such detection technique should be simple, small in size and low cost in order to be available for everybody and to be integrated into a smart portable device for example.

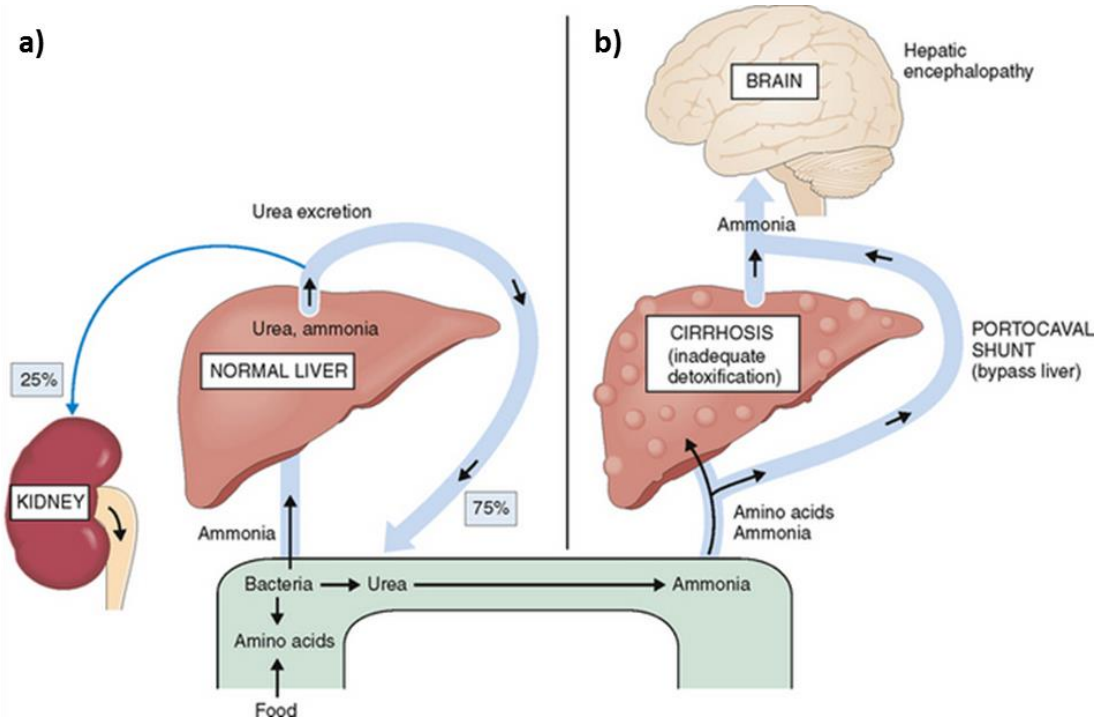

Figure 1. Schematic illustration of ammonia cycle in human body of a) normal liver, b) in the case cirrhosis where the liver cannot degrade the entering ammonia. The excess of ammonia in the blood can be transferred to the brain and cause hepatic encephalopathy [2].

Chemical sensors are offering a simple, low cost and small size sensing device. Recently, chemical sensors field has witnessed a great development. It is enough to count the number of publications in the specialized scientific journals "Sensors and Actuators" as well as in the specialized congresses "Eurosensors" (the 31th edition will take place in Paris, September 2017) and "International Meeting on Chemical Sensors". Figure 2 illustrates the evolution of the number of articles related to gas sensors listed on ScienceDirect since the 1974s. In parallel to the development of research, the industrial market for chemical sensors has also shown very strong growth (+9.6%/year) since the end of 2000s with a volume estimated by Global Industry Analysts Inc. about $13 billion in 2011 and it is expected to reach $31.2 billion by 2020 [3]. The necessity of chemical sensors in many fields such as environmental and food safety, air quality automobile, and recently in exhaled breath analysis leads to notable progress. Among the most developed sensors to date, gas sensors based on semiconductor materials are not only well adapted to microelectronic techniques but also incorporate a wide variety of materials such as metal oxides, semiconductor polymers and other composites. Chemical sensors based on metal

oxides are the most used because of their good sensitivity to gases. They were developed and marketed for the first time by Seiyama and Taguchi in the 1960s [4]. They used ZnO and then SnO_2 as sensitive materials for the detection of liquefied petroleum gases. Consequently, much research has been carried out to improve the performance of these chemical sensors. Among these oxides, tin dioxide is the most used and studied sensor because of its good sensitivity to gases and its chemical stability during operation in a polluted atmosphere. Despite these advantages, SnO_2 sensors faced major shortcomings such as a lack of selectivity and high power consumption due to the high operating temperature (300-500 °C).

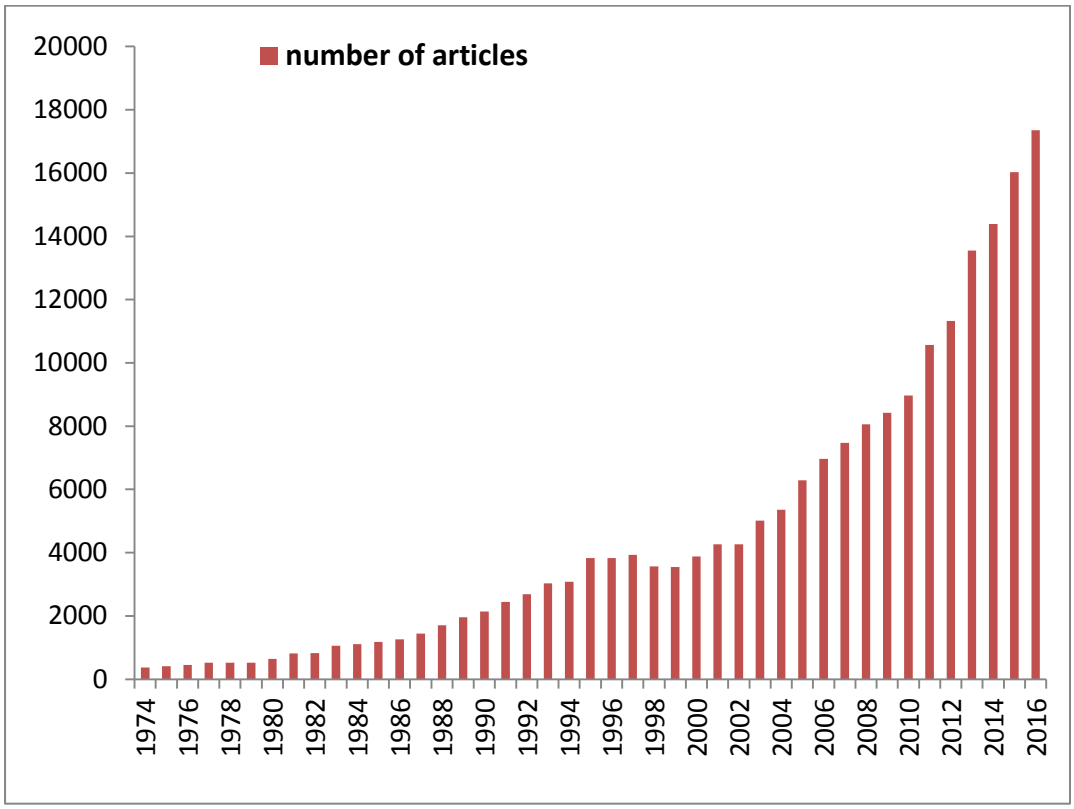

Figure 2. The number of published papers in ScienceDirect on gas sensors throughout the years.

In order to meet the breath analysis application, one of the major challenges is to have a selective gas sensor. In addition to selectivity, an ideal gas sensor should be sensitive to low concentration of gases with fast response and recovery times. Metal oxides surface functionalization by organic molecules could be incorporated in clinical and laboratory diagnostic tool in order to fulfil these requirements [5].

In the laboratory of SPIN center in Saint Etienne, especially in the group of Process of Solid Transformation and Instrumentation (PTSI), SnO_2 sensors have been well studied during the past 30 years for many applications, mainly for the industrial ones. The enhancements of the SnO_2 sensors, depending on the application, were achieved in different ways such as doping by other metal or metal oxide. For the breath analysis application, special improvement of SnO_2 sensor should be applied to fulfil all the requirements. In addition, such sensor is supposed to be integrated in the smart portable devices, so it should operate at room temperature.

The group of Valérie Stambouli at LMGP laboratory of Grenoble works on SnO_2 surface functionalization for the development of biosensors. They have experience on the functionalization of metal oxide surfaces especially SnO_2.

So, the idea is to try to incorporate functionalized sensors in the application of breath analysis. This work focuses on the organic functionalization of existing SnO_2 sensor from Saint Etienne laboratory. The functionalization is first started by the attachment of APTES because it can act as a substrate for grafting of different molecules. Functionalization of APTES can be achieved in vapor and liquid phases. Vapor phase silanization was carried out at LMGP according to previous reported synthesis procedures. Liquid silanization was developed at PTSI by studying the effect of different synthesis parameters. SnO_2 functionalized by APTES was used as substrate to attach different functional groups. The different functionalized sensors were tested under ammonia and other gases in a dedicated test bench at Saint Etienne.

Therefore, this is an approach to obtain organic-inorganic materials which are expected to have special interactions with gases at low operating temperature.

This thesis is divided into four chapters as following:

Chapter 1 presents a bibliographic study on chemical sensors, in particular SnO_2 based gas sensors. The advantages and the blocking points of SnO_2 sensors are highlighted as well as the possible ways tested in the literature to improve their performance. Afterwards, a short review about breath analysis for disease diagnosis is presented. Finally, a brief review about organic surface functionalization is proposed.

Chapter 2 presents the experimental procedures for the preparation of SnO_2 sensors to be functionalized. The synthesis procedures of functionalization as well as the different characterization techniques used in this work are exposed.

Chapter 3 is essentially dedicated to the physico-chemical characterizations of pure and functionalized SnO_2 sensors by multiple techniques. In addition, the influence of synthesis parameters of APTES modified SnO_2 is investigated.

Chapter 4 is devoted to the electrical characterization of the different functionalized sensor. Tests are carried out under ammonia and other interfering gases such as ethanol, carbon monoxide and acetone. A sensing mechanism is proposed in this chapter.

In the end, the conclusion and some outlook of the present work are proposed.

References

[1] S. DuBois, S. Eng, R. Bhattacharya, S. Rulyak, T. Hubbard, D. Putnam, D.J. Kearney, Breath Ammonia Testing for Diagnosis of Hepatic Encephalopathy, Dig. Dis. Sci. 50 (2005) 1780–1784.

[2] W.R. Kelly, The liver and biliary system, Pathol. Domest. Anim. 2 (1993) 319–406.

[3] Market Research Report Collections - WWW.StrategyR.com.

[4] N. Taguchi, A Metal Oxide Gas Sensor," Japanese Patent No.45-38200, 1962.

[5] N. Kahn, O. Lavie, M. Paz, Y. Segev, H. Haick, Dynamic Nanoparticle-Based Flexible Sensors: Diagnosis of Ovarian Carcinoma from Exhaled Breath, Nano Lett. 15 (2015) 7023–7028.

Chapter 1. **Bibliographic study**

1.1. General review about chemical gas sensor

A chemical sensor is a device that transforms chemical information, such as concentration or composition of a sample to be analyzed into a useful signal (electrical or optical). Typically, chemical sensors consist of two main parts, a receptor and a transducer arranged as illustrated in Figure 1-1. The receptor is composed from a sensitive material allowing the recognition of the target compound with which it interacts. Transducer system transforms the interaction between the target compound and the sensitive element into a measurable quantity. This interaction is recognized in most cases by a variation of the physical characteristics of the sensitive material (conductance, temperature, permittivity, mass, etc.). A chemical gas sensor is therefore capable of providing information representative of the presence or concentration of a chemical compound in a gaseous mixture. Separator can be introduced in a sensor to eliminate the particles in the gas sample, e.g. a membrane.

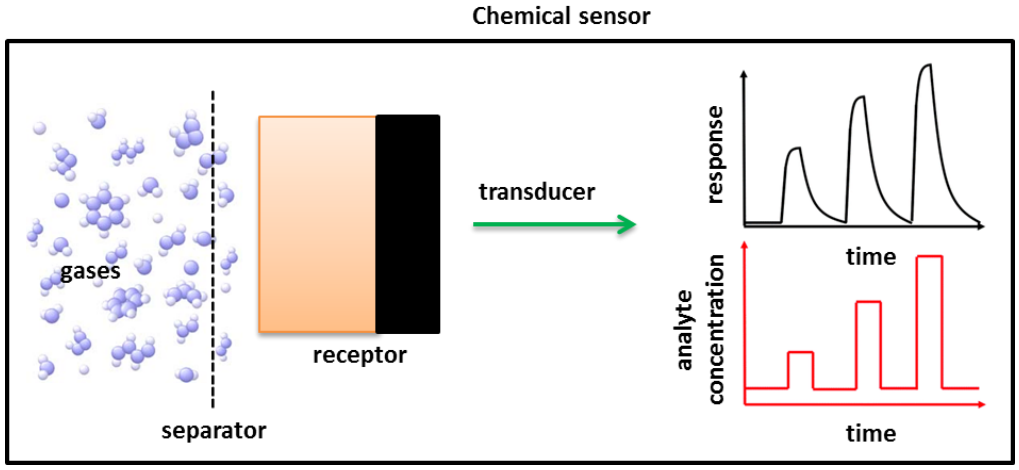

Figure 1-1. Schematic diagram of the different parts of chemical sensor [1].

A chemical sensor is not an autonomous system but is one of the essential components of an analyzer. Other parts such as transporting the analyzed sample to the sensor, conditioning the sample, processing the signal from the sensor, etc. may complement the chemical sensor according to the specifications of the application.

1.2. Different families of chemical gas sensors

The chemical sensors are classified according to the principle of transducer. Several transduction principles are now being commercially exploited for the detection of gases. At the present time, measurements of gas concentrations (gas analyzers) are generally based on physical principles such as Mass Spectrometry, Ultraviolet or Infra-red Absorption Spectrophotometry or Chromatography. These systems are very efficient but also very voluminous and very expensive, which reduces their use in the analysis of samples of gases taken from the real environment. The so-called "real-time" measurement has therefore lead to numerous sensor developments based on different principles. Table 1-1 gives an overview of various families of gas sensors. These include sensors based on infrared absorption that are most commonly used in safety systems and for high-precision gas analyzers. Each type of the sensors presented in this simplified table has advantages and disadvantages in terms of certain characteristics such as selectivity, stability, energy consumption and cost. Despite their lack of selectivity and long-term stability, semiconductor gas sensors has been marketed and widely spread since 1968, because they offer many advantages such as price, portability, sensitivity, response time, etc. They are widely used in automotive, indoor/outdoor controlling of gases and healthy applications. For the advantages stated above, semiconductor gas sensors are the object of particular attention both in research and industrial level. However, some blocking points remain problematic such as selectivity which prevents the desired performance with these systems from being achieved. From several decades, research laboratories are still trying to develop new sensors always more efficient, while remaining small in size and inexpensive.

Table 1-1. Classification of various chemical sensors.

Type	Measured variable	Sensor example
Electrochemical sensors	Electromotive force	Electrochemical cell
Calorimetric	Temperature	Pellistor
Optical gas sensors	Absorption peak	Photoionization detector
Gravimetric	Frequency	Quartz microbalance sensors
Conductometric	Electrical conductivity	Metal oxide gas sensors

1.3. Main characteristics of gas sensors

In the ideal case, a gas sensor must provide information about the nature and concentration of a chemical compound. As with any instrument, several criteria can generally be taken into account when defining the performance of a sensor. In the field of chemical sensors, these criteria are often the sensitivity, selectivity and stability. In addition, reversibility, response and recovery time, limit of detection and reproducibility should be taken in consideration.

1.3.1. Sensitivity

The first quality that is sought for a sensor is its sensitivity to gases. The sensitivity is a parameter which expresses the variation of the sensor response as a function of the variation of the concentration of a gas. A gas sensor is said to be sensitive if a small change in concentration causes a large variation in the output signal. In other word, the sensitivity is the slope of the calibration curve. The curve of sensor response versus the concentrations of the target gas is usually named the calibration curve. This curve is generally highly non-linear, so the sensitivity is not constant. Therefore, it is defined, for a given concentration of gas, by the relative or fractional variation of conductance (or resistance or other variable). The general formula of sensitivity is thus given as equation (1).

$$S_i = \frac{dR}{d[C]_i} \quad (1)$$

With S_i: the sensitivity to gas i, dR: variation in sensor response (sensor output, resistance or conductance, etc.), $d[C]_i$: the change in concentration of gas i, and $\frac{dR}{d[C]_i}$: the variation of sensor response over the concentration variation of gas i.

The sensitivity is measured in units of output quantity per units of input quantity (Ω/ppm, Hz/ppm, etc.).

In order to compare different sensor sensitivities, relative and differential responses should be used. According to the literature, the sensor response can be written in four forms as shown in equations 2, 3, 4 and 5 depending on the value of response with respect to the initial state of the sensor (base line). When the response is in decreasing form with respect to the base line, equations 2 or 4 can be used, otherwise equations 3 or 5 is applied.

If we consider "G" (conductance) as sensor response, relative sensor response calculations are given in equations 2 and 3. Normalized sensor response calculations are shown in equations 4 and 5.

$$G_{relative} = \frac{G_0 - G}{G_0} \quad (2)$$

$$G_{relative} = \frac{G - G_0}{G} \quad (3)$$

With $G_{relative}$: relative sensor response.

$$G_{normalized} = \frac{G}{G_0} \quad (4)$$

$$G_{normalized} = \frac{G_0}{G} \quad (5)$$

With $G_{normalized}$: normalized sensor response,

G_0: the conductance value under base gas atmosphere (generally air) or a fixed concentration value of the given target gas,

G: Corresponds to the value of the conductance under a concentration of the target gas.

1.3.2. Selectivity

Selectivity is defined as the ability of a sensor to respond to a certain gas in the presence of interfering gases. It is a parameter to be taken into account regarding the applications in real atmospheres, because the sensor is often used to detect a gas in an atmosphere containing several gases.

1.3.3. Stability

The notion of stability is associated with problems of temporal drifts. These drifts are detected by an evolution of the responses (amplitude, shape) for a given gas or by the evolution of the baseline with the time under the same conditions. These drifts can have several origins, such as

problem of reversibility or the instability of its surface [2]. There are two types of drifts: short-term drift (e.g. observed after switching on) and long term (due to the instability of sensor).

1.3.4. Reversibility

It relates to the ability of the sensor to return to its initial state in absence of the target compound to be detected. In the case of a non-return to the initial conditions, we speak about poisoning of the sensor.

1.3.5. Response and recovery times

The response time is often defined as the time taken by the sensor to reach 90 % of the steady-state sensor response when exposed to the gas. The recovery time is the time taken to return to 10% above the initial value in air after cutting off the gas injection. The sensor is said to be with high performance, when it responds with less time needed. The response-recovery time depends not only on the sensor itself but also on the measurement conditions such as the dimensions of measuring chamber, gas flow, and readout electronics. Thus, the conditions where the test is carried out should be mentioned with the value of the sensor response and recovery times.

1.3.6. Limit of detection (LOD)

LOD corresponds to a signal equal 3 times the standard deviation of the conductance baseline noise. Values above the LOD indicate the presence of target gas, while values below LOD indicate that no analyte is detectable.

1.3.7. Reproducibility

The reproducibility of a gas sensor reflects its ability to produce the same response for the same gaseous atmosphere. The system is reproducible if it responds to a gas in the same way regardless of the number of measurements and the time between measurements. Reproducibility includes response-recovery time and mainly the sensitivity.

Moreover, there is the notion of technological reproducibility from sensor to sensor. It is possible to manufacture two sensors having the same physical and geometrical characteristics. The

deposition of sensitive layers is particularly important because it determine the reproducibility of the sensors in most cases.

As a conclusion, each of these performances is of course more or less crucial depending on the applications: an application such as the air quality in the passenger compartment of a car will prefer the response time and the reproducibility rather than the low detection threshold. Another application such as human breath analysis will be more seeking for the lower detection limits of gases. In these two cases, the smallness of the sensor is not necessarily a priority, contrary to an instrumented textile application. This shows that it is almost impossible to design a generic sensor without considering dedicated application.

1.4. Metal oxide gas sensors

1.4.1. Historical background

Conductometric semiconductors metal oxide also known as chemo-resistive gas sensors, are based on metal oxide sensing layer. Actually they constitute one of the most investigated groups of gas sensors due to their variety of sensitive material and preparation methods. They have attracted the attention in gas sensors applications under atmospheric conditions due to their simplicity of use, large number of detectable gases in many application fields, flexibility in production and low cost [3–6]. In addition, chemical sensors based on metal oxides have other advantages such as portability, very large change in film conductance upon exposure to a reference gas, and fast response time etc. In the 1950s, Brattain et al. [7] and Heiland [8] have found that the electrical properties of a porous layer of semiconductor oxide deposited on a ceramic substrate are substantially affected in the presence of a low concentration of oxidizing or reducing gas. The oxidizing gases like oxygen generate acceptor surface states in the semiconductors, whereas the reducing gases such as carbon monoxide (CO) cause donor states (n-and p-type semiconductors). Following this work, a lot of research has been carried out on metal oxides for the detection of gases. Seiyama et al. [9] were have firstly proposed a ZnO-based sensor in 1962 for the detection of liquefied petroleum gas (LPG). Many other metal oxides were described in the literature such as Cr_2O_3, Mn_2O_3, CuO, Co_3O_4, NiO, SrO, In_2O_3, WO_3, TiO_2, V_2O_3, Fe_2O_3, Nb_2O_5, MoO_3, Ta_2O_5, La_2O_3, CeO_2, Nd_2O_3, and SnO_2 [10,11]. These

oxides are operated at elevated temperature between 300 °C and 650 °C, which does not represent favorable operating conditions of the sensors in terms of stability, repeatability and energy consumption [12]. Among these oxides, tin dioxide is the most used and studied because of its good sensitivity to gases and its chemical stability during operation in a polluting atmosphere.

1.4.2. Tin dioxide (SnO_2) gas sensors

Tin dioxide is the inorganic compound with the formula SnO_2. Tin (IV) dioxide also called stannic oxide is the most extensively studied gas sensing material and it is the dominant choice for solid state gas sensors. SnO_2 has been chosen due to its unique physical and chemical properties such as wide band gap (3.6 eV), dielectric constant, accuracy or repeatability at the present stage of development, environmental-friendliness and synthesis easiness. Its electronic configuration is [kr] $4d^{10}$. SnO_2 is usually regarded as an oxygen-deficient n-type semiconductor. The mineral form of SnO_2 is called cassiterite, and this is the main source of tin. This oxide of tin is the most important raw material in tin chemistry. It crystallizes with the rutile structure, where the tin atoms are 6 coordinate and the oxygen atoms three coordinate, and the lattice parameters are a = b = 4.737Å and c = 3.185Å as shown in Figure 1-2.

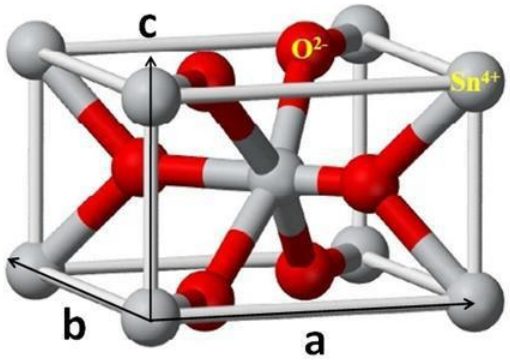

Figure 1-2. Unit cell of rutile SnO_2 [13].

SnO_2 materials is also used as electrode material in solar cells, light emitting diodes, flat panel displays, and other optoelectronic devices [14]. SnO_2 can be in different forms that have several useful properties, including that of a transparent conductive film which is used to define LCD

alphanumeric and graphic patterns. To achieve robustness and durability in its role as a gas sensor, SnO_2 is usually prepared in the form of a ceramic [15] which is sintered onto a substrate, commonly the alumina. The first gas sensor based on SnO_2 for the detection of flammable/explosive gases was developed by TAGUSHI in 1962 [16]. In 1968, the research on metal oxide gas sensors led to the commercialization of the first sensor based on semiconductor oxide under the name Figaro TGS (Taguchi Gas Sensor) for the detection of domestic gas leakage [17]. This Japanese company then proposed different versions of SnO_2-based sensors for the detection of natural gas (1980), hydrogen sulfide (1981), CO (1983). In total, the number of SnO_2 sensors currently used in Japan can be estimated at more than 80 million. Today, there are many companies offering this type of sensors, such as Figaro, FIS, MICS, etc. [18].

1.5. Electrical properties of SnO_2 thick film: effect of gas adsorption

In general, for a semiconductor, the conduction type originates from the creation of structural defects arising from stoichiometric deviations or doped impurities. In a real case, surface of a metal oxide can be imagined as a crystal which is cut, where the bonds between atoms on the surface are broken and defects in topology (gaps) appear. This intrinsic state is due to the abrupt discontinuity of the crystal lattice. Extrinsic states are due to the presence of foreign species on the surface of the solid and the interaction with the surrounding gaseous phase.

Usually SnO_2 is operated in ambient air which contains about 20.95% of oxygen. In the initial electronic situation (vacuum), oxygen interacts with surface vacancies of SnO_2 which induces upward band bending (i.e. surface energy barrier for electrons that trying to travel from the bulk to the surface) [6] as shown in Figure 1-3. In this case, the surface is charged negatively and the concentration of the electrons in the SnO_2 conduction band decreases leading to the reduction of the conductivity compared with flat band. Oxygen acts as electron acceptor on SnO_2 surface. In the vicinity of the surface of solid (bulk), there is therefore a zone of depletion poor in major carriers, comprising only positively ionized defects. The conductivity in the vicinity of the surface is consequently low. This interaction is favored at 300-450 °C because maximum amount of O^- appears on the surface at this temperature range [4].

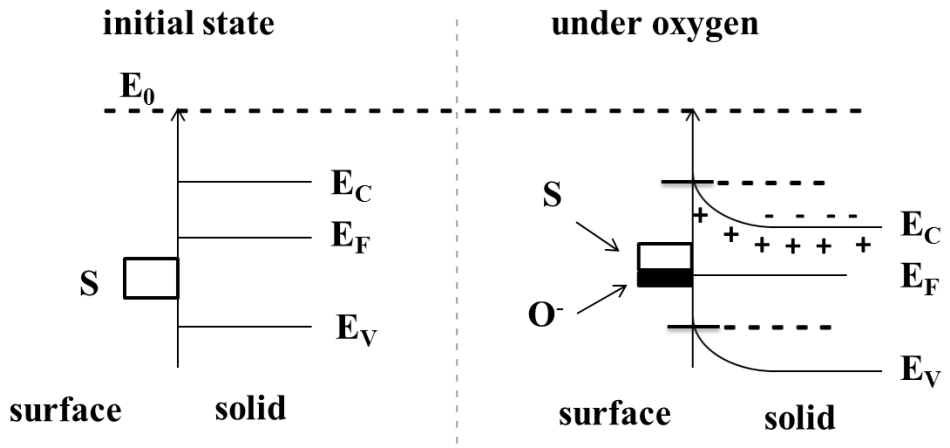

Figure 1-3. Simplified model illustrating the flat band (left) and the band banding upon exposure to O_2 (right) of n-type semiconductor metal oxides. The adsorption of oxygen as O^-, leads to band bending. E_C, E_V, E_F and S refer to energy of conducting band, valence band, the Fermi level, and surface vacancy respectively [6].

Conversely, if the gas is donor that is created for example by the adsorption of hydrogen, the surface is positively charged and there is accumulation of the free carriers in its vicinity. In both cases, the electron transfer between the volume and the surface will stop when the Fermi levels of the surface and the solid are equal. However, this transfer will result in a curvature of the conduction and valence levels in order to ensure the continuity of the latter between the surface and the solid.

The reaction mechanisms of gas detection in air are governed by the oxygen concentration and the type of species adsorbed on the surface of the sensitive material. The type and the concentrations of the adsorbed oxygen on the surface depend mainly on the operation temperature.

1.5.1. Adsorption of oxygen at the surface of SnO_2

In the case of metal oxides material such as SnO_2, the presence of oxygen is necessary for the detection of reducing gases. In this case, the reducing gases react preferentially with the chemisorbed oxygen and rarely with the material directly [2,19]. The adsorbed oxygen is therefore the precursor of the detection by oxidation reaction of the reducing gases. In addition, oxygen reacts with the SnO_2 and has an effect on the concentration of charge carriers of the

material, which consequently modifies its conductivity as shown before. Depending on the operating temperature, oxygen can exist as O_2, O_2^-, O^-, and O^{2-} adsorbed on the surface (with different reactivity) of the sensitive layer [4,20]. The evolution of these species on the surface of SnO_2 with the temperature can be summarized in Figure 1-4.

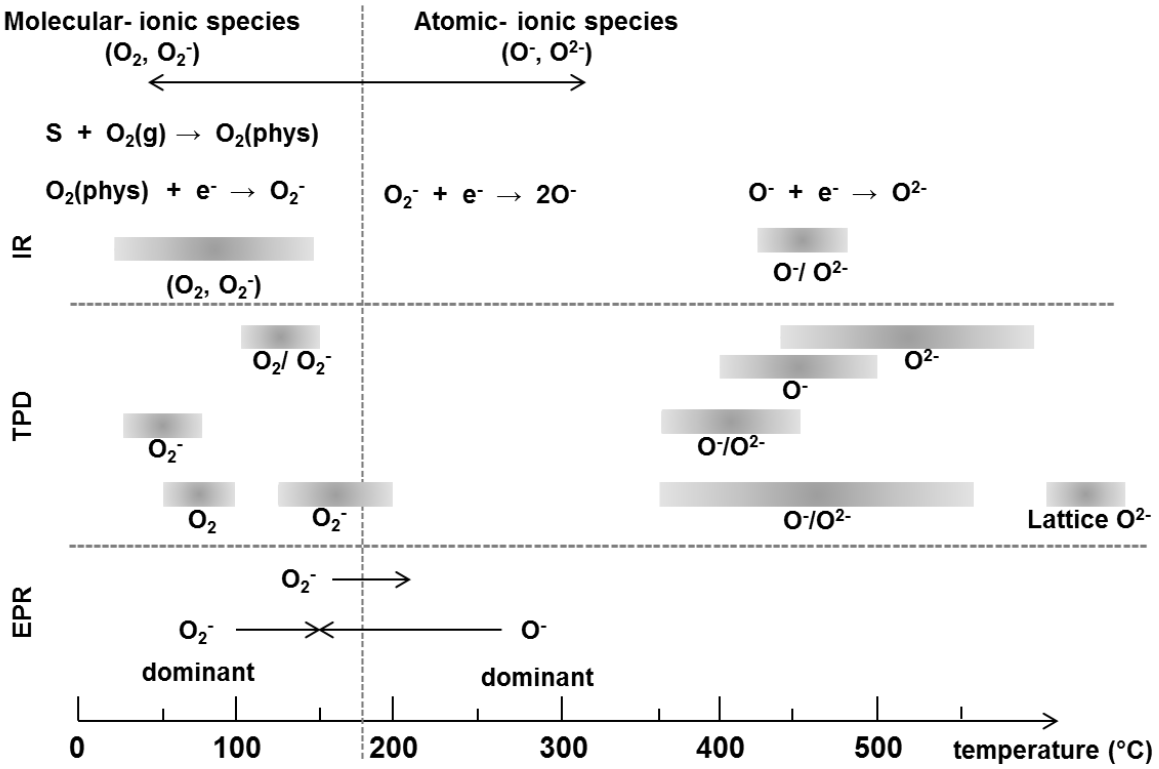

Figure 1-4. Literature study of diverse oxygen species detected at different temperatures at SnO_2 material surface by IR (infrared analysis), TPD (temperature programed desorption), and EPR (electron paramagnetic resonance) [4,20].

The reported surface oxygen species (Figure 1-4) were mainly observed with spectroscopic techniques (TPD, EPR and IR) on the surface of SnO_2 [4,20]. At the temperatures of interest in this study, which is between 25 and 200 °C, the oxygen species exist in neutral (O_2) and ionic molecular (O_2^--s) forms adsorbed on the adsorption sites (s) of SnO_2 grains. Equations (6) and (7) show how the physisorption of oxygen gas on SnO_2 takes place. The adsorbed oxygen on surface in the form of O_2 takes electron from the bulk SnO_2 and is transformed into adsorbed molecular oxygen (O_2^--s). This process decreases the conductivity of whole SnO_2.

$$O_2 + s \leftrightarrow O_2\text{-}s \quad (6)$$

$$O_2\text{-}s + e^- \leftrightarrow O_2^-\text{-}s \quad (7)$$

At temperature between 200 °C and 400 °C, the dominant species is O^- which derived from O_2^- as shown in equation (8). This step leads to decrease the electrons in the conduction band of SnO_2.

$$O_2^-\text{-}s + e^- + s \leftrightarrow 2O^-\text{-}s \quad (8)$$

At elevated temperature (>400 °C), the adsorbed oxygen ion transform to double ionic as shown in equation (9). Here, chemosorbed oxygen takes electrons from the conduction band of SnO_2.

$$O^-\text{-}s + e^- \leftrightarrow O^{2-}\text{-}s \quad (9)$$

Each of these reactions (equations (7), (8) and (9)) leads to decrease in the conductance of the whole metal oxide film by extracting electrons from its conduction band. Furthermore, these various types of oxygen at different temperatures affect the response of sensor to oxidizing and reducing gases. The description of the reaction mechanisms for detecting a gaseous compound by a sensitive surface of SnO_2 requires attention to its surface morphology. Generally, the semiconductor films used in gas detection consist of contiguous crystallites (Figure 1-5).

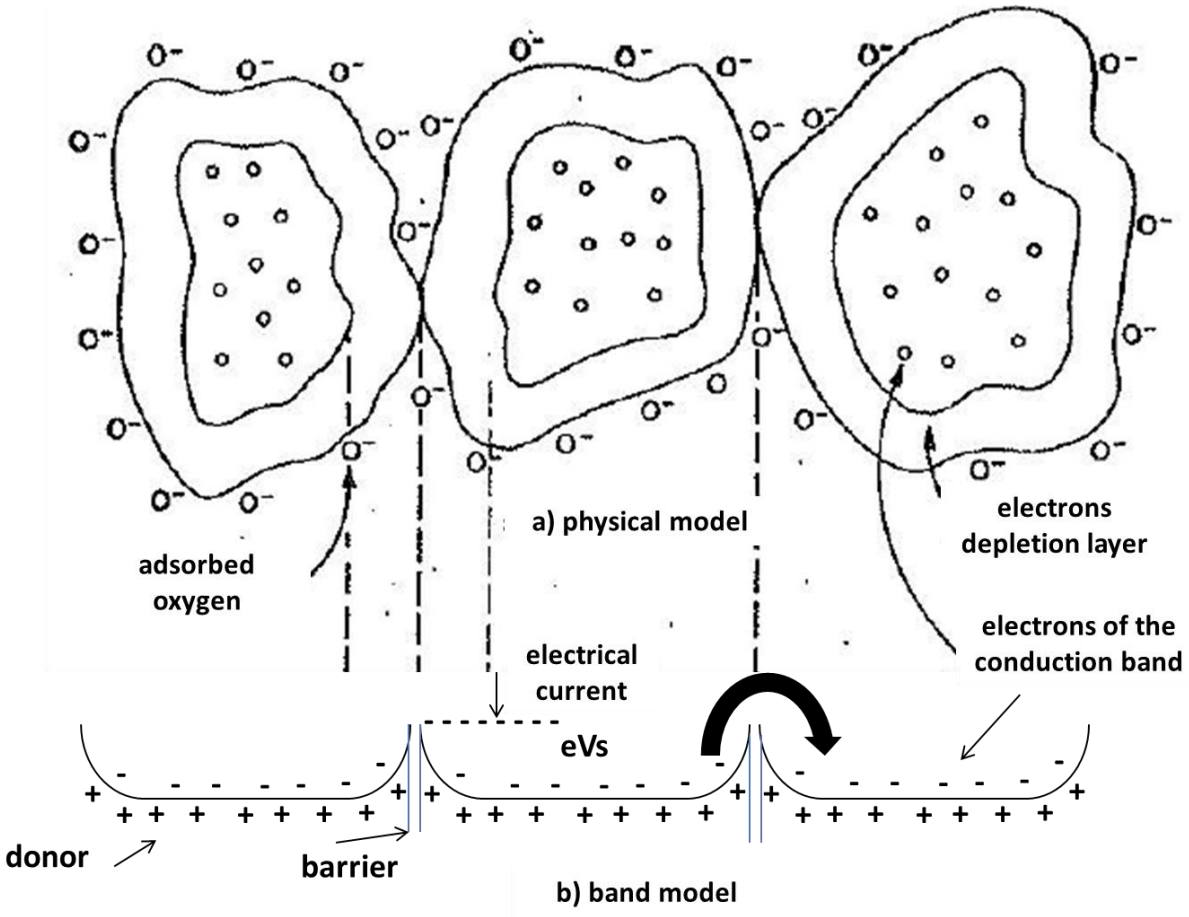

Figure 1-5. Potential barrier appearance at the grain boundaries [21,22], eVs is the potential barrier.

During the adsorption of negatively charged species at the surface (O^- for example), an electronic depletion zone is formed at the surface of the grains and also at the grain boundaries. This results in the formation of a potential barrier that modulates the electron flow from one grain to another. This surface resistance will thus dominate the overall resistance of the material and leads to a decrease in the conductivity of the whole film. The length of the depletion layer between two neighbor grains is known as Schottky barrier. When Schottky barrier between the grains increases, the transfer of electrons become more difficult, so conductance decreases. As a result, any phenomenon tending to vary the oxygen content adsorbed will cause a change in the electrical conductance of the sensitive material. For example, a reduction in the amount of adsorbed oxygen is induced either by decreasing the oxygen content in the surrounding atmosphere or by consuming this oxygen by heterogeneous reaction at the surface. This is the

basic principle that generates the electrical responses of the SnO_2-based gas sensors. For these devices, the conductance of the sensitive layer is expressed by equation (10).

$$G = G_0 \,.\, \exp\left(-\frac{eV_s}{k_B T}\right) \tag{10}$$

Where,

G: Conductance of the sensitive layer,

G_0: Conductivity obtained under reference gas (air),

eVs: Energy of the potential barrier,

k_B: Boltzmann constant,

T: Absolute temperature.

Moreover, the conductivity is the product of two important factors: the number of carrier electrons or holes and the carrier mobility (eVs), which is defined as the ease with which a carrier moves through a material. Hence, the conductance is controlled by the temperature, which modulates the electrons number in the conduction band of SnO_2.

1.5.2. Principle of detection of reducing and oxidizing gases

When SnO_2 is exposed to gases other than oxygen present in the air, a chemical reaction may occur with the pre-adsorbed oxygen species. The reactions are essentially redox reactions. For example, reducing gas such as carbon monoxide (CO), interacts with the adsorbed oxygen ion and is transformed to carbon dioxide (CO_2) as shown in equation (11). CO gas consumes the adsorbed surface oxygen, giving back electrons to the conduction band. This will reduce the depletion layer which leads to increases in conductance. The reaction of CO on the surface of SnO_2 is well studied before because it is the most simple gas (i.e. typical reaction gives CO_2) [23,24]. This reaction takes place preferentially at sensor operating temperature between 250 °C and 400 °C.

$$CO + O^-\text{-}s \rightarrow CO_2 + e^- + s \tag{11}$$

In contrast, the reaction of oxidizing gas with the surface results in more oxygen ions in the surface. This reaction will lead to decrease in conductance of the sensor. Therefore, SnO_2 exhibits

two types of responses: increasing or decreasing in conductance in different magnitude, depending on the concentration, the type of gas and the operating temperature.

1.5.3. Adsorption of water (H_2O)

Water vapor is an essential element to be investigated at ambient temperature. Indeed, water vapor in the breath of the human is very elevated (100% of relative humidity at 37 °C). Water vapor acts as an interfering gas for the detection of gases related to the detection of diseases by its interaction with the surface of SnO_2. As the functionalization will be carried out at low temperature (<100 °C), the adsorbed water on the surface of SnO_2 will later participate in the attachment of organic molecules on the surface. Therefore, the effect of water is of great interest for our study.

The results from the literature of TPD and IR studies are summarized in Figure 1-6 [20]. At temperatures of our interest (<100 °C), water is adsorbed by physisorption or hydrogen bond on the surface of the SnO_2 in molecular form. But, at temperature higher than 200 °C, water is adsorbed in the form of hydroxyl groups (OH) and molecular water is no longer present. IR and TPD have shown the presence of OH groups on SnO_2. However, the interaction mechanism of adsorbed water with SnO_2 once the temperature increases is still under discussion. Many studies assume homolytic dissociation of adsorbed water molecule on the surface of SnO_2 into two OH groups. One is an “isolated” hydroxyl bond to Sn and the other is a “rooted” OH group generated from lattice oxygen [25,26]. Others authors say that the hydroxyl groups are generated from an acid/ base reaction of HOH sharing its electronic pair with Sn (Lewis acid site), and leaving the weakly bonded proton (H^+). This proton can react with the lattice oxygen which acts as Lewis base or with adsorbed oxygen [27].

It is experimentally proven that SnO_2 based sensors exhibit reversible increase in surface conductance in presence of water vapor at temperature above 200 °C. These reversible changes in conductance are related to the presence and disappearance of OH groups on the surface [28]. Likely, at room temperature, the conductivity of SnO_2 increases on exposure to water vapor [29,30]. There are three types of mechanism to explain the increase of surface conductivity. Two different types have been proposed by Heiland and Kohl [31]. The first one attributes the role of the electron donor to the ‘rooted’ OH group, this one including lattice oxygen according to equation (12).

$$H_2O + Sn + O_{lat} \leftrightarrow (HO\text{-}Sn) + (O_{lat}H)^+ + e^- \quad (12)$$

where Sn and O_{lat} are tin and oxygen atoms in the lattice, (HO-Sn) is referred to as an isolated hydroxyl or OH group and $(O_{lat}H)^+$ is the rooted one.

The second mechanism of Heiland and Kohl takes into account the possibility of the reaction between the hydrogen atom and the lattice oxygen, and the binding of the resulting hydroxyl group to the Sn atom. The resulting oxygen vacancy will produce additional electrons as shown in equation (13).

$$H_2O + 2Sn + O_{lat} \leftrightarrow 2(HO\text{-}Sn) + V_O^{2+} + 2e^- \quad (13)$$

where V_O^{2+} is an oxygen vacancy on Sn.

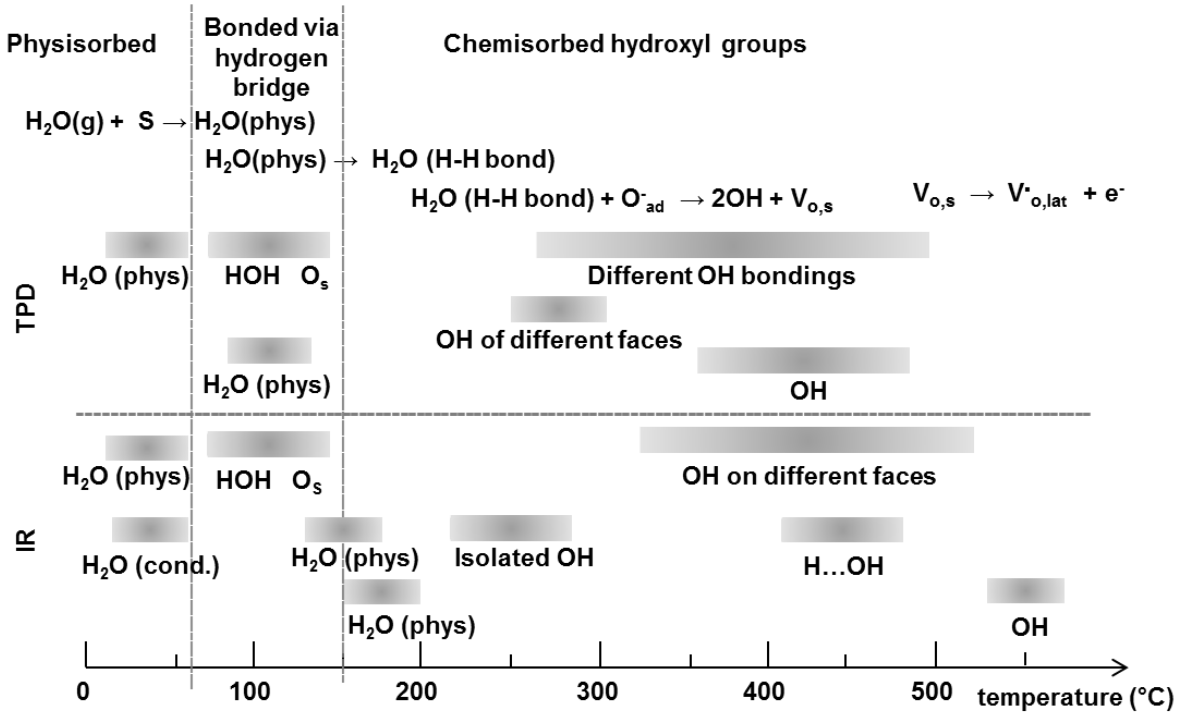

Figure 1-6. Literature study of water-related species formed at different temperatures on SnO_2 surface. Results were detected by IR and TPD [20].

Morrison [32], as well as Henrich and Cox [33], consider an indirect effect. These interactions could be the interaction between either the hydroxyl group or the hydrogen atom originating from the water molecule with acid or basic group, which are also acceptor surface states. They supposed that their electronic affinity could change after the interaction. It could also be the influence of the co-adsorption of H_2O on the adsorption of another adsorbate, which could be an electron acceptor. Henrich and Cox suggested that the pre-adsorbed oxygen could be displaced by H_2O adsorption. In any of these mechanisms, the particular state of the surface plays a major role due to the fact that it considers that surface defects will increase the dissociative adsorption. These hydroxyl groups act as donor states. This implies an increase in the conductivity of the sensitive layer.

1.5.4. Modulation of temperature

Under ambient conditions, the most abundant reactive gases present are oxygen and water vapor. As shown before, the operating temperature affects the quantity and quality of adsorbed species on the surface of SnO_2. These variations with the change of temperature affect the conductance and the interactions with gases. For example, the temperature affects the response of SnO_2 sensor to reducing gases according to the following processes:

- Dissociative adsorption of oxygen (molecular oxygen does not interact with reducing gases). Generally, this process begins at T > 170–200 °C to form atomic oxygen atoms.
- Adsorption of reducing gases molecules and conversion into oxidized form. This process is influenced by the type of reducing gas; for example, detection of H_2 or CH_4 in contrast to CO, which requires dissociative adsorption of molecules.
- Desorption of reducing gas.
- Desorption of chemisorbed oxygen.

The first two processes determine the decrease in sensitivity at low operating temperatures. In addition, the last two determine the drop of the sensitivity at high temperatures. The competition between these processes determines the temperature of maximum sensitivity. It means that gases have specific combination of adsorption/desorption parameters and reaction rates can have different temperature profiles of sensor response. Therefore, these gases have to be selectively recognized [34]. Each gas has a specific reaction rate and specific sensitive temperature as shown

in Figure 1-7. Thus, sensors operated at different temperatures will show a degree of selectivity [35].

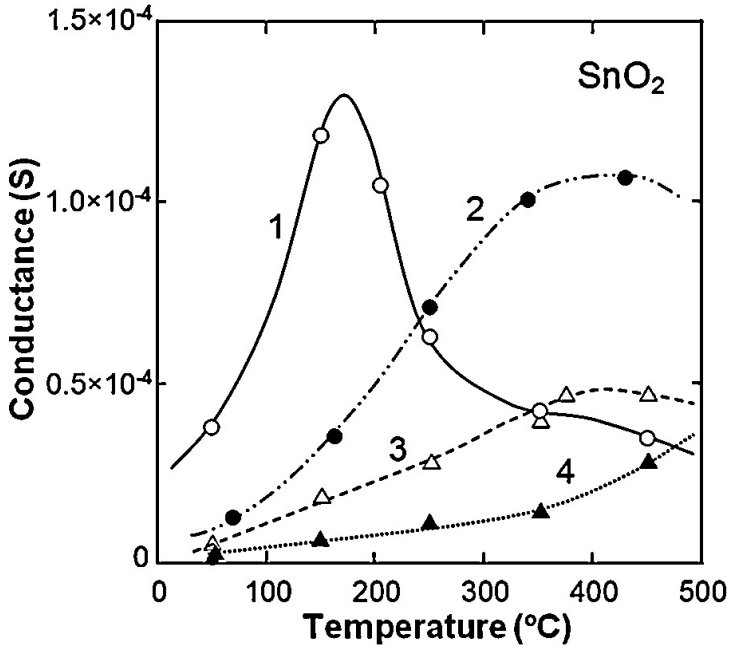

Figure 1-7. Temperature dependances of conductivity response of SnO_2 thick films to (1) C_2H_5OH (50 ppm), (2) H_2 (500 ppm), (3) CO (300 ppm), (4) CH_4 (1000 ppm), in dry synthetic air [35].

Therefore, by changing operation temperature it is possible to create conditions where the response to one gas will exceed considerably the response to other one.

1.6. Conductometric room temperature gas sensors

1.6.1. General description

As already mentioned, the semiconductor gas sensors are operated at temperatures above 200 °C in order to increase reaction kinetics and sensitivity. In addition to the fact that the installation of a heating circuit on the sensor induces technological constraints, it also has an increase in manufacturing and operating costs of the devices. The working at elevated temperature could affect the stability of these devices with time. This phenomenon is mainly due to the diffusion of the oxygen in the network and to the dilation-agglomeration of the grains. Operation at high temperature is also undesirable for safety reasons when detecting the combustible gases [36,37]. Efforts have been made in recent years to develop new sensitive materials operating at lower

temperatures or even at ambient temperature. These new Conductometric gas sensors are mostly made up of conductive polymers, nanostructured thin films (nanoparticles, nanowires, integration of carbon nanotubes), composite materials (combination of metal oxides), or metal oxide layers modified by the addition of various catalysts (doping elements).

1.6.2. Conductive polymer based gas sensors

The use of conducting polymers in the field of gas sensor is of high interest because they are operated at room temperature. Conductive polymers refer to macromolecules which have the property of carrying charges (electrons or holes). They possess a conjugate structure allowing the delocalization of the electrons along the macromolecular skeleton. This extended π-conjugated system of the conducting polymers has single and double bonds alternating along the polymer chain.

Recently, conducting polymers such as polyaniline (PANI), polypyrrole, polythiophene have been widely investigated as an active layer for the development of gas sensors operating at room temperature [38]. They are characterized by good conductivity, high sensitivity, short response time at room temperature and good mechanical properties. These improved characteristics allow facile fabrication of sensors, thus making them popular [39]. However, conducting polymer based sensors have disadvantages such as lack of selectivity and low stability. Thus, the major challenge in conducting polymer-based sensors is enhancing their selectivity and stability. Among these conducting polymers, PANI is the most investigated recently.

Polyaniline has been widely investigated as room temperature gas sensors. The structural properties of PANI can be modified conveniently by adding metals, metal-oxides, organic molecules, or carbon nanotubes [40–43] which in many cases improve the selectivity and stability. The modification of PANI films by SnO_2 nanoparticles can produce a sensor highly selective and responsive to NH_3 [44]. Working at room temperature improves the reproducibility and stability of gas sensors. Table 1-2 lists some gas sensors based on PANI conductive polymer operating at ambient temperature. As shown, PANI can be used for the detection of various gases such as ammonia, hydrogen and LPG gases. Concerning the PANI detection mechanism, many explanations were proposed in the literature including acid-base and redox reactions [45]. PANI

can exist in different oxidation states depending on the pH. Thus, PANI can change its oxidation state upon interaction with acidic or basic gases. This variation of oxidation states affects the conductance of the film [46]. Despite these advantages of PANI-based gas sensors, they still have very low sensitivity for the detection at low gas concentrations.

Table 1-2. Different sensors based on pure and modified polyaniline material.

Sensitive material	Operating temperature (°C)	Detected gas	Reference
polyaniline nanowires	25	NH_3 (25-500 ppm)	[47]
polyaniline nanofibers	25	H_2	[48]
polyaniline/TiO_2	25	LPG	[49]
Polyaniline/palladium	25	H_2	[50]
polyaniline	25	NH_3 (5-1000 ppm)	[51]
polyaniline/SnO_2	25	NH_3 (100–500 ppm)	[44]

1.6.3. SnO_2 modified by other metal oxides gas sensors

The operating temperature of the gas sensor can also be decreased by using a composite of metal oxides. This combination leads to a modification of the electronic structure of the composite oxides and consequently induces the formation of a high resistance between the grains of different types. The combination of metal oxides forms p-n type heterojunctions, for example in the case of the following composite oxides: CuO (p)/SnO_2 (n), ZnO (p)/SnO_2 (n) [52], and La_2CuO_4 (p)/ZnO (n) [53]. Selim et al. [54] have fabricated a ZrO_2-doped SnO_2 sensor for the detection of H_2S at room temperature. Similarly, Patel et al. [55] have shown that thin films composed of a mixture of indium and tin oxide (In_2O_3/ SnO_2) are sensitive to methanol at low temperature.

1.6.4. SnO_2 with addition of metals or carbon

Several authors have shown that the addition of noble metals or carbon nanotubes to the metal oxide influences the operating temperature of the sensor as well as its selectivity. In this

direction, Tadeev et al. [56] have shown that the addition of additives such as Pd and Pt to SnO_2 layer decreases the optimal CO detection temperature from 400 °C to 100 °C. Chaparadza et al. [57] found that SnO_2 doped with 0.1% of Sb showed a high Cl_2 response and selectivity with respect to compounds Br_2, HCl, NO, NO_2, $CHCl_3$, NH_3 and H_2 at room temperature. This sensor has a relatively short response time (~ 60 s). Wei et al. [36] also revealed that the doping of the SnO_2 layers with very small amounts of the mono-walled carbon nanotubes (SWNT) improves sensitivity to NO_2 at room temperature.

1.7. Breath analysis application: focus on ammonia and SnO_2

1.7.1. Breath analysis

Recently, one of the main challenges in disease diagnoses field is how we can detect the disease when we are still feeling healthy. Today, it is highly requested to have the capability of predicting healthy people who are going to develop a disease in the future using very simple and affordable device. This approach is relying on chemical biomarker or so-called volatile organic compounds (VOCs). These compounds basically are chemical analytes which are emitted as results of the disease evolvements in the human body into the blood stream. These analytes should be emitted outside the human body because they have high vapor pressure. They can do it either throughout the urine, feces, skin, or breath. The detection of these volatile disease biomarkers throughout the breath would be the most beneficial [58]. This type of diagnosis is characterized by the non-invasiveness of the sample collection [59]. Each type of disease has a unique gases fingerprint in the breath exactly as people have a unique fingerprint that discriminates a person from another person [60]. Thus, breath analysis permits to know whether the patient is healthy or has a disease, as well as it can predict the healthy people who have high risk to get a disease in the future. This is a critical point because if the disease can be identified at very early stages, the survival rates can be increased by several folds [61]. For this mission, the gas sensor is supposed to interact selectively with biomarker gases if it present in the breath. This type of sensors could be installed a smart phone. Once the person talk over the phone, the smart phone will react to the content of the breath and it will analyze the results. This is a quite important approach because it allows every person to get a diagnosis of the diseases without going into the clinic.

Exhaled breath of the human contains water vapor, nitrogen, oxygen, carbon dioxide, carbon monoxide, ammonia, and a mixture of VOCs [62,63]. These gases are expired in air saturated with water vapor. Normally, the breath content varies from each individual person qualitatively and quantitatively [64]. Table 1 illustrates the major contents of the human breath. Elevated levels of a number of these gases indicate a systemic disorders and extra pulmonary organ failures.

Table 1-3. Major human breath content for health person [64].

Exhaled Breath	Concentration
Nitrogen	78.04%
Oxygen	16%
Carbon dioxide	4%–5%
Hydrogen	<5ppm
Carbon monoxide	0–6 ppm
Acetone and Ethanol	<1 ppm

Ammonia is one of the disease biomarker. Indeed, ammonia in humans is converted to urea in the liver and then passes to urine through the kidney, while unconverted ammonia is excreted in breath at 10 ppb for healthy subjects [65]. The ammonia concentration in exhaled air increases in case of malfunctioning of liver and kidney reaching more than 1 ppm in presence of renal failure [66,67].

1.7.2. Ammonia

Ammonia gas has basic character and it is lighter than air, colorless under ambient temperature and pressure conditions, emitting a pungent odor (its olfactory concentration limit is generally between 5 and 25 ppm). It is stable at room temperature (thermal decomposition at 450 °C-550 °C).

This gas is widely used in many sectors of the chemical industry, including petroleum and fuel chemistry, metal processing, and paper industries. Ammonia in the atmosphere comes mainly

from agricultural activities (fertilizers and animal waste). It is also used as a refrigerant gas. It is also found in cigarette smoke and certain household products [68].

Although often present in the environment, ammonia is considered as toxic gas, which can have adverse health effects such as irritation of the ocular system. In addition, it causes severe lung damage. This compound is also harmful to our ecosystem. It can form explosive mixtures with air in the range of 15 to 28% by volume. The contact of ammonia with certain products such as mercury, halogens, calcium, and silver oxide is a source of fires and explosions. Because of its toxicology and chemical reactivity, the use of ammonia is submitted to a number of regulations. For information purposes, in France, the short-term exposure limit value measured over a maximum of 15 min is set at 20 ppm (14 mg/m^3). In addition, the threshold toxic limit value put to protect workers from long-term, measured over the duration of a workstation for 8 h, is 10 ppm ($7mg/m^3$). Thus, ammonia gas sensors are needed for the early detection of possible leakages from such systems.

1.7.3. Detection of ammonia by metal oxide gas sensors

Many techniques were described in the literature for the detection of ammonia gas. Among all, metal oxide-based gas sensors are the most frequently used and investigated at high and at low temperatures. Metal-oxide, mostly based on SnO_2 sensors have been manufactured and tested in the largest quantities [69,70]. Several examples of ammonia sensors reported in the literature are shown in Table 1-4. For the detection of ammonia gas, Metal oxides can be used as pure, composite and doped. Among all material present, SnO_2 is the most powerful for the detection of ammonia. Many techniques were applied to improve the sensing performance of SnO_2 to ammonia gas such as doping with another metal, SnO_2/carbon nanotubes [71], and hybrid sensors like SnO_2/polyaniline [72]. However, all the reported sensors are limited with respect to sensor selectivity and the ability to detect very low concentrations of NH_3 (in the range of ppb). Therefore, the presented sensors do not fulfill needs for the detection of ammonia in the human breath. To develop a selective and sensitive ammonia gas sensor based on SnO_2 material, it is essential to investigate the sensing mechanism.

Table 1-4. Conductometric metal oxide sensors for the detection of ammonia.

Material	Analyte	Temperature (°C)	Concentration (ppm)	Reference
SnO_2 (ultrathin film)	NH_3	25	5-30	[73]
SnO_2 (nanoparticles)	NH_3	25	50	[74]
SnO_2 (ultrathin film)	NH_3	25	9	[75]
ZnO	NH_3	25	40-160	[76]
ZnO/Cr_2O_3	NH_3	25	20	[77]
WS_2	NH_3	25	1-10	[78]
TeO_2	NH_3	25	10-100	[79]
Sb doped SnO_2	NH_3	25	50	[80]
SnO_2/MWNTs	NH_3	25	60-800	[71]
SnO_2/SWNTs	NH_3	25	1-100	[81]
SnO_2/polyaniline	NH_3	25	100-500	[44]
SnO_2/polyaniline	NH_3	25	100	[82]
TiO_2/polyaniline	NH_3	25	20-100	[83]
Camphor sulfonic acid doped PANi-TiO_2	NH_3	25	20-100	[84]
Camphor sulfonic acid doped PANi-SnO_2	NH_3	25	100	[85]
Polypyrrole-reduced graphene oxide hybrid	NH_3	25	10	[86]
graphene oxide-silver nanoparticles	NH_3	25	15-100	[87]
Pd/SnO_2/ reduced graphene oxide	NH_3	25	5-300	[88]
SnO_2	NH_3	100, 400	500	[89,90]
ZnO	NH_3	200	2-100	[91]
TiO_2	NH_3	300, 350	43-156	[92]

1.7.4. Interactions of ammonia with SnO_2 gas sensors at high temperature

Numerous models have been proposed trying to explain the detection mechanism of ammonia by metal oxides based sensors [93]. It is now well known that the interactions of gases with metal oxide sensitive layer lead to change in the conductivity of gas sensor. The oxygen species (O_2^-, O^-, OH, O^{2-}, etc.) adsorbed on the surface of the metal oxide interact with reducing gases at high temperatures (> 150 °C.) which leads to an increase in the conductance of the film. Thus, in the presence of ammonia, the oxidation reactions (14), (15) and (16) can occur depending on the operating temperature where the oxygenated species are predominant at the surface.

$$NH_3 + s \leftrightarrow NH_3\text{-}s \quad (14)$$

$$2NH_3\text{-}s + 3O^-\text{-}s \rightarrow N_2 + 3H_2O + 3e^- + 5s \quad (15)$$

$$2NH_3\text{-}s + 3O^{2-}\text{-}s \rightarrow N_2 + 3H_2O + 6e^- + 5s \quad (16)$$

The same mechanism has also been proposed by Wagh et al. [94]. Shao et al. [95] modeled the adsorption of ammonia on a surface of SnO_2: the retained mechanism consists in an NH_3 dehydrogenation reaction chain to form N_2 as shown in equations (17) and (18).

$$NH_3\text{-}s + O(lat) \rightarrow NH_2 + H\text{-}O(lat) + s \quad (17)$$

$$NH_2 + NH_2 \rightarrow N_2H_4 \xrightarrow{-H} N_2H_3 \xrightarrow{-H} N_2H_2 \xrightarrow{-H} N_2H \xrightarrow{-H} N_2 \quad (18)$$

All the proposed mechanisms lead to the formation of N_2 at the end of the adsorption of ammonia at temperature above 150 °C. These interactions give electrons to the conduction band of metal oxide (equations (15) and (16)) which leads to the increase in the conductance of whole film. However, at temperature less than 150 °C, the sensor response becomes in opposite sense (decrease in conductance) which makes the mechanism of interactions more complicated due to

the presence of many types of adsorbed species on the surface in atomic and molecular forms [74,76].

1.7.5. Interactions of ammonia with SnO_2 gas sensors at ambient temperature

As shown before, the interaction of ammonia with n-type semiconductors at temperature more than 150 °C like SnO_2 leads to increase in conductance of the whole film. In contrast, at ambient temperature, decrease in conductance was observed for SnO_2, rhodium doped SnO_2, WO_3, and CeO_2 [96] upon exposure to ammonia. This means that another mechanism takes place, other than the one showed before. Research has been carried out in this direction, but the mechanisms are still barely known to date.

Sipra Choudhury et al. [73] have studied the sensitivity of ultra-thin films of SnO_2 to ammonia at room temperature. The electrical current of these films decreases upon exposure to ammonia gas (15-30 ppm) as reported in Figure 1-8. The electrical current is proportional to the conductance. This means that the conductance of SnO_2 decreases when it exposed to ammonia. This response is generated as a result of the decrease in carrier mobility during ammonia adsorption. Betty et al. [75], detected ammonia at room temperature by ultra-thin SnO_2 using electrical impedance spectroscopy. These sensors showed a rapid increase in their electrical resistance in the presence of ammonia.

Reversibility of detection suggests that the ammonia molecules adsorb and easily desorb on the surface of SnO_2 at room temperature. This is due to the low interaction energy between the hydrogen of ammonia and the surface oxygen of SnO_2 compared with N-H bond of ammonia itself (E_{N-H-O} = 5 kcal.mol^{-1} for ammonia-SnO_2, E_{N-H} = 93 kcal.mol^{-1} for ammonia molecule). According to these authors, the adsorbed ammonia can function as active diffusion centers, thus reducing the mobility of the free carriers and consequently increase the resistance. This is due to the fact that the mean free path of the free charge carriers is comparable to the grain size.

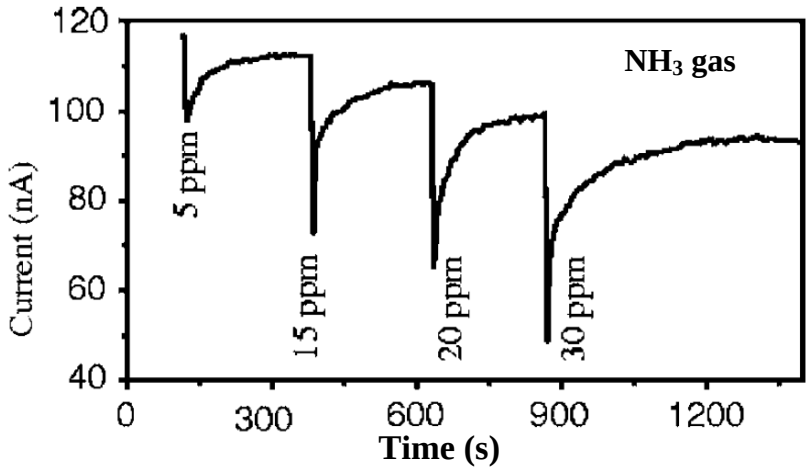

Figure 1-8. Response curve of SnO_2 sensor to ammonia gas at room temperature [73]. The current is proportional to conductance.

Likely, Kamalpreet Khun Khun et al. [74], have found that SnO_2 sensor exhibits an decrease in the electrical conductance in presence of ammonia at temperature between 25 to 200 °C. They supposed that there is compensation between two different reactions. The first reaction is as mentioned in equation (15) before, which leads to increase in sensor conductance. The second is the reaction of ammonia with molecular adsorbed oxygen ion (O_2^-), producing nitrogen monoxide gas (NO) according to equation (19). In presence of oxygen, NO can be easily transformed into NO_2 which is very good oxidizing agent. The reaction of NO_2 with SnO_2 at ambient temperature leads to the decrease in conductance of the sensor. Therefore, the second reaction is the predominant one because the conductance actually decreases when SnO_2 sensor exposed is to ammonia at ambient temperature.

$$4NH_3 + 5s\text{-}O_2^- \rightarrow 4NO + 6H_2O + 5s + 5e^- \quad (19)$$

In summary, research on SnO_2-based sensors operating at room temperature is still very limited. Efforts are still needed to understand the mechanisms of detection as well as the correlation between the nature of the response and the concentration of ammonia at low temperatures. These interactions will be discussed more in details in the next chapters.

1.8. SnO_2 surface functionalization

Many possibilities exist to enhance the performance of SnO_2 gas sensors such as selectivity, sensitivity, response/recovery time and stability with time. Selectivity of the gas sensor to a specific target gas in the presence of a mixture of gases is necessary for many applications in which the gas origin is of interest. However, in most cases, the gases often produce very similar sensor responses except when reducing and oxidizing gases are being compared. For example, gases such as ethanol, carbon monoxide and methane have appreciable cross-sensitivity which hinders the development of gas sensor able to distinguish these species [97]. The techniques which were developed for improving the selectivity of SnO_2 gas sensors includes the control of the sensor operating temperature [35], addition of gas filter [35], small amount of noble metals [98–100], oxides mixture [101,102], hybrid film of SnO_2 and organic materials [45,103] as discussed before.

1.8.1. Organic surface functionalization

Inorganic and organic compounds have been proposed as gas sensing materials, and have gained increasing development respectively due to some particular advantages. Inorganic compounds have generally high chemical and thermal stability that allows their application under different operating conditions.

Organic functionalization is the modification of the surface of a material by reactive end groups for further modification, protective layers, biological or gas sensors, catalysis, solar batteries, etc. These modifications lead to change in physical and chemical properties of the surface and later change in sensing response. The attached organic groups act as chemical antennas on the surface of sensor. The design of organically modified surfaces is a rapidly expanding field of research in material science, in which the central purpose is access to materials possessing tunable properties in different areas. These modifications involve attaching organic polymers to metal oxide or grafting of monolayer onto the surface using appropriate functional molecules.

Organic compounds are described by a synthetic versatility and reactivity, which makes it possible to modulate the molecular structure of the sensing materials to enhance the selectivity toward a target analyte [104,105]. As shown before, the organic sensing materials such as conducting polymers can show response to target analyte at ambient temperature, which has a

suitable operating and attractive outlook [38,106–108]. Nevertheless, there are many drawbacks for using single inorganic or single organic sensing materials. Gas sensors based on inorganic sensing layer have high operating temperature and low selectivity. As for organic sensing materials, the drawbacks are poor chemical stability, and mechanical strength that restrict their practical application. The addition of the advantages of organic and inorganic materials is with high interest. In the past decade, various organic/ inorganic hybrid sensors were synthesized by intercalation of inorganic particles in organic film, as for example, the intercalation of SnO_2 particles in conducting polymers like polyaniline [85,109–111]. It can be also the inverse by surface functionalization of SnO_2 film by polyaniline [112]. These sensors have enhanced sensing performances to several toxic or harmful gases for example NH_3, ethanol, methanol, H_2S and acetone etc. Molecular modification is another way to organically modify metal oxide surface which provides a better control of the density and orientation of the organic component at the surface.

Molecular layers of organic molecules can interact with the substrate in two different ways, either by physisorption or covalent bond formation. Physisorbed molecules retain their base structure upon adsorption, whereas molecules can decompose and be covalently attached in the chemisorption process, for example, dissociation upon adsorption on a hydroxyl terminated oxide surface [113]. These molecules possess a head chemical functionality (ethoxysilanes) with high affinity to bind with metal oxide surface and a tail with desired chemical composition (e.g. amine group). The self-assembly of ethoxysilanes terminated with amine group, in particular 3-aminopropyltriethoxysilane (APTES), is in the focus of this dissertation.

The following section of the thesis will focus on possible covalent surface modification strategies of SnO_2 sensor. Thick SnO_2 films produced by screen printing technique will be intended to be functionalized by organic film to modify their sensitive properties to gases like ammonia.

1.8.2. Covalent functionalization

1.8.2.1. Self-assembled monolayer on SnO_2

Many attachment methods have been used to covalently modify the surface of metal oxide by organic self-assembled monolayers (SAMs). As shown in Figure 1-9, carboxylic acid, alkenes, alkynes, amines, phosphoric acid, catechol and silane groups can be used in functionalization

[114]. Among all of these methods, the most commonly used method to covalently functionalize metal oxide surfaces is through the self-assembly of organofunctional alkoxysilane and chlorosilane molecules. Silane technique can be applied onto the majority of metal oxide materials. The interest of SAMs comes from the ability to form very dense, stable, and highly ordered structures. In addition, the molecules to be grafted can arrange upon adsorption reaction with the substrate (SnO_2). Depending on the end functional groups, SAMs can selectively interact with gas. In this case, metal oxide sensitivity may be changed with SAMs of organic molecules bearing the desired functional groups. The process to functionalize a metal oxide by silane products is known as silanization. Silanes are existing in different bases (alkoxysilane and chlorosilane) and different end functional groups as shown in Figure 1-10. Figure 1-11 gives a schematic representation of the formation of APTES monolayer terminated with amine onto silicon surface. It should be noted that this chemistry is mostly investigated on SiO_x surfaces; other hydroxylated oxides surfaces can be modified as well (e.g. SnO_2 [115], Al_2O_3 [116]). Previously, many papers have reported the silanization by APTES on silicon nanowires-based sensor devices [117–119]. APTES functionalized silicon films were used as pH sensors, biosensors, and gas sensors.

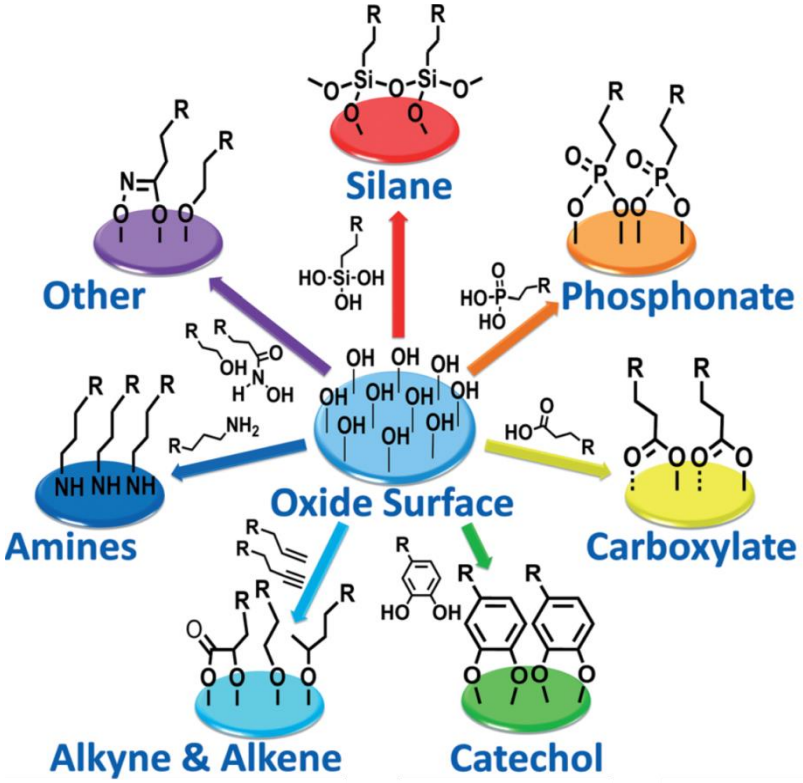

Figure 1-9. Different approaches towards surface functionalization of metal oxides surface [114].

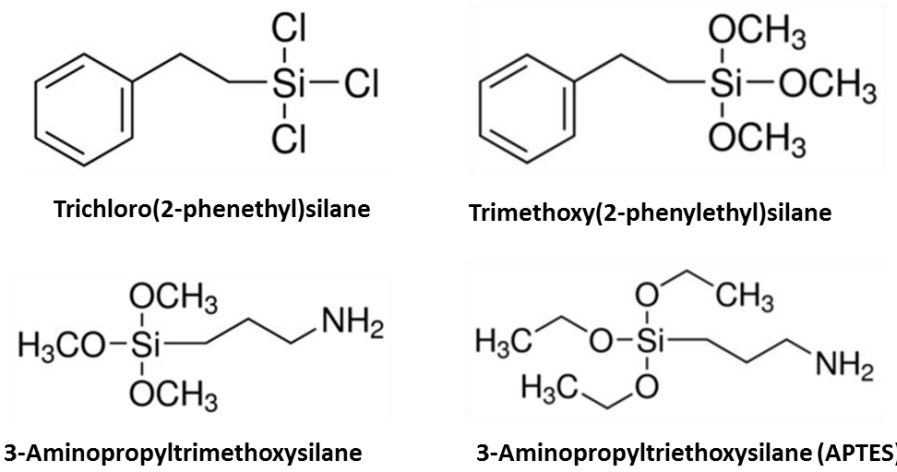

Figure 1-10. Some examples of silane products.

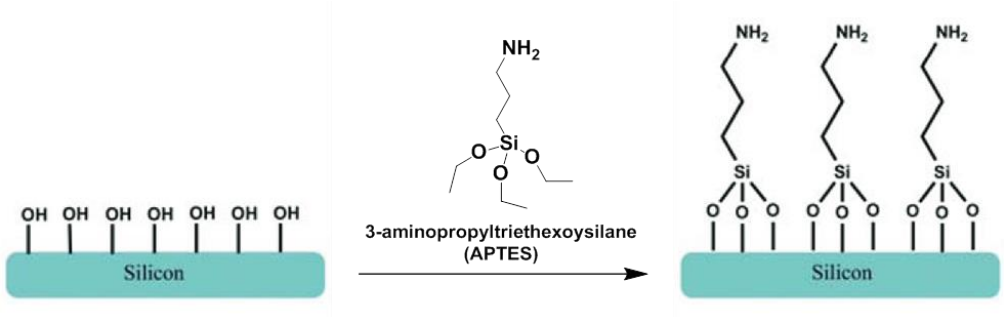

Figure 1-11. Schematic representation of the silanization process by APTES on silicon substrate [120].

As in SiO_x, functionalizing SnO_2 by organic molecules could be of special interest to improve sensitivity, selectivity, and electrical properties in gas sensor applications and others. Among all the silane products, APTES is the most used in silanization of metal oxide surfaces.

1.8.2.2. Silanization mechanism

Normally, metal oxide surfaces are terminated with hydroxyl groups under atmospheric conditions as mentioned before. These -OH groups are the active sites where the condensation reactions can take place. The major pathway to covalently modify OH-terminated oxide surfaces via self-assembly is the use of condensation reactions. Silanes with reactive groups, such as, methoxy-, chloro- and ethoxysilanes (ethoxysilanes in the case of APTES), are converted to hydroxysilanes in contact with water. Then, condensation reaction between -OH groups of

APTES and the -OH of SnO_2 surface takes place. The resulting silanol moieties can then react with each other via another condensation reaction producing siloxane bonds. Besides covalent linkage, the interaction of APTES with metal oxide film can be also in form of physisorption, hydrogen bonding, or electrostatic attachment [120]. Thus, annealing after silanization is important to remove all the non-covalent bonded APTES.

The hydrolysis of chlorosilane or ethoxysilanes to hydroxysilanes is a key step in the silanization. It controls the final quality and morphology of the SAMs. The incomplete hydrolysis results in incomplete monolayer, while excessive hydrolysis leads to polymerization of silane on the surface of metal oxide. In addition, the same effects are observed if the surface of metal oxide does not have sufficient amount of adsorbed water. In these cases, creation of OH groups on the surface is needed and it can be done by plasma activation or by immersing in NaOH solution for 2 h [121,122].

To the best of our knowledge, the properties of APTES films such as thickness, orientation, and the density of the monolayer have essentially been investigated on silicon oxide [123–125]. However, only a few studies on the preparation of APTES layer deposited on thick SnO_2 film have been explored, although the development of low cost films is of high interest [126]. APTES modified SnO_2 could have a special interaction with gases or can served as a substrate for further modifications.

1.8.2.3. Silanization by 3-aminopropyltriethoxysilane

Silanization is the most widely process used to modify surface properties of hydroxide terminated oxide substrates [125,127–131]. 3-aminopropyltriethoxysilane (APTES) is commonly used to introduce terminal amine functionality to the surface. In most cases, APTES is used as intermediate step for further modifications such as coupling reaction with acyl chloride and carboxylic acid [132–134] to attach a variety of materials such as DNA, proteins and polymers [115,135,136]. The main advantage of an aminosilane monolayer on the surface of metal oxide is the rapid formation of covalent bonds between the oxide surface and the anchoring groups. This covalent linkage stabilizes the monolayer and facilitates further modifications with the conservation of monolayer integrity [114]. Furthermore, APTES has bulky alkoxy groups that improve the stability of the resulting monolayer as shown by Linford et al. increasing hydrolytic stability using bulky alkoxy side [137]. One major drawback of this molecule is the possibility of

polymerization, which can occur if the reaction conditions are not carefully controlled [138]. The functionalization of metal oxide surface by APTES can be carried out in liquid or in the vapor phase [126].

1.8.2.4. Liquid phase silanization

The first silane-based self-assembled monolayer produced in liquid silanization was reported by Sagiv in 1980 [128]. In general, a hydroxylated surface like SnO_2 is introduced into a solution of a silane dissolved in an organic solvent. Many factors affect the nature of monolayer such as APTES concentration, reaction time, reaction temperature, type of solvent, and water in the reaction solution. The study of silanization parameters was carried out mostly on silicon oxide [136]. It has been shown that keeping the film in 50 mM of APTES dissolved in toluene for 12 h at room temperature is sufficient to have successful grafting. Water in the reaction mixture plays an essential role in the silanization process. When the water quantity is too low, incomplete silane layer formed; however, too much water can lead to polymerization of silane producing multilayers [131,139,140]. Ethanol [141], toluene [142], methanol [143], are among the solvents used in liquid silanization. Ethanol has high capacity to dissolve water, so it can be ideal in liquid silanization to have well covered SnO_2. Thus, it could be ideal to carry out the silanization in hydrous solution. The reaction at room temperature and the ease of controlling the reaction parameters are the advantages of liquid silanization. In gas sensor application it is essential to have very dense layer of silane to inhibit the direct interaction of gases with substrate which can change the response. The interaction of gases with the surface of Conductometric gas sensors can increase or decrease the conductance of metal oxide film. Thus the effect of substrate (SnO_2) and the attached organic film could be opposite. In this case, the sensor response could be reduced or annulled by the compensation of two interactions.

1.8.2.5. Vapor phase silanization

Vapor phase deposition of silane is another way of functionalization. It was first reported by Haller in 1978 [144]. He carried out the silanization by APTES on silicon and gallium arsenide in vapor phase. Vapor silanization is very interesting because it decreases the polymerization of APTES molecules and lead to monolayer formation [145]. This high-quality film of APTES is

needed for many applications like biosensors [126]. It is achieved by exposing the metal oxide to APTES vapor for several hours in closed system at temperature between 50 and 120 °C. This process is generally accomplished in dry atmosphere to prevent the polymerization of APTES. However, to start the reaction, water is essential to reduce the ethoxy groups to hydroxyl. Chidsey et al. [146] investigated a new method to add very little and controlled amount of water molecules to the reaction process from the dehydration of $MgSO_4 \cdot 7H_2O$. Actually, the miss of experience of many chemists with gas-phase reaction, limits the use of vapor silanization.

In this thesis, the functionalization of thick SnO_2 film by APTES in vapor and liquid phases will be studied. The effect of synthesis parameters will be investigated in liquid phase silanization. APTES modified films will be conserved as a reactive substrate for further modifications.

1.8.2.6. Functionalization of APTES modified SnO_2 by organic functional groups

The interesting point of molecularly functionalized materials is the large number of chemical and structural modifications available. The modifications with organic functional groups having different polarities could change the sensor response to specific gases depending on their polarity [147]. These interactions could be dipole-dipole, induced dipole or diffusion between the molecular layers. Many parameters can be adapted in functionalization like chain length, backbone conformation, end functional groups (electron donating/withdrawing groups). It can be carried out starting with APTES combined with acyl chloride molecules bearing alkyl, benzene, acid, or ester functional groups (Figure 1-12). These devices were tested under some aliphatic alcohol and alkanes molecules. The functionalized field effect transistors have shown responses to a wide variety of volatile organic compounds like alcohols and alkanes etc. (see Figure 1-13). The electrostatic field of the molecular layer can generate charge carriers in the silicon field effect transistor interface. Adsorption of volatile organic compounds (VOCs) on the molecular layer can take place in two types: first type is the adsorption on the surface of the molecular layer, and the second type is the diffusion between the molecular layers. For the first type, the interactions could be dipole-dipole or induced dipole. If the tested gas and the end functional group of the molecular layer are polar the interactions are called dipole-dipole, while if one of them is non-polar, in this case the interaction is named induced dipole [59,147]. When VOCs adsorb on the molecular layer's surface, they are attached to the functional groups on the surface.

Thus, the attachment of gases on the molecular layer's surface is controlled by the properties of surface functional groups. For example, alkyl and benzene functional groups are electron donating groups. In this case, the gas negative pole bonds to the functionalized molecular layer's surface. Under these situations, the dipole moment orientation of the adsorbed VOCs is similar to the molecular layer. As a result, adsorption of gases induces change in the molecular layer's dipole moment. Furthermore, the changes in the dipole moment of the functionalized film lead to change in the electrical properties. Moreover, the type of molecular functional groups on the surface also controls the diffusion of VOCs in the molecular layer. For example, ester functional group has methyl groups at the end. In this case, the steric hindrance prevents the diffusion of VOCs in the molecular layer.

Functionalized silicon nanowire field effect transistors have exhibited response to various VOCs. However, these field effect transistor sensors still lack of selectivity. These effects could be very interesting when they are applied on SnO_2 gas sensor.

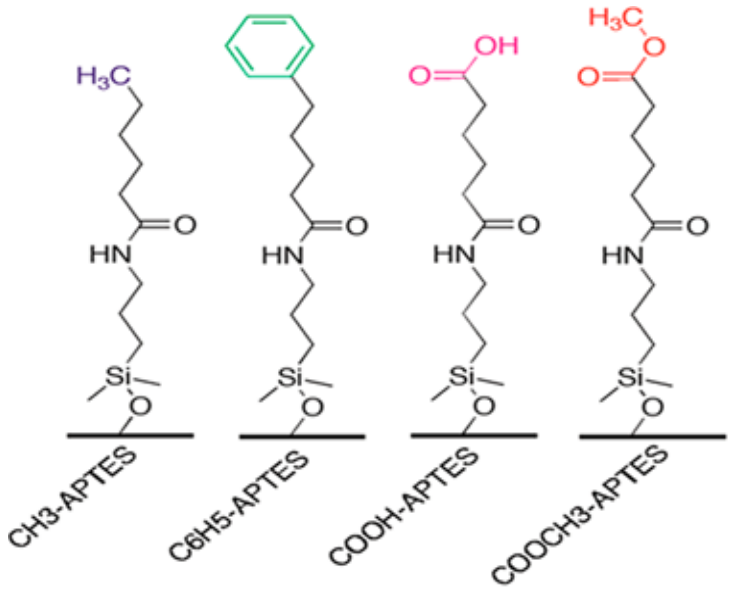

Figure 1-12. Schematic illustration of APTES layer modified with different functional groups [147].

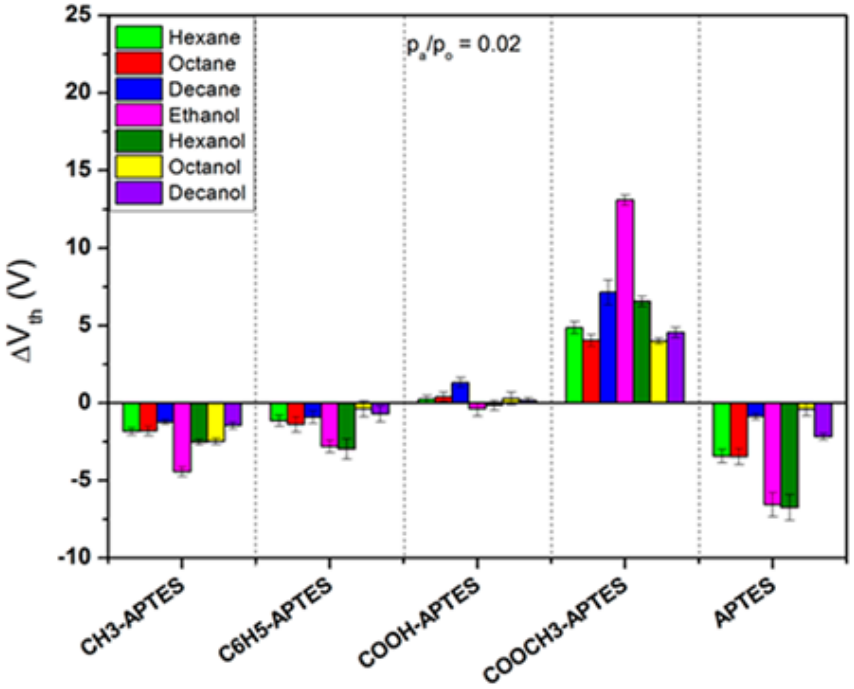

Figure 1-13. The sensor response of APTES modified silicon nanowire field effect transistors, with and without modifications by various functional groups upon exposure to different gases at p_a/p_o = 0.02, (where p_a and p_o are the VOC's partial pressure and vapor pressure at a given temperature, respectively). ΔV_{th} is the threshold voltage [147].

The principal advantage offered by organic materials is the promise for better chemical specificity. The organic–SnO_2 gas sensors could be expected to exhibit a specific response to a particular gas. Ichiro Matsubara et al. [148] have reported an organically hybridized SnO_2 gas sensors. The functionalization was carried out by attaching aminosilane film first. Second, these amines groups react with another molecule which contains carboxylic acid for coupling reaction. Normally, the reaction between amine group and carboxylic acid is carried out in presence of coupling reagent like 1-ethyl-3-(3-dimethylaminopropyl)-carbodiimide. In addition, these molecules can be ended with either benzene, dimethyl benzene, or dihydroxyl benzene as shown in Figure 1-14.

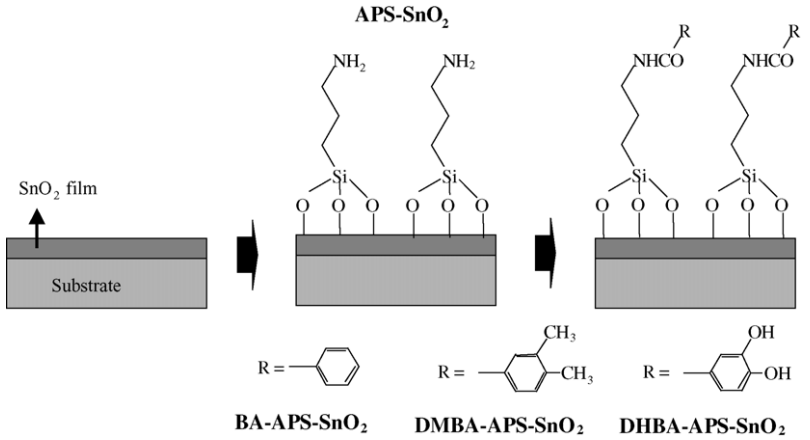

Figure 1-14. Schematic illustrating the organically hybridized SnO_2 thin film sensors [148].

The electrical characterization was done by measuring the change in resistance of the modified surface upon exposure to reducing gas (CO, CH_4 and H_2) at 150 °C. The response of BA–APS–SnO_2 and DMBA–APS–SnO_2 samples to these gases was the same as unmodified SnO_2. DHBA–APS–SnO_2 sample exhibits increasing in resistance upon exposure to CO gas, which is in opposite sense with respect to pure SnO_2 at temperature between 100 and 170 °C (Figure 1-15). This type of response is related to the interactions of CO gas with the grafted organic component. There are hydrogen bonds between the hydroxyl groups of organic layer and the SnO_2 surface. These hydrogen bonds results in decrease of the depth of space-charge region of SnO_2. As CO is a polar molecule, it can break these hydrogen bonds which in turn increase the resistance. The response of DHBA–APS–SnO_2 to H_2 gas was supposed to be related to typical oxidation reaction on the surface of SnO_2. Thus, the functionalized sensor with DHBA shows selectivity to CO gas with respect to other reducing gas. However, this sensor cannot be selective in the presence of oxidizing gases because the response will be in the same direction (decrease in resistance). In addition, the sensor detection limit to CO gas is very high (30000 ppm) and the operating temperature is relatively elevated for organically modified sensor.

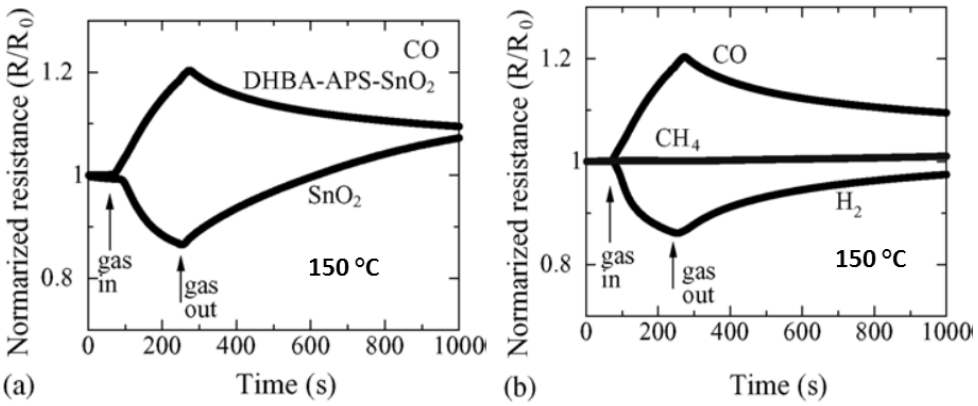

Figure 1-15. The response curves of (a) DHBA–APS–SnO_2 and SnO_2 sensors to 3 vol.% CO balanced with air at 150 °C and (b) DHBA–APS–SnO_2 sensor to 3 vol.% H_2, CO, and CH_4 balanced with air at 150 °C [148].

1.9. Conclusions

As a result of this bibliographic study, gas sensors can be used for the detection of many gases such as ammonia. Metal oxide materials have attracted the attention in gas sensors applications under atmospheric conditions due to their simplicity of use, large number of detectable gases and thus application fields, flexibility in production and low cost. Among many metal oxides, SnO_2 was chosen due to its unique physical and chemical properties such as large energy gap and environmental-friendliness. In addition, SnO_2 shows high sensitivity to many target compounds, but at high operating temperatures (300-500 °C, [149]) with very low selectivity. At low operating temperature, SnO_2 has very low sensitivity and selectivity to gases. Many techniques were developed for improving the selectivity of SnO_2, including the control of the sensor operating temperature, composite SnO_2, and organically material functionalization. High operating temperature needs high energy consumption, response can change with time, and SnO_2 is not sensitive to some gases also at high temperature. The chemically reactive surface of SnO_2 provides a powerful platform for modification with various organic molecular layers for the selective detection of gases. Molecular modifications of SnO_2 can be done by grafting organic groups or by conducting polymers. The most convenient way for grafting of organic function group is organosilane (e.g. APTES) using one or two reaction steps. The second step can be coupling reaction to introduce the desired functional group or to attach biological molecules. However, research on organically functionalized SnO_2-based sensors is still very limited and

efforts are still needed to develop such sensors. Furthermore, the silanization by APTES of SnO_2 thick film is poorly studied.

Our objective is the organic functionalization of SnO_2 to prepare sensitive sensor to low ammonia concentrations, with high selectivity. Up to our knowledge, an ambient temperature ammonia sensor based on molecular modification of SnO_2 has not been reported. Another objective is to reduce the power consumption by decreasing the operating temperature, since the sensor will be used later for smart devices and portable applications.

In the next work, SnO_2 sensitive layer will be functionalized with organic molecules to enhance the sensor performance to ammonia. This sensor should be operated at ambient temperature to prevent the organic layer from thermal degradation. It is important to investigate the consequences of working at ambient temperature with respect to the sensing mechanism of pure SnO_2 to compare it later with the modified one.

References

[1] L. Huang, Z. Wang, X. Zhu, L. Chi, Electrical gas sensors based on structured organic ultra-thin films and nanocrystals on solid state substrates, Nanoscale Horiz. 1 (2016) 383–393.

[2] K. Ihokura, J. Watson, The Stannic Oxide Gas Sensor Principles and Applications, CRC Press, 1994.

[3] D.E. Williams, Semiconducting oxides as gas-sensitive resistors, Sens. Actuators B Chem. 57 (1999) 1–16.

[4] N. Barsan, M. Schweizer-Berberich, W. Göpel, Fundamental and practical aspects in the design of nanoscaled SnO_2 gas sensors: a status report, Fresenius J. Anal. Chem. 365 (1999) 287–304.

[5] G. Korotcenkov, Gas response control through structural and chemical modification of metal oxide films: state of the art and approaches, Sens. Actuators B Chem. 107 (2005) 209–232.

[6] N. Barsan, D. Koziej, U. Weimar, Metal oxide-based gas sensor research: How to?, Sens. Actuators B Chem. 121 (2007) 18–35.

[7] W.H. Brattain, J. Bardeen, Surface Properties of Germanium, Bell Syst. Tech. J. 32 (1953) 1–41.

[8] G. Heiland, Zum Einfluß von adsorbiertem Sauerstoff auf die elektrische Leitfähigkeit von Zinkoxydkristallen, Z. Für Phys. 138 (1954) 459–464.

[9] T. Seiyama, S. Kagawa, Study on a Detector for Gaseous Components Using Semiconductive Thin Films., Anal. Chem. 38 (1966) 1069–1073.

[10] C. Wang, L. Yin, L. Zhang, D. Xiang, R. Gao, Metal Oxide Gas Sensors: Sensitivity and Influencing Factors, Sensors. 10 (2010) 2088–2106.

[11] G. Korotcenkov, B.K. Cho, Engineering approaches for the improvement of conductometric gas sensor parameters, Sens. Actuators B Chem. 188 (2013) 709–728.

[12] G. Korotcenkov, Metal oxides for solid-state gas sensors: What determines our choice?, Mater. Sci. Eng. B. 139 (2007) 1–23.

[13] A. Valleron, Etude et optimisation de capteurs de gaz a base de dioxyde d'etain en conditions d'une ligne d'echappement automobile, Thesis, Ecole Nationale Supérieure des Mines de Saint-Etienne, 2011.

[14] H. Gourari, M. Lumbreras, R. Van Landschoot, J. Schoonman, Elaboration and characterization of SnO_2–Mn_2O_3 thin layers prepared by electrostatic spray deposition, Sens. Actuators B Chem. 47 (1998) 189–193.

[15] I. K, Tin oxide gas sensor for deoxydising gases, New Mater New Sci Electrochem Technol. 43 (1981).

[16] N. Taguchi, A Metal Oxide Gas Sensor," Japanese Patent No.45-38200, 1962.

[17] T. Seiyama, N. Yamazoe, S. Yamauchi, Chemical Sensor Technology, Elsevier Science Ltd. 1, 2, 3, and 4 (1988).

[18] http://www.figarosens.com, http://www.fisinc.co.jp, http://www.appliedsensors.com, http://www.citytech.com, http://www.microchem.com.

[19] R.I. Masel, Principles of Adsorption and Reaction on Solid Surfaces, John Wiley & Sons, 1996.

[20] N. Barsan, U. Weimar, Conduction Model of Metal Oxide Gas Sensors, J. Electroceramics. 7 (2001) 143–167.

[21] M.E. Franke, T.J. Koplin, U. Simon, Metal and Metal Oxide Nanoparticles in Chemiresistors: Does the Nanoscale Matter?, Small. 2 (2006) 36–50.

[22] A. Vergara, E. Llobet, Sensor Selection and Chemo-Sensory Optimization: Toward an Adaptable Chemo-Sensory System, Front. Neuroengineering. 4 (2012) 19.

[23] J.F. Boyle, K.A. Jones, The effects of CO, water vapor and surface temperature on the conductivity of a SnO_2 gas sensor, J. Electron. Mater. 6 (1977) 717–733.

[24] S. Emiroglu, N. Barsan, U. Weimar, V. Hoffmann, In situ diffuse reflectance infrared spectroscopy study of CO adsorption on SnO_2, Thin Solid Films. 391 (2001) 176–185.

[25] M. Henzler, W. Göpel, Oberflächenphysik des Festkörpers, (1994).

[26] F. Hernandez-Ramirez, S. Barth, A. Tarancon, O. Casals, E. Pellicer, J. Rodriguez, A. Romano-Rodriguez, J. Morante, S. Mathur, Water vapor detection with individual tin oxide nanowires, Nanotechnology. 18 (2007) 424016.

[27] M.A. Barteau, Site requirements of reactions on oxide surfaces, J. Vac. Sci. Technol. A. 11 (1993) 2162–2168.

[28] B. Gillot, J.-F. Ferriot, G. Dupré, A. Rousset, Study of the oxidation kinetics of finely-divided magnetites. II - Influence of chromium substitution, Mater. Res. Bull. 11 (1976) 843–849.

[29] Q. Kuang, C. Lao, Z.L. Wang, Z. Xie, L. Zheng, High-Sensitivity Humidity Sensor Based on a Single SnO2 Nanowire, J. Am. Chem. Soc. 129 (2007) 6070–6071.

[30] M. Li, L.J. Qiao, W.Y. Chu, A.A. Volinsky, Water pre-adsorption effect on room temperature SnO_2 nanobelt ethanol sensitivity in oxygen-deficient conditions, Sens. Actuators B Chem. 158 (2011) 340–344.

[31] G. HEILAND, D. KOHL, Physical and Chemical Aspects of Oxidic Semiconductor Gas Sensors A2 - SEIYAMA, Tetsuro, in: Chem. Sens. Technol., Elsevier, Amsterdam, 1988: pp. 15–38.

[32] S.R. Morrison, The Chemical Physics of Surfaces, 2 edn, Plenum Press, New York, New York, 1990.

[33] V. Henrich, P. Cox, The Surface Science of Metal Oxides, Cambridge University, N. Y. (1994).

[34] A. Valleron, C. Pijolat, J.-P. Viricelle, P. Breuil, J.-C. Marchand, S. Ott, M. Pardo, G. Sberveglieri, Exhaust Gas Sensor Based On Tin Dioxide For Automotive Application, in: AIP, (2009) 450–451.

[35] G. Tournier, C. Pijolat, Selective filter for SnO_2-based gas sensor: application to hydrogen trace detection, Sens. Actuators B Chem. 106 (2005) 553–562.

[36] B.-Y. Wei, M.-C. Hsu, P.-G. Su, H.-M. Lin, R.-J. Wu, H.-J. Lai, A novel SnO_2 gas sensor doped with carbon nanotubes operating at room temperature, Sens. Actuators B Chem. 101 (2004) 81–89.

[37] E. Comini, G. Faglia, G. Sberveglieri, UV light activation of tin oxide thin films for NO_2 sensing at low temperatures, Sens. Actuators B Chem. 78 (2001) 73–77.

[38] Conducting Polymer Gas Sensors, Sens. Actuators. 20 (1989) 287–292.

[39] P.N. Bartlett, S.K. Ling-Chung, Conducting polymer gas sensors Part III: Results for four different polymers and five different vapours, Sens. Actuators. 20 (1989) 287–292.

[40] A.A. Athawale, S.V. Bhagwat, P.P. Katre, Nanocomposite of Pd–polyaniline as a selective methanol sensor, Sens. Actuators B Chem. 114 (2006) 263–267.

[41] A.Z. Sadek, W. Wlodarski, K. Shin, R.B. Kaner, K. Kalantar-zadeh, A polyaniline/WO_3 nanofiber composite-based ZnO/64° YX $LiNbO_3$ SAW hydrogen gas sensor, Synth. Met. 158 (2008) 29–32.

[42] G.D. Khuspe, M.A. Chougule, S.T. Navale, S.A. Pawar, V.B. Patil, Camphor sulfonic acid doped polyaniline-tin oxide hybrid nanocomposites: Synthesis, structural, morphological, optical and electrical transport properties, Ceram. Int. 40 (2014) 4267–4276.

[43] J. Yun, S. Jeon, H.-I. Kim, Improvement of NO gas sensing properties of polyaniline/MWCNT composite by photocatalytic effect of TiO_2, J. Nanomater. 2013 (2013) 3.

[44] N.G. Deshpande, Y.G. Gudage, R. Sharma, J.C. Vyas, J.B. Kim, Y.P. Lee, Studies on tin oxide-intercalated polyaniline nanocomposite for ammonia gas sensing applications, Sens. Actuators B Chem. 138 (2009) 76–84.

[45] H. Bai, G. Shi, Gas sensors based on conducting polymers, Sensors. 7 (2007) 267–307.

[46] B. Lakard, S. Carquigny, O. Segut, T. Patois, S. Lakard, Gas Sensors Based on Electrodeposited Polymers, Metals. 5 (2015) 1371–1386.

[47] C.V. Tuan, M.A. Tuan, N.V. Hieu, T. Trung, Electrochemical synthesis of polyaniline nanowires on Pt interdigitated microelectrode for room temperature NH_3 gas sensor application, Curr. Appl. Phys. 12 (2012) 1011–1016.

[48] A.Z. Sadek, W. Wlodarski, K. Kalantar-Zadeh, C. Baker, R.B. Kaner, Doped and dedoped polyaniline nanofiber based conductometric hydrogen gas sensors, Sens. Actuators Phys. 139 (2007) 53–57.

[49] D.S. Dhawale, R.R. Salunkhe, U.M. Patil, K.V. Gurav, A.M. More, C.D. Lokhande, Room temperature liquefied petroleum gas (LPG) sensor based on p-polyaniline/n-TiO_2 heterojunction, Sens. Actuators B Chem. 134 (2008) 988–992.

[50] H.-S. Li, M. Josowicz, D.R. Baer, M.H. Engelhard, J. Janata, Preparation and Characterization of Polyaniline-Palladium Composite Films, J. Electrochem. Soc. 142 (1995) 798–805.

[51] L. Kumar, I. Rawal, A. Kaur, S. Annapoorni, Flexible room temperature ammonia sensor based on polyaniline, Sens. Actuators B Chem. 240 (2017) 408–416.

[52] J.H. Yu, G.M. Choi, Selective CO gas detection of CuO-and ZnO-doped SnO_2 gas sensor, Sens. Actuators B Chem. 75 (2001) 56–61.

[53] D.H. Yoon, J.H. Yu, G.M. Choi, CO gas sensing properties of ZnO–CuO composite, Sens. Actuators B Chem. 46 (1998) 15–23.

[54] M. Soliman Selim, Room temperature sensitivity of (SnO_2–ZrO_2) sol–gel thin films, Sens. Actuators Phys. 84 (2000) 76–80.

[55] N.G. Patel, P.D. Patel, V.S. Vaishnav, Indium tin oxide (ITO) thin film gas sensor for detection of methanol at room temperature, Sens. Actuators B Chem. 96 (2003) 180–189.

[56] A.V. Tadeev, G. Delabouglise, M. Labeau, Influence of Pd and Pt additives on the microstructural and electrical properties of SnO_2-based sensors, Mater. Sci. Eng. B. 57 (1998) 76–83.

[57] A. Chaparadza, S.B. Rananavare, Room temperature Cl_2 sensing using thick nanoporous films of Sb-doped SnO_2, Nanotechnology. 19 (2008) 245501.

[58] C. Di Natale, R. Paolesse, E. Martinelli, R. Capuano, Solid-state gas sensors for breath analysis: A review, Anal. Chim. Acta. 824 (2014) 1–17.

[59] B. Wang, J.C. Cancilla, J.S. Torrecilla, H. Haick, Artificial Sensing Intelligence with Silicon Nanowires for Ultraselective Detection in the Gas Phase, Nano Lett. 14 (2014) 933–938.

[60] N. Shehada, J.C. Cancilla, J.S. Torrecilla, E.S. Pariente, G. Brönstrup, S. Christiansen, D.W. Johnson, M. Leja, M.P.A. Davies, O. Liran, N. Peled, H. Haick, Silicon Nanowire Sensors Enable Diagnosis of Patients via Exhaled Breath, ACS Nano. 10 (2016) 7047–7057.

[61] N. Shehada, G. Brönstrup, K. Funka, S. Christiansen, M. Leja, H. Haick, Ultrasensitive Silicon Nanowire for Real-World Gas Sensing: Noninvasive Diagnosis of Cancer from Breath Volatolome, Nano Lett. 15 (2015) 1288–1295.

[62] M. Barreto, M.P. Villa, C. Olita, S. Martella, G. Ciabattoni, P. Montuschi, 8-Isoprostane in Exhaled Breath Condensate and Exercise-Induced Bronchoconstriction in Asthmatic Children and Adolescents, Chest. 135 (2009) 66–73.

[63] P. Montuschi, P.J. Barnes, G. Ciabattoni, Measurement of 8-Isoprostane in Exhaled Breath Condensate, in: D. Armstrong (Ed.), Adv. Protoc. Oxidative Stress II, Humana Press, Totowa, NJ, 2010: pp. 73–84.

[64] T. Mathew, P. Pownraj, S. Abdulla, B. Pullithadathil, Technologies for Clinical Diagnosis Using Expired Human Breath Analysis, Diagnostics. 5 (2015) 27–60.

[65] S. Capone, A. Forleo, L. Francioso, R. Rella, P. Siciliano, J. Spadavecchia, D.S. Presicce, A.M. Taurino, Solid state gas sensors: state of the art and future activities, J. Optoelectron. Adv. Mater. 5 (2003) 1335–1348.

[66] S. DuBois, S. Eng, R. Bhattacharya, S. Rulyak, T. Hubbard, D. Putnam, D.J. Kearney, Breath Ammonia Testing for Diagnosis of Hepatic Encephalopathy, Dig. Dis. Sci. 50 (2005) 1780–1784.

[67] A.T. Güntner, M. Righettoni, S.E. Pratsinis, Selective sensing of NH_3 by Si-doped α-MoO_3 for breath analysis, Sens. Actuators B Chem. 223 (2016) 266–273.

[68] Mineral Commodities Summaries, 2015.

[69] G. Sberveglieri, Recent developments in semiconducting thin-film gas sensors, Sens. Actuators B Chem. 23 (1995) 103–109.

[70] H.-P. Hübner, S. Drost, Tin oxide gas sensors: an analytical comparison of gas-sensitive and non-gas-sensitive thin films, Sens. Actuators B Chem. 4 (1991) 463–466.

[71] N. Van Hieu, L.T.B. Thuy, N.D. Chien, Highly sensitive thin film NH_3 gas sensor operating at room temperature based on SnO_2/MWCNTs composite, Sens. Actuators B Chem. 129 (2008) 888–895.

[72] S.B. Kondawar, S.P. Agrawal, S.H. Nimkar, H.J. Sharma, P.T. Patil, Conductive polyaniline-tin oxide nanocomposites for ammonia sensor, Adv. Mater. Lett. 3 (2012).

[73] S. Choudhury, C.A. Betty, K.G. Girija, S.K. Kulshreshtha, Room temperature gas sensitivity of ultrathin SnO_2 films prepared from Langmuir-Blodgett film precursors, Appl. Phys. Lett. 89 (2006) 071914.

[74] K. Khun Khun, A. Mahajan, R.K. Bedi, SnO_2 thick films for room temperature gas sensing applications, J. Appl. Phys. 106 (2009) 124509.

[75] C.A. Betty, S. Choudhury, K.G. Girija, Discerning specific gas sensing at room temperature by ultrathin SnO_2 films using impedance approach, Sens. Actuators B Chem. 173 (2012) 781–788.

[76] A. Ghosh, Y. Gudage, R. Sharma, R. Mane, S. Han, Room temperature ammonium gas sensing behavior of upright-standing ZnO nano-sheets, Sens. Transducers. 98 (2008) 1–5.

[77] D.R. Patil, L.A. Patil, P.P. Patil, Cr_2O_3-activated ZnO thick film resistors for ammonia gas sensing operable at room temperature, Sens. Actuators B Chem. 126 (2007) 368–374.

[78] X. Li, X. Li, Z. Li, J. Wang, J. Zhang, WS_2 nanoflakes based selective ammonia sensors at room temperature, Sens. Actuators B Chem. 240 (2017) 273–277.

[79] S. Sen, K.P. Muthe, N. Joshi, S.C. Gadkari, S.K. Gupta, Jagannath, M. Roy, S.K. Deshpande, J.V. Yakhmi, Room temperature operating ammonia sensor based on tellurium thin films, Sens. Actuators B Chem. 98 (2004) 154–159.

[80] K. Khun Khun, A. Mahajan, R.K. Bedi, Nanostructured Sb doped SnO_2 thick films for room temperature NH_3 sensing, Chem. Phys. Lett. 492 (2010) 119–122.

[81] N. Duc Hoa, N. Van Quy, Y. Suk Cho, D. Kim, Nanocomposite of SWNTs and SnO_2 fabricated by soldering process for ammonia gas sensor application, Phys. Status Solidi A. 204 (2007) 1820–1824.

[82] G.D. Khuspe, S.T. Navale, D.K. Bandgar, R.D. Sakhare, M.A. Chougule, V.B. Patil, SnO_2 nanoparticles-modified polyaniline films as highly selective, sensitive, reproducible and stable ammonia sensors, Electron. Mater. Lett. 10 (2014) 191–197.

[83] S.G. Pawar, M.A. Chougule, S.L. Patil, B.T. Raut, P.R. Godse, S. Sen, V.B. Patil, Room Temperature Ammonia Gas Sensor Based on Polyaniline-TiO_2 Nanocomposite, IEEE Sens. J. 11 (2011) 3417–3423.

[84] S.G. Pawar, S.L. Patil, M.A. Chougule, B.T. Raut, P.R. Godase, R.N. Mulik, S. Sen, V.B. Patil, New Method for Fabrication of CSA Doped PANi- TiO_2 Thin-Film Ammonia Sensor, IEEE Sens. J. 11 (2011) 2980–2985.

[85] G.D. Khuspe, S.T. Navale, M.A. Chougule, V.B. Patil, Ammonia gas sensing properties of CSA doped PANi-SnO_2 nanohybrid thin films, Synth. Met. 185–186 (2013) 1–8.

[86] J. Sun, X. Shu, Y. Tian, Z. Tong, S. Bai, R. Luo, D. Li, C.C. Liu, Facile preparation of polypyrrole-reduced graphene oxide hybrid for enhancing NH_3 sensing at room temperature, Sens. Actuators B Chem. 241 (2017) 658–664.

[87] Q.T. Tran, H.T.M. Hoa, D.-H. Yoo, T.V. Cuong, S.H. Hur, J.S. Chung, E.J. Kim, P.A. Kohl, Reduced graphene oxide as an over-coating layer on silver nanostructures for detecting NH_3 gas at room temperature, Sens. Actuators B Chem. 194 (2014) 45–50.

[88] P.-G. Su, L.-Y. Yang, NH_3 gas sensor based on Pd/SnO_2/RGO ternary composite operated at room-temperature, Sens. Actuators B Chem. 223 (2016) 202–208.

[89] A. Forleo, L. Francioso, S. Capone, F. Casino, P. Siciliano, O. Tan, H. Hui, Wafer-level fabrication and gas sensing properties of miniaturized gas sensors based on inductively coupled plasma deposited tin oxide nanorods, Procedia Chem. 1 (2009) 196–199.

[90] A. Forleo, L. Francioso, S. Capone, F. Casino, P. Siciliano, O.K. Tan, H. Hui, Fabrication at wafer level of miniaturized gas sensors based on SnO_2 nanorods deposited by PECVD and gas sensing characteristics, EUROSENSORS XXIII. 154 (2011) 283–287.

[91] N.L. Hung, E.S. Ahn, H.C. Jung, H.J. Kim, D.J. Kim, Synthesis and gas sensing properties of ZnO nanostructures, J. Korean Phys. Soc. 57 (2010) 1784–1788.

[92] D. Biskupski, B. Herbig, G. Schottner, R. Moos, Nanosized titania derived from a novel sol–gel process for ammonia gas sensor applications, Sens. Actuators B Chem. 153 (2011) 329–334.

[93] P. Clifford, D. Tuma, Characteristics of semiconductor gas sensors II. Transient response to temperature change, Sens. Actuators. 3 (1982) 255–281.

[94] M.S. Wagh, G.H. Jain, D.R. Patil, S.A. Patil, L.A. Patil, Modified zinc oxide thick film resistors as NH_3 gas sensor, Sens. Actuators B Chem. 115 (2006) 128–133.

[95] F. Shao, M.W.G. Hoffmann, J.D. Prades, J.R. Morante, N. López, F. Hernández-Ramírez, Interaction Mechanisms of Ammonia and Tin Oxide: A Combined Analysis Using Single Nanowire Devices and DFT Calculations, J. Phys. Chem. C. 117 (2013) 3520–3526.

[96] L. Wang, H. Huang, S. Xiao, D. Cai, Y. Liu, B. Liu, D. Wang, C. Wang, H. Li, Y. Wang, Q. Li, T. Wang, Enhanced Sensitivity and Stability of Room-Temperature NH3 Sensors Using Core–Shell CeO_2 Nanoparticles@Cross-linked PANI with p–n Heterojunctions, ACS Appl. Mater. Interfaces. 6 (2014) 14131–14140.

[97] R. Moos, A Brief Overview on Automotive Exhaust Gas Sensors Based on Electroceramics, Int. J. Appl. Ceram. Technol. 2 (2005) 401–413. doi:10.1111/j.1744-7402.2005.02041.x.

[98] S. Tian, X. Ding, D. Zeng, J. Wu, S. Zhang, C. Xie, A low temperature gas sensor based on Pd-functionalized mesoporous SnO_2 fibers for detecting trace formaldehyde, RSC Adv. 3 (2013) 11823.

[99] A. Cabot, J. Arbiol, J.R. Morante, U. Weimar, N. Barsan, W. Göpel, Analysis of the noble metal catalytic additives introduced by impregnation of as obtained SnO_2 sol–gel nanocrystals for gas sensors, Sens. Actuators B Chem. 70 (2000) 87–100.

[100] D.D. Trung, N.D. Hoa, P.V. Tong, N.V. Duy, T.D. Dao, H.V. Chung, T. Nagao, N.V. Hieu, Effective decoration of Pd nanoparticles on the surface of SnO_2 nanowires for enhancement of CO gas-sensing performance, J. Hazard. Mater. 265 (2014) 124–132.

[101] W. Zeng, T. Liu, Z. Wang, Enhanced gas sensing properties by SnO_2 nanosphere functionalized TiO_2 nanobelts, J. Mater. Chem. 22 (2012) 3544.

[102] N. Van Hieu, H.-R. Kim, B.-K. Ju, J.-H. Lee, Enhanced performance of SnO_2 nanowires ethanol sensor by functionalizing with La_2O_3, Sens. Actuators B Chem. 133 (2008) 228–234.

[103] L. Geng, Y. Zhao, X. Huang, S. Wang, S. Zhang, S. Wu, Characterization and gas sensitivity study of polyaniline/SnO_2 hybrid material prepared by hydrothermal route, Sens. Actuators B Chem. 120 (2007) 568–572.

[104] S. Nardis, D. Monti, C.D. Natale, A. D'Amico, P. Siciliano, A. Forleo, M. Epifani, A. Taurino, R. Rella, R. Paolesse, Preparation and characterization of cobalt porphyrin modified tin dioxide films for sensor applications, 17th Euopean Conf. Solid-State Transducers Univ. Minho Guimares Port. Sept. 21-24 2003. 103 (2004) 339–343.

[105] X. Ma, M. Wang, G. Li, H. Chen, R. Bai, Preparation of polyaniline–TiO_2 composite film with in situ polymerization approach and its gas-sensitivity at room temperature, Mater. Chem. Phys. 98 (2006) 241–247.

[106] W.-S. Huang, B. D, D.H. and A. G, MacDiarmid, Polyaniline, a Novel Conducting Polymer Morphology and Chemistry of its Oxidation and Reduction in Aqueous Electrolytes, J Chem SOC. 82 (1986) 2385–2400.

[107] A. Joshi, D.K. Aswal, S.K. Gupta, J.V. Yakhmi, S.A. Gangal, ZnO-nanowires modified polypyrrole films as highly selective and sensitive chlorine sensors, Appl. Phys. Lett. 94 (2009) 103115.

[108] S. Wang, Y. Kang, L. Wang, H. Zhang, Y. Wang, Y. Wang, Organic/inorganic hybrid sensors: A review, Sens. Actuators B Chem. 182 (2013) 467–481.

[109] A.Z. Sadek, W. Wlodarski, K. Shin, R.B. Kaner, K. Kalantar-Zadeh, A Room Temperature Polyaniline/SnO_2 Nanofiber Composite Based Layered ZnO/64Â° YX $LiNbO_3$ SAW Hydrogen Gas Sensor, in: Optoelectron. Microelectron. Mater. Devices 2006 Conf. On, IEEE, 2006: pp. 208–211.

[110] C. Murugan, E. Subramanian, D.P. Padiyan, Enhanced sensor functionality of in situ synthesized polyaniline–SnO_2 hybrids toward benzene and toluene vapors, Sens. Actuators B Chem. 205 (2014) 74–81.

[111] G.D. Khuspe, S.T. Navale, M.A. Chougule, S. Sen, G.L. Agawane, J.H. Kim, V.B. Patil, Facile method of synthesis of polyaniline-SnO_2 hybrid nanocomposites: Microstructural, optical and electrical transport properties, Synth. Met. 178 (2013) 1–9.

[112] C. Li, Y. Wang, M. Wan, S. Li, Rectifying effect of soluble polyaniline films, Synth. Met. 39 (1990) 91–96.

[113] R. Helmy, A.Y. Fadeev, Self-assembled monolayers supported on TiO_2: comparison of $C_{18}H_{37}SiX_3$ (X= H, Cl, OCH_3), $C_{18}H_{37}Si$ (CH_3) 2Cl, and $C_{18}H_{37}PO$ $(OH)_2$, Langmuir. 18 (2002) 8924–8928.

[114] S.P. Pujari, L. Scheres, A.T.M. Marcelis, H. Zuilhof, Covalent Surface Modification of Oxide Surfaces, Angew. Chem. Int. Ed. 53 (2014) 6322–6356.

[115] V. Stambouli, M. Labeau, I. Matko, B. Chenevier, O. Renault, C. Guiducci, P. Chaudouët, H. Roussel, D. Nibkin, E. Dupuis, Development and functionalisation of Sb doped SnO_2 thin films for DNA biochip applications, Sens. Actuators B Chem. 113 (2006) 1025–1033.

[116] X. Wang, Y. Chen, K.A. Gibney, S. Erramilli, P. Mohanty, Silicon-based nanochannel glucose sensor, Appl. Phys. Lett. 92 (2008) 013903.

[117] Y. Chen, X. Wang, S. Erramilli, P. Mohanty, A. Kalinowski, Silicon-based nanoelectronic field-effect pH sensor with local gate control, Appl. Phys. Lett. 89 (2006) 223512–223512.

[118] M. Lin, C. Chu, L. Tsai, H. Lin, C.-S. Wu, Y. Wu, Y. Wu, D.-B. Shieh, Y. Su, C. Chen, Control and detection of organosilane polarization on nanowire field-effect transistors, Nano Lett. 7 (2007) 3656–3661.

[119] Y. Engel, R. Elnathan, A. Pevzner, G. Davidi, E. Flaxer, F. Patolsky, Supersensitive detection of explosives by silicon nanowire arrays, Angew. Chem. Int. Ed. 49 (2010) 6830–6835.

[120] R.G. Acres, A.V. Ellis, J. Alvino, C.E. Lenahan, D.A. Khodakov, G.F. Metha, G.G. Andersson, Molecular Structure of 3-Aminopropyltriethoxysilane Layers Formed on Silanol-Terminated Silicon Surfaces, J. Phys. Chem. C. 116 (2012) 6289–6297.

[121] P. Serre, C. Ternon, V. Stambouli, P. Periwal, T. Baron, Fabrication of silicon nanowire networks for biological sensing, Sens. Actuators B Chem. 182 (2013) 390–395.

[122] V. Stambouli, A. Zebda, E. Appert, C. Guiducci, M. Labeau, J.-P. Diard, B. Le Gorrec, N. Brack, P.J. Pigram, Semiconductor oxide based electrodes for the label-free electrical detection of DNA hybridization: Comparison between Sb doped SnO_2 and $CdIn_2O_4$, Electrochimica Acta. 51 (2006) 5206–5214.

[123] M. Ben Haddada, J. Blanchard, S. Casale, J.-M. Krafft, A. Vallée, C. Méthivier, S. Boujday, Optimizing the immobilization of gold nanoparticles on functionalized silicon surfaces: amine- vs thiol-terminated silane, Gold Bull. 46 (2013) 335–341.

[124] N. Herzer, S. Hoeppener, U.S. Schubert, Fabrication of patterned silane based self-assembled monolayers by photolithography and surface reactions on silicon-oxide substrates, Chem. Commun. 46 (2010) 5634.

[125] A. Ulman, Formation and structure of self-assembled monolayers, Chem. Rev. 96 (1996) 1533–1554.

[126] M. Le, C. Jimenez, E. Chainet, V. Stambouli, A Label-Free Impedimetric DNA Sensor Based on a Nanoporous SnO_2 Film: Fabrication and Detection Performance, Sensors. 15 (2015) 10686–10704.

[127] B.M. Silverman, K.A. Wieghaus, J. Schwartz, Comparative Properties of Siloxane vs Phosphonate Monolayers on A Key Titanium Alloy, Langmuir. 21 (2005) 225–228.

[128] J. Sagiv, Organized monolayers by adsorption. 1. Formation and structure of oleophobic mixed monolayers on solid surfaces, J. Am. Chem. Soc. 102 (1980) 92–98.

[129] S.R. Wasserman, G.M. Whitesides, I.M. Tidswell, B.M. Ocko, P.S. Pershan, J.D. Axe, The structure of self-assembled monolayers of alkylsiloxanes on silicon: a comparison of results from ellipsometry and low-angle x-ray reflectivity, J. Am. Chem. Soc. 111 (1989) 5852–5861.

[130] J. Ohlhausen, K. Zavadil, Time-of-flight secondary ion mass spectrometry measurements of a fluorocarbon-based self-assembled monolayer on Si, J. Vac. Sci. Technol. A. 24 (2006) 1172–1178.

[131] A.Y. Fadeev, T.J. McCarthy, Trialkylsilane Monolayers Covalently Attached to Silicon Surfaces: Wettability Studies Indicating that Molecular Topography Contributes to Contact Angle Hysteresis, Langmuir. 15 (1999) 3759–3766.

[132] J. Tiller, P. Berlin, D. Klemm, A novel efficient enzyme-immobilization reaction on NH_2 polymers by means of L-ascorbic acid, Biotechnol. Appl. Biochem. 30 (1999) 155–162.

[133] S. Onclin, B.J. Ravoo, D.N. Reinhoudt, Engineering silicon oxide surfaces using Self-Assembled monolayers, Angew. Chem. Int. Ed. 44 (2005) 6282–6304.

[134] S.D. Cook, K.A. Thomas, J.F. Kay, M. Jarcho, Hydroxyapatite-coated titanium for orthopedic implant applications., Clin. Orthop. 232 (1988) 225–243.

[135] L. Cecchetto, A. Denoyelle, D. Delabouglise, J.-P. Petit, A silane pre-treatment for improving corrosion resistance performances of emeraldine base-coated aluminium samples in neutral environment, Appl. Surf. Sci. 254 (2008) 1736–1743.

[136] N. Aissaoui, L. Bergaoui, J. Landoulsi, J.-F. Lambert, S. Boujday, Silane Layers on Silicon Surfaces: Mechanism of Interaction, Stability, and Influence on Protein Adsorption, Langmuir. 28 (2012) 656–665.

[137] F. Zhang, K. Sautter, A.M. Larsen, D.A. Findley, R.C. Davis, H. Samha, M.R. Linford, Chemical Vapor Deposition of Three Aminosilanes on Silicon Dioxide: Surface Characterization, Stability, Effects of Silane Concentration, and Cyanine Dye Adsorption, Langmuir. 26 (2010) 14648–14654.

[138] J.A. Howarter, J.P. Youngblood, Optimization of Silica Silanization by 3-Aminopropyltriethoxysilane, Langmuir. 22 (2006) 11142–11147.

[139] K. Wen, R. Maoz, H. Cohen, J. Sagiv, A. Gibaud, A. Desert, B.M. Ocko, Postassembly Chemical Modification of a Highly Ordered Organosilane Multilayer: New Insights into the Structure, Bonding, and Dynamics of Self-Assembling Silane Monolayers, ACS Nano. 2 (2008) 579–599.

[140] J. Gun, J. Sagiv, On the formation and structure of self-assembling monolayers: III. Time of formation, solvent retention, and release, J. Colloid Interface Sci. 112 (1986) 457–472.

[141] A. Zebda, M. Labeau, J.-P. Diard, V. Lavalley, V. Stambouli, Electrical resistivity dependence of semi-conductive oxide electrode on the label-free electrochemical detection of DNA, Sens. Actuators B Chem. 144 (2010) 176–182.

[142] G. Tan, L. Zhang, C. Ning, X. Liu, J. Liao, Preparation and characterization of APTES films on modification titanium by SAMs, Thin Solid Films. 519 (2011) 4997–5001.

[143] A.R. Morrill, D.T. Duong, S.J. Lee, M. Moskovits, Imaging 3-aminopropyltriethoxysilane self-assembled monolayers on nanostructured titania and tin (IV) oxide nanowires using colloidal silver nanoparticles, Chem. Phys. Lett. 473 (2009) 116–119.

[144] I. Haller, Covalently attached organic monolayers on semiconductor surfaces, J. Am. Chem. Soc. 100 (1978) 8050–8055.

[145] J.-R. Li, J.C. Garno, Elucidating the role of surface hydrolysis in preparing organosilane nanostructures via particle lithography, Nano Lett. 8 (2008) 1916–1922.

[146] R.D. Lowe, M.A. Pellow, T.D.P. Stack, C.E.D. Chidsey, Deposition of Dense Siloxane Monolayers from Water and Trimethoxyorganosilane Vapor, Langmuir. 27 (2011) 9928–9935.

[147] B. Wang, H. Haick, Effect of Functional Groups on the Sensing Properties of Silicon Nanowires toward Volatile Compounds, ACS Appl. Mater. Interfaces. 5 (2013) 2289–2299.

[148] I. Matsubara, K. Hosono, N. Murayama, W. Shin, N. Izu, Organically hybridized SnO_2 gas sensors, Sens. Actuators B Chem. 108 (2005) 143–147.

[149] N. Dufour, Y. Veyrac, P. Menini, F. Blanc, C. Talhi, B. Franc, C. Ganibal, C. Wartelle, K. Aguir, Increasing the sensitivity and selectivity of metal oxide gas sensors by controlling the sensitive layer polarization, Sens. IEEE, (2012) 1–4.

Chapter 2. **Materials and methods**

2.1. Introduction

This chapter will focus on the methods of fabrication and characterization of organically functionalized SnO_2 sensitive layer. The synthesis of the desired sensors is carried out by deposition of SnO_2 film on alumina substrate followed by molecular functionalization. The deposited SnO_2 film will be organically functionalized in two steps. The first step is the silanization by APTES. As shown before, APTES can be deposited using vapor or liquid phases. The second step is the functionalization of APTES modified SnO_2 by molecules bearing different end functional groups. For these syntheses, it is essential to be sure that the functionalization on SnO_2 film is well achieved. Hence, the different characterization techniques used and their principle will be presented in this chapter. Finally the parameters of the electrical characterization under gases will be described.

2.2. Sensor fabrication

It is essential to know the different parts of conductometric gas sensors to study their performances. A typical metal oxide gas sensor is composed of sensitive layer, which can be made of SnO_2, ZnO, etc. in form of thin film, thick film, nanowire, or pellet. It can be deposited over a substrate such as alumina (Al_2O_3), glass ceramics, flexible, and silicon substrates. The sensitive layer is connected with gold electrodes in order to measure its electrical characteristics. Heating the sensors is needed to favor the interactions of the target compound with the sensitive film. For that, the sensor can be self-heated by attaching a platinum resistor on the other side of the substrate or by an external heater. Such device generally operates in air in presence of humidity and target gases. The most important part is the sensing film composition. Moreover, the particles size and the thickness of the sensing layer play important role in sensing behavior. SnO_2 thick film is generally deposited on a substrate by screen printing or inkjet technologies. For all the sensors used in this work, thick SnO_2 film was deposited on alumina substrate by screen printing. Thus, SnO_2 ink is needed for printing it in this process.

2.2.1. Ink preparation

SnO_2 ink should have acceptable rheological characteristics such as the viscosity and the ratio of solvent to powder. The optimized ink composition was reported before in our laboratory by Jean-Paul Viricelle et al. [1]. This ink was prepared by grinding 4 g of SnO_2 (Prolabo Company, sieved at 200 µm) with mortar and pestle for 5 min, and added to 1.7 g of organic binder (ESL® V400A) and then stirred with 25 drops of organic solvent (ESL® 404). The ink was homogenized 3 times (90:30 µm; 30:10 µm; 15:5 µm) by three roll mill EXAKT 80E/120E machine.

2.2.2. Deposition of sensing element

The sensor elements except the gold electrodes attached to SnO_2 which are made by sputtering, are deposited by screen printing technique. Screen printing has advantages over other deposition techniques such as low cost, and ease of use. In general, screen printing is a simple and an automated manufacturing technique which allows the production of very porous and robust chemical sensors with a good reproducibility. The thickness of the film can be adjusted by controlling the distance between screen and substrate or by deposition of several layers. In addition, screen printing permits to produce many sensors at the same time.

In this work, a semi-automatic screen printer (Aurel Model C890) was used. Thick-film screen made from a woven mesh of polymer is mounted under tension on a stainless steel frame. The mounted screen has open-mesh areas through which the desired pattern can be printed. The screen is held in position within a screen-printing machine (screen holder) at a distance of 0.3 mm from the surface of the substrate. The paste (ink) is poured onto the top surface of the stencil, and a rubber squeegee traverses the screen under pressure. This action brings the screen in contact with the substrate and forces the ink through the open areas. The demanded pattern is thus deposited onto the substrate as shown in Figure 2-1.

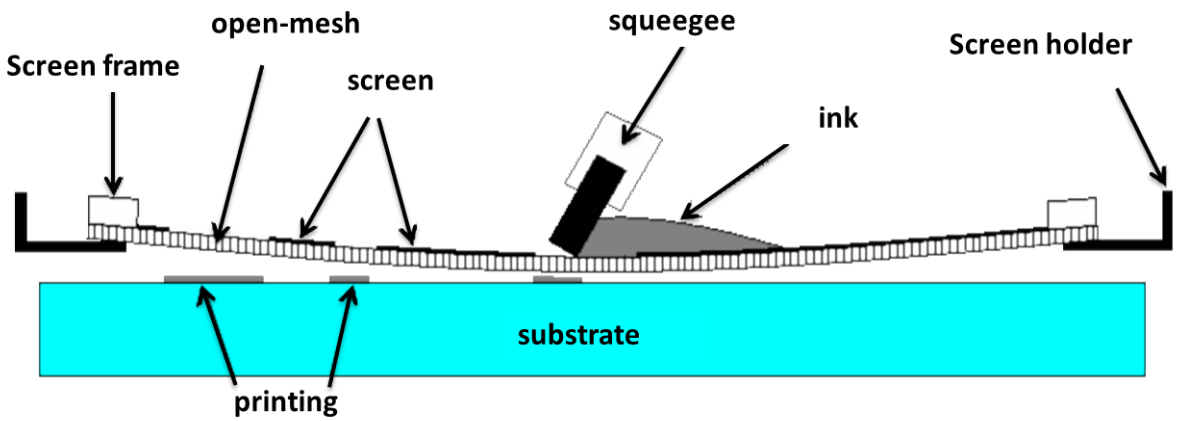

Figure 2-1. Schematic representation of screen printing technique [2].

For each sensor element a specific ink, annealing temperature and screen were used. These different parts with its properties are presented in Table 2-1. For the synthesis of the used sensors, Pt-resistor to heat the sensitive layer was printed on the heating side of alumina substrate (Al_2O_3, purity of 96%). On the two faces of Al_2O_3 substrate, screen printed gold electrodes were deposited as shown in Figure 2-2. A dielectric film was deposited on Pt-heater to prevent the interactions of Pt with gases. Finally, two successfully screen printed layers of SnO_2 are deposited on sputtered gold electrodes which are in turn (~0.6 µm thickness and 1 mm distance between the electrodes) deposited by sputtering on Al_2O_3 substrate (sensing side). Each screen printed element was dried in an oven (MEMMERT UM/SM 100) to evaporate the solvent and annealed in muffle furnace (Thermolyne furnace 48000) to remove the organic binder according to Table 2-1. This furnace allows controlling the ramp (10 °C/min) and the dwell temperature and time (700 °C, 10 h for SnO_2). The image of fabricated sensor is shown in Figure 2-2.

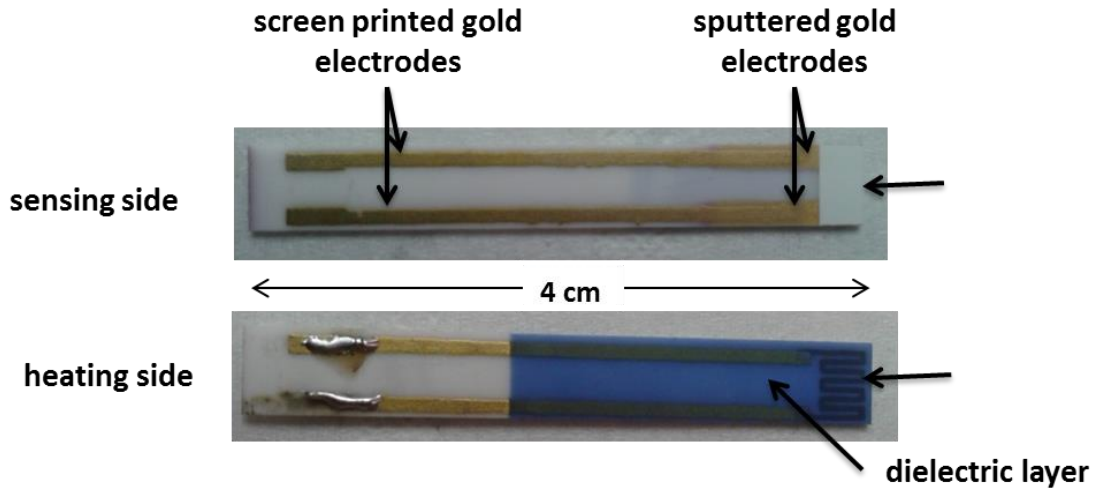

Figure 2-2. The two sides of SnO_2 sensor elaborated by screen printing.

Table 2-1. Different sensor elements deposition parameters.

Screen printed element	Ink	Drying	Annealing	Screen mesh count (threads per square inch)
Platinum heater	ESL 5545	100 °C, 10 min	980 °C, 1 h	325
Gold electrodes	ESL 8880-G	100 °C, 10 min	850 °C, 1 h	-
Dielectric film	ESL 4917	100 °C, 10 min	850 °C, 1 h	180
Sensitive film (SnO_2)	As-prepared	100 °C, 10 min	700 °C, 10 h	180

2.2.3. Surface modification of SnO_2 sensor by APTES molecule

In this work, the silanization of SnO_2 by APTES was performed in vapor and liquid phases. The presence of hydroxyl group at the surface of SnO_2 is essential to allow the condensation reaction with the hydroxyl groups of APTES. Thus, the first step is the creation of hydroxyl groups on SnO_2 surface followed by reaction with APTES in vapor or liquid phases. The silanization leads to the formation of APTES film on SnO_2 terminated with amine groups as shown in figure Figure 2-3. Vapor phase deposition was carried out at LMGP laboratory of Grenoble with standard synthesis parameters. Liquid phase deposition was developed at the Ecole des Mines of Saint Etienne by investigating the effects of silanization parameters.

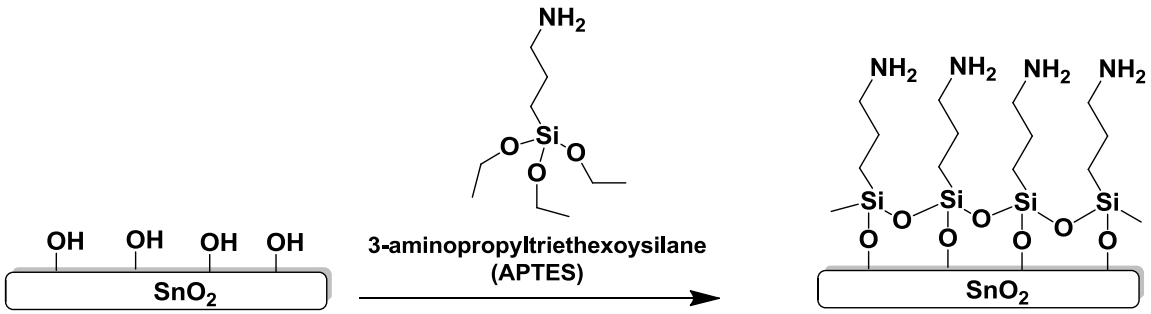

Figure 2-3. Theoretical schematic representation of the silanization process.

2.2.3.1. Vapor phase silanization

The silanization of SnO_2 film by 3-aminopropyltriethoxysilane (Acros-Organics) in vapor phase has been described elsewhere [3]. First, the SnO_2 films were immersed for 5 min in acetone, ethanol and distilled water successively to remove contaminants, and then dried under argon gas. Second, films were treated by air/oxygen plasma (air/O_2 pressure =0.4 torr, homemade machine) for 4 min to clean the sample surface from residual impurities and to create hydroxyl groups at the surface of SnO_2. Third, the SnO_2 sample and APTES (liquid) were placed side by side in a Teflon holder as shown in Figure 2-4. The installation of SnO_2 samples and 150 µL of APTES was conducted in a dry atmosphere to avoid the humidity in the Teflon holder. Then, the Teflon pot was sealed and heated for 1 h at 80 °C. After 1 h silanization, the samples were rinsed with absolute ethanol. Finally, the films were annealed at 110 °C for 1 h to eliminate water trapped in the deposited APTES layer.

Figure 2-4. Installation of the SnO_2 samples and APTES solution in the Teflon pot.

2.2.3.2. Liquid phase silanization

The creation of hydroxyl groups on SnO_2 surface was achieved by heating the film at 500 °C in humid atmosphere (around 70 %RH at 20 °C) for 1 h. Subsequently, the SnO_2 films were dipped in solution of APTES under stirring as presented in Figure 2-5. The liquid phase grafting of APTES has to take into account the influence of three main parameters: anhydrous or hydrous APTES solution, APTES concentration, and reaction time. All the solutions in different liquid synthesis procedures were prepared in absolute ethanol. The silanization was performed by immersing the SnO_2 films in the APTES solution, without or with water (5vol %H_2O), with three different APTES concentrations (1, 50 or 500 mM) at room temperature and for various durations: 5 min, 30 min, 4 h, and 5 h. After silanization, the films were rinsed with absolute ethanol, dried with N_2 and annealed at 110 °C for 1 h. The optimized silanization procedures (discussed in the next chapter) will be applied to synthesize SnO_2-APTES sensor for the next step of functionalization.

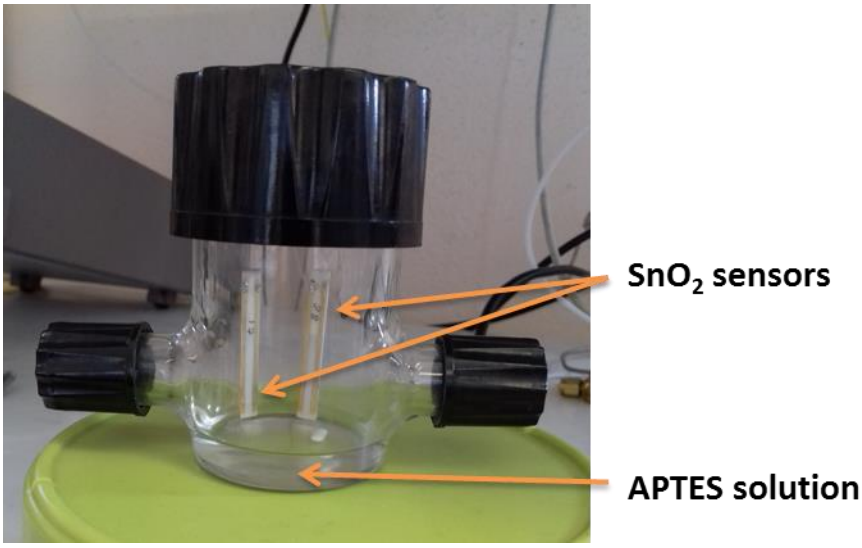

Figure 2-5. Photograph of the experimental setup of sensors in liquid phase silanization process.

2.2.4. Modification of APTES by functional groups

The produced SnO_2-APTES film acts as an intermediate step for further modification. The next step of functionalization is the reaction of amine groups of APTES with acyl chloride (acid chloride). Acyl chloride is a reactive group regarding the reaction with amine which leads to the

formation of amide bond. This reaction is known as Schotten-Baumann reaction [4]. Schotten-Baumann reaction leads to productions of one equivalent acid. This acid protonates the unreacted amine groups of APTES which lead to the formation of salt and reduce the reaction yield. The addition of triethylamine base is to neutralize this acid and pushes the reaction forward the formation of amide. In our case, acyl chloride molecule contains alkyl, acid or ester end functional groups on the other side. The main advantage of this reaction is that the end functional group is conserved after the reaction. A schematic illustration of the second step functionalization is reported in Figure 2-6.

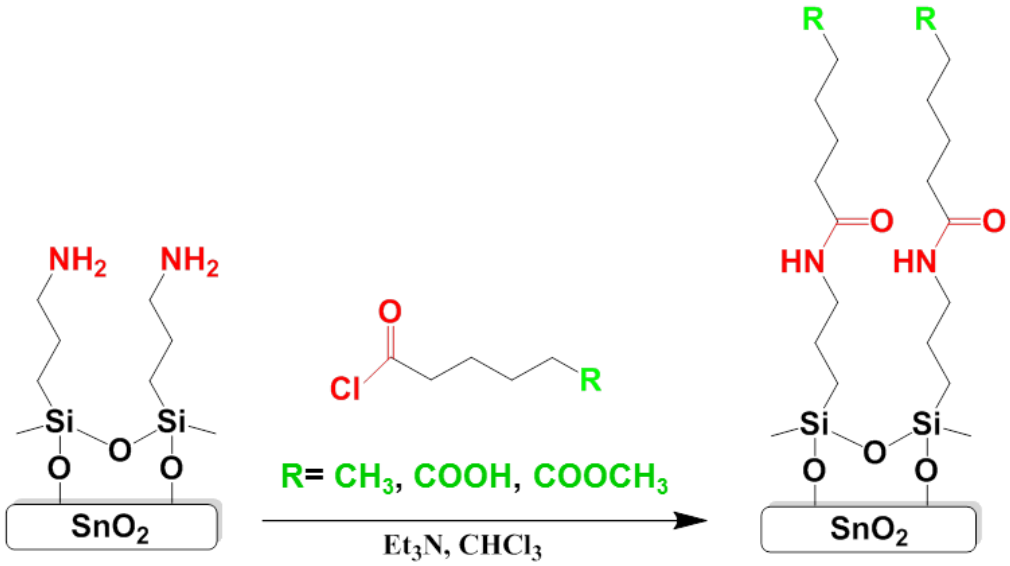

Figure 2-6. Schematic illustration of SnO_2-APTES-ester, SnO_2-APTES-acid, and SnO_2-APTES-alkyl synthesis steps.

Practically, the SnO_2-APTES sensors were immersed in a solution containing an acyl chloride product with 5 µL of triethylamine (Fluka) in 10 mL of chloroform as solvent. The different acyl chloride concentrations are 10 mM of hexanoyl chloride (98%, ALDRICH, alkyl: $C_6H_{11}ClO$), 50 mM of 1,4-butanedicarbonyl chloride (98%, Fluka, acid: $C_6H_8Cl_2O_2$), or 10 mM of methyl adipoyl chloride (96%, Alfa Aesar, ester: $C_7H_{11}ClO_3$). These different solutions were kept for 12 h under stirring. This reaction was carried out in a setup as shown in Figure 2-5. The sensors were then rinsed with chloroform and dried under N_2 flow (sensors: SnO_2-APTES-alkyl, SnO_2-APTES-acid and SnO_2-APTES-ester). This step of SnO_2 sensors functionalization leads to covalent attachment of alkyl, acid and ester end functional groups.

2.3. Methods of characterization

Pure and functionalized SnO_2 films have been characterized by different physico-chemical analytical techniques, namely Scanning Electron Microscopy (SEM), X-ray diffraction (XRD), Total Attenuated Reflectance Fourier Transform Spectroscopy (ATR-FTIR), and X-ray Photoelectron Spectroscopy (XPS). An indirect method was also used to investigate the presence of APTES molecules on SnO_2 surface by measuring the contact angles. Alexa Fluor fluorescent molecules and citrated gold nanoparticles have also been implemented to test the reactivity of APTES film on SnO_2. Electrical characterizations under gases were carried out to test the effect of functionalization on the sensors performance.

2.3.1. Scanning Electron Microscopy

The scanning electron microscopy (SEM) technique was used to characterize the morphology of elaborated SnO_2 thick films and the APTES modified SnO_2 after deposition of gold nanoparticles. This technique mainly exploits the detection of the emitted secondary electrons from the surface excited by electron beam. The emitted secondary electrons give information about the topology and the composition of the analyzed specimen. SEM observations were carried out at the LMGP laboratory in Grenoble by XL30 microscope (Philips, Eindhoven, Netherlands).

2.3.2. X-ray diffraction

X-ray diffraction allows to determine the atomic arrangement and the interatomic distances in the crystal lattices and to estimate the average particle size. XRD was used in this study to determine the average size particle of SnO_2 film. For that, Siemens D5000 Diffractometer having X-ray tube with anticathode of copper was used. The machine is of configuration $\theta/2\theta$. The diffracted X-ray was detected by an AR monochromator detector.

2.3.3. Attenuated Total Reflection-Fourier Transform Infrared Spectroscopy

Infrared Spectroscopy is a very useful tool for characterization, since it provides information about the composition and the structure of materials. In addition, FTIR has high sensitivity, high resolution and quickness of measurement.
Basically, an IR spectrometer is composed of source, monochromator and receptor. Normally, if the vibrational frequency of the molecule equals the frequency of the electromagnetic radiation, absorption can take place. As an approximation, the larger the strength of the bond the higher the frequency of its original vibration. Furthermore, the higher the masses of the atoms attached to the bond the lower the wavenumber of the original vibration. In general, the band intensity is proportional to the number of groups and the polarity of the bonds.

The domain of the infrared (IR) electromagnetic spectrum can be divided into three regions according to wavelengths: far-IR between 10 and 400 cm^{-1}, mid-IR between 400 and 4000 cm^{-1}, and the near-IR between 4000 and 12500cm^{-1}. According to these regions, different phenomena are observed in IR spectroscopy. During the reflection of the incident beam, a part of this beam penetrates into the medium of the lower refraction index before undergoing reflection. This penetration causes an evanescent wave. This evanescent wave can interact with the studied molecule. During the penetration to the second medium, a part of the incident light can be absorbed by tested sample and therefore the reflected ray has less energy than the incident ray. In this case, it becomes possible to detect an absorption spectrum. It is one of the techniques of infrared spectroscopy that has evolved mostly in recent years.

Recently, the most used IR technique to characterize the solid surfaces is Attenuated Total Reflection (ATR). ATR requires a crystal where the sample to be analyzed is deposed on it. ATR is operated by measuring the changes that occur in a totally internally reflected infrared beam, when the beam comes in contact with a sample. An infrared beam is focused to an optically dense crystal (diamond, Ge, ZnSe, etc.) with a high refractive index at a certain angle. In this case, it is possible to generate an evanescent wave that extends beyond the surface of the crystal into the sample held in contact with the crystal as shown in Figure 2-7. This evanescent wave protrudes between 0.5 μm and 5 μm beyond the crystal surface and into the sample. The quality of the contact between the crystal and the sample plays an important role in the quality of the spectrum: bad contact could reduce the total attenuated reflection and leads to irregular baselines and to the

observation of few vibrational bands [5]. In our case, diamond crystal was used with 1 mm × 1 mm in size which allows making good contact between the sample to be analyzed and the diamond. The evanescent wave will be attenuated or altered in regions of the infrared spectrum where the sample absorbs energy. The attenuated energy from each evanescent wave is reflected back to the IR beam, which then exits the opposite end of the diamond and is passed to the detector in the IR spectrometer. The system then can generate an infrared spectrum.

The spectra presented in this study were collected in the region of the middle infrared. This region corresponds on the one hand to the spectral fingerprints of the functional groups constituting the grafted molecules on the surface, and on the other hand to the transparency ranges of the ATR diamond crystal. ATR-spectra were recorded using a Golden Gate Diamond VERTEX 70 (Germany) spectrometer from Bruker with a DTGS detector operated at 4 cm^{-1} resolution in Saint Etienne (Figure 2-8). 64 scans were collected in each run. Absorbance mode was used for the collection of all spectra.

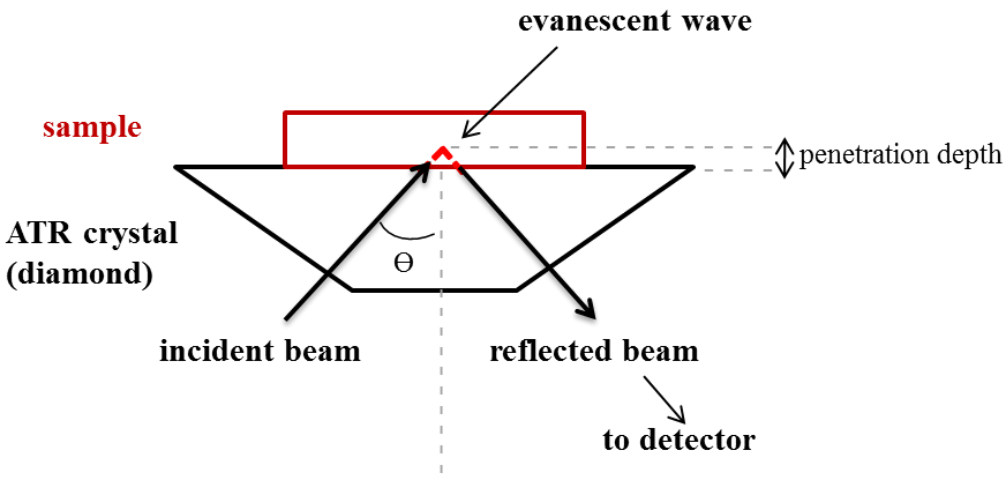

Figure 2-7. Schematic representation of ATR-FTIR detection principle [6].

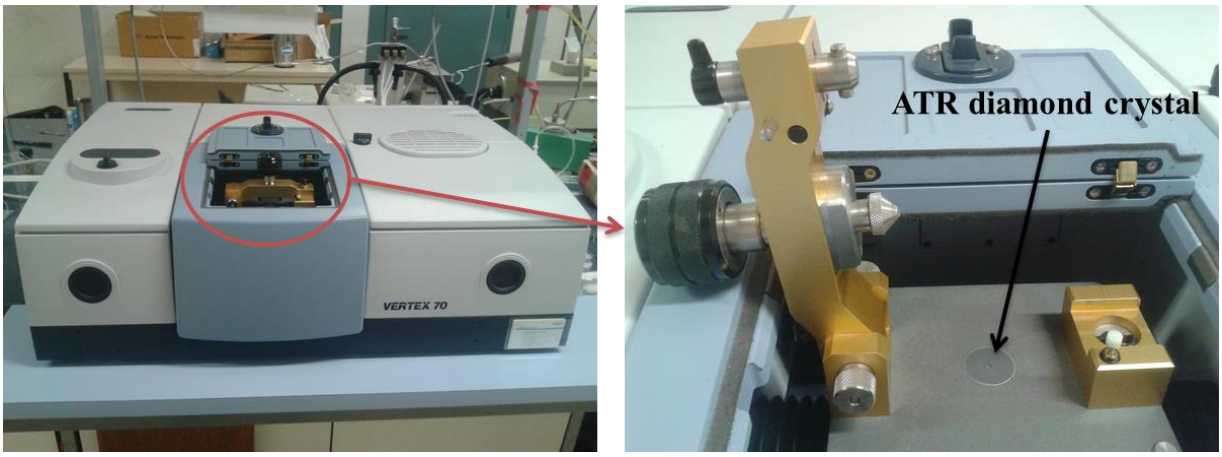

Figure 2-8. ATR-FTIR machine VERTEX 70 with diamond crystal.

In this thesis, IR technique will be used for the characterization of the functionalized sensors by APTES and other functional groups. As mentioned before, APTES grafting can be carried out in vapor or liquid phase. It will be essential to be sure that the functionalization is well achieved before testing the sensors under gas. In addition, IR analysis will be used to compare the vapor and liquid silanization as well as the effect of synthesis parameters on the nature of the APTES film in liquid phase.

2.3.4. X-ray Photoelectron Spectroscopy

2.3.4.1. Working principle

X-ray Photoelectron Spectroscopy (XPS) or Electron Spectroscopy for Chemical Analysis (ESCA) is extensively used to examine the chemical composition of material surfaces. XPS was developed in 1960 by Kai Siegbahn and his research group [7]. It can analyze surface of a material over a depth ranging from 3 nm to 10 nm. This method is non-destructive and applicable to all elements with high sensitivity except hydrogen and helium. The information obtained are the elemental chemical composition (with a detection threshold of the order of 0.3 atomic %) and the nature of the chemical forms of the elements present on the analyzed depth. Generally, the experiments are carried out at room temperature. XPS measurements are accomplished in ultra-high vacuum atmosphere (10^{-7} Pa) to avoid contamination of the sample and to prevent the interaction of gases with incident X-rays and emitted electrons. The photon source is an X-ray tube.

In XPS technique, the sample is irradiated with X-ray photons of energy hν causing the ionization of its atoms by photoelectric effect [8,9]. During the interaction of photons with the atom, part of their energy is used to eject photoelectron away from the atom. This part is the binding energy (BE). Any electron (core and valence) with a binding energy less than hν can be ejected into the vacuum with specific kinetic energy (KE). The measurement of the kinetic energy of the emitted photoelectrons makes it possible to determine their binding energy as shown in equations (20 and (21. Each atom has core electrons with the specific binding energy.

$$h\nu = BE + KE + \phi \tag{20}$$

$$BE = h\nu - KE - \phi \tag{21}$$

ϕ is the work function induced by the analyzer, it is generally constant about 4~5 eV.

The photoelectron is the electron which is emitted from the lowest energy levels (Figure 2-9a). When a core electron is removed, leaving vacancy, this is followed by an electronic rearrangement in which an electron with higher energy level (L_1 for example) occupies the vacant space on the inner layer. The released energy can be used for ejecting an Auger electron (Figure 2-9b).

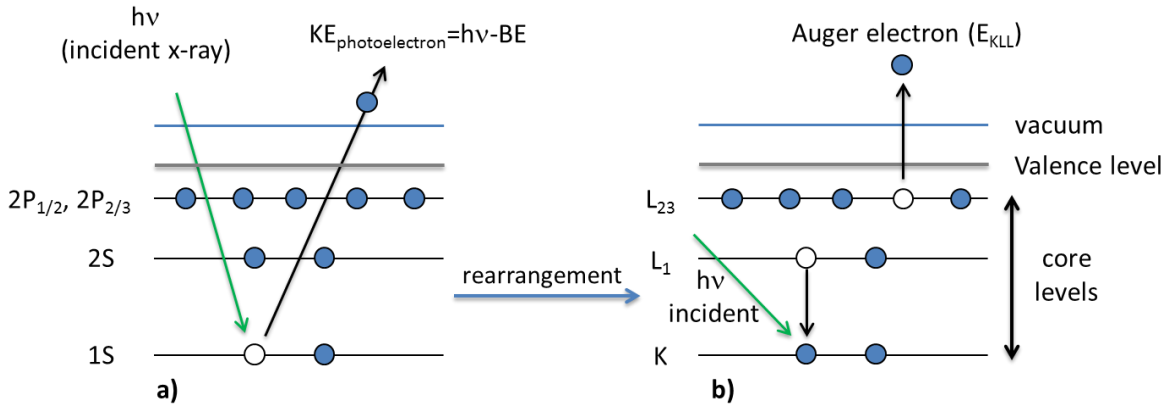

Figure 2-9. The diagram showing the process of photo-emission.

So, XPS counts electrons ejected from the surface of the sample when irradiated by X-rays. Its results are quantitative and qualitative in terms of peak intensities and positions. The peak position gives information about the elemental and chemical composition of material, while the peak intensity indicates the quantity of material on the surface. Chemical shift of each atom with respect to its environment can be obtained, so it is possible to distinguish the different chemical

bond on the surface [10]. Under these circumstances it will be possible to carry out qualitative and quantitative characterization of APTES after different silanization processes.

2.3.4.2. Quantitative analysis

The intensity of the detected photoelectron peak of an element A (I_A) can be written as shown in equation (32).

$$I_A = KT_A N_A \sigma_A \lambda_A^M \cos\theta \, k_A^M \tag{22}$$

with

K constant depending on instrumental factors and analysis conditions (K is the same for all elements during the analysis of a given specimen),

T_A the transmission function of the spectrometer at a kinetic energy corresponding to the photoelectron peak A,

N_A the atomic concentration per unit volume of the element x,

σ_A the photoionization cross section of the core level A,

λ_A^M the inelastic mean free path for an electron A in the matrix M.

θ the escape angle of photoelectrons with respect to the normal of the surface of the analyzed specimen, and

$k_A^M = \exp\left(-\frac{d_M}{\lambda_A^M \cos\theta}\right)$ the attenuation factor of an electron of A in the matrix M, for example the attenuation of Sn 4d peak by grafted APTES on the surface.

In the next chapter, this equation will be used to calculate the concentration of APTES molecules on SnO_2 after silanization.

2.3.4.3. Experimental procedures used

The analysis were performed with a Thermo VG Thetaprobe instrument with a focused monochromatic Al Kα source (hν=1486.7 eV, 400 µm spot size). Photoelectrons were analyzed using a concentric hemispherical analyzer operating in the constant ΔE mode. The energy scale was calibrated with sputter-cleaned pure reference samples of Au, Ag and Cu in order that the Au 4f7/2, Ag 3d5/2 and Cu 2p3/2 were positioned at a binding energies of respectively 84, 386.2 and 932.7 eV. Spectra were recorded in the binding energy range of 0–1200 eV with step size of 1 eV and pass energy of 300 eV for survey scans, step size of 0.1 eV and pass energy of 50 eV for narrow C 1s, O1s, N 1s, Si 2p, Sn 4d and Sn 3d scans. The two pass energies give energy resolution (width of the Ag 3d5/2 peak) measured on sputter clean silver samples of respectively 1 eV and 0.5 eV. During XPS experiments, charge compensation was achieved by irradiation of the sample with a system combining a diffuse beam of low energy electrons and low energy ions. Optimum charge compensation was achieved in order to have the narrower-shape of the tail at the low binding energy of Sn 3d peak. Analysis of the different components of C 1s, O 1s, N 1s and Si 2p photoelectron peaks were carried out using synthetic line shapes consisting of a convolution product of a Gaussian function with 30% of a lorentzian function. To study APTES thermal stability, SnO_2-APTES films were in-situ annealing at 200 °C, 300 °C, 400 °C and 500 °C, for 4 h in a preparation chamber connected to the spectrometer at a pressure of 5.10^{-9} mbar .

As a conclusion, the aims from XPS analysis are to carry out qualitative and quantitative characterization of the different functionalized films. Qualitative analysis comprises the detection of different characteristic APTES peaks and the shape of the film. However, quantitative analysis will deal with the thickness and the concentration of APTES on SnO_2. In addition, XPS will be used to study the thermal stability of the APTES deposited layer on SnO_2 under different operating temperature.

2.3.5. Contact angle measurements

The value of contact angle is a quantitative measurement using a drop of liquid (deionized water). It reflects the ability of a liquid to spread on a surface by wettability. The method consists in measuring the angle value formed by the intersection of the liquid-solid interface and the liquid-vapor interface (geometrically acquired by applying a tangent line from the contact point along

the liquid-vapor interface in the droplet profile) as shown in Figure 2-10. In practice, a drop of distilled water is deposited using a syringe on the surface of the film to be characterized. The measurement of the contact angle allows to characterize the wettability of a surface and to verify presence of an organic film deposited on the surface of metal oxide. By attaching the organic film on SnO_2, the contact angle is supposed to vary. The contact angle measurement was made at the LMGP laboratory in Grenoble using an optical instrument type Krüss equipped with a CCD camera connected to a graphic card that records the profile of the drop by contrast (Figure 2-11). The image processing software DSA10-Mk2 (Drop Shape Analysis system) makes possible to extract the contact angle of both sides from the recorded image.

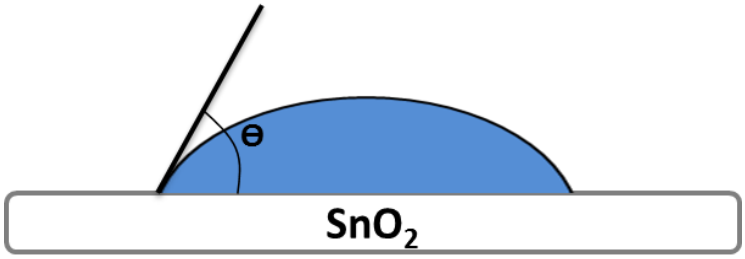

Figure 2-10. Schematic representation of contact angle measurement.

Figure 2-11. Krüss DSA10-Mk2 contact angle machine.

2.3.6. Physico-chemical modifications of APTES

2.3.6.1. Alexa Fluor fluorescent molecules

APTES modified SnO_2 films are used as intermediate step for further surface modifications. The chemical reactivity of APTES film with respect to coupling reactions was determined by using Alexa Fluor® 488 carboxylic acid, succinimidyl ester molecule ($\lambda_{exitation} = 488\,nm$). Alexa Fluor product was purchased from Life Technologies. These florescent molecules react specifically with the primary amines of APTES that lead eventually to florescence on SnO_2 film as shown in Figure 2-12. To study the feasibility of employing fluorescent molecules on APTES films, two SnO_2 samples, one with APTES (SnO_2-APTES) and the other without APTES, were immersed for one hour in a mixture of 4 µL of Alexa Fluor and 3 mL of solution of sodium carbonate and sodium bicarbonate, with pH =9, at room temperature. Afterwards, the samples were rinsed with absolute ethanol. Alexa Fluor molecules were detected by epifluorescence measurements using an BX41M optical microscope (Olympus, Tokyo, Japan), fitted with a 100 W mercury lamp, a cyanide Cy3 dichroic cube filter (excitation 550 nm, emission 580 nm) and a cooled Spot RT monochrome camera (Diagnostic, Sterling Heights, MI, USA). The intensity of film fluorescence was measured by Fluorescence Spectrometer (Tecan Infinite M1000) in order to determine qualitatively the APTES on the surface of SnO_2 film. The fluorescence intensity measurements were carried out at 494 nm as excitation wavelength and 517 nm emission wavelength with an integration time of 20 µs and a settle time of 10 ms.

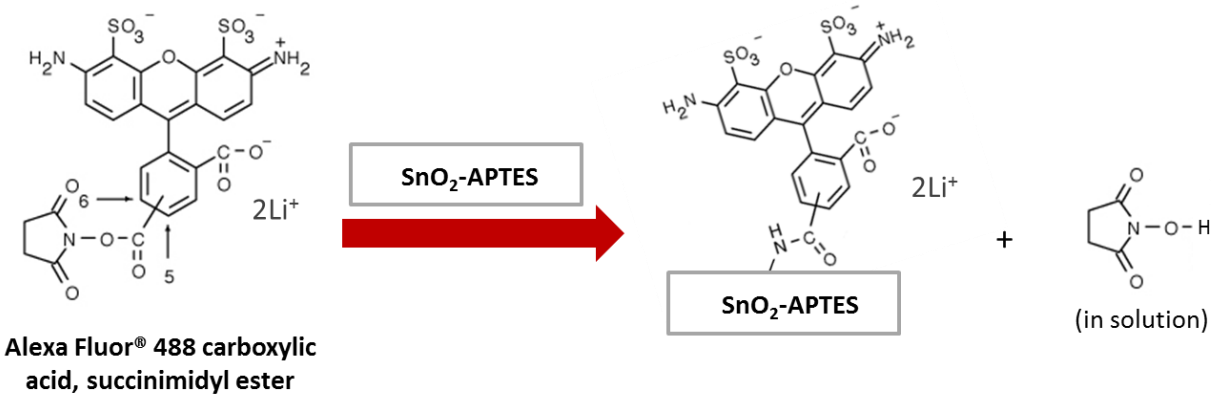

Figure 2-12. Schematic representation of SnO_2 modified Alexa Fluor® 488 carboxylic acid, succinimidyl ester.

2.3.6.2. Citrated gold nanoparticles

SnO_2-APTES was modified by 20 nm gold nanoparticles stabilized by citrate groups (Figure 2-13, fabricated by CEA Grenoble). These citrate groups are physisorbed on the surface of gold nanoparticles. The primary amine groups of APTES react with the citrate groups. This reaction leads to the physisorption of gold nanoparticles onto SnO_2-APTES. The reaction was carried out through dipping the two samples, with and without APTES modification, in suspension solution containing gold nanoparticles as shown in Figure 2-14. After 1.5 h reaction, the two samples were rinsed gently with distilled water.

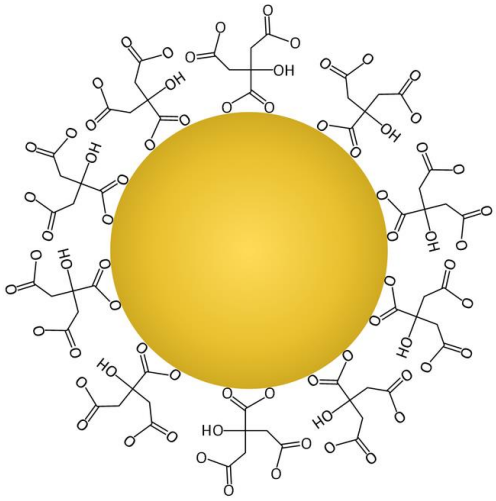

Figure 2-13. Citrated gold nanoparticle.

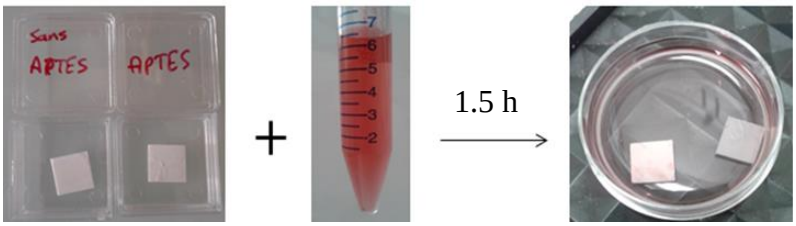

Figure 2-14. The functionalization steps of SnO_2-APTES by citrated gold nanoparticle.

2.3.7. Electrical characterizations

We have developed a home-made test bench at the "Ecole des Mines Saint-Etienne" as presented in Figure 2-15 to test the sensors under gases. In this test bench, two sensors are installed, each one is in an 80 cm^3 glass chamber under constant gas flow of 15 l/h. The test bench is provided with gas mass flow controllers (Brooks) which allows controlling the concentrations of different gases at same time by PC computer. LabVIEW program allows controlling the temperature of the sensors as well as the concentration of gases. In addition, the test bench is equipped with water bubbler to test the sensors under different relative humidity (RH) balanced with air at 20 °C. Thus, this system can generate a mixture of gases at different parameters like amount of oxygen, humidity, sensor temperature, and gases concentration. Conductance measurements were performed by electronic unit equipped with voltage divider circuit that permits measuring the conductance of the SnO_2 film as function of time or temperature. The most used technique for measuring the conductance of metal oxide film is voltage divider. It is a simple method to measure the conductance of surface as shown in Figure 2-16. In a simple electrical circuit, the fixed reference resistor (r) and the tested sensor (R) are connected in series with 1 volt generator (E). As the tested sensor and the reference resistor are connected in series so they have the same value of current. In this case, the current can be written as in equation (23) according to Ohm's law. This equation allows to calculate the resistance as in equation (24) of the tested sensor and of course its conductance (equation (25)). For example, with "r" equal 10 kΩ we can measure conductance values between 10^{-6} and 10^{-3} Ω^{-1}. This technique of measurement is included in the electronic card.

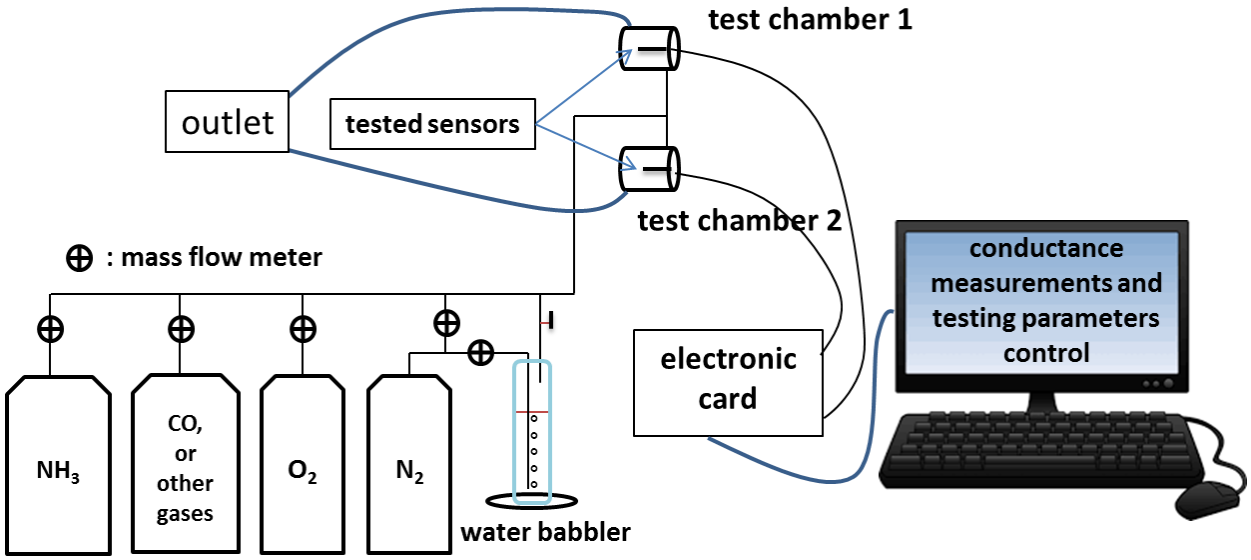

Figure 2-15. Schematic diagram of the homemade test bench.

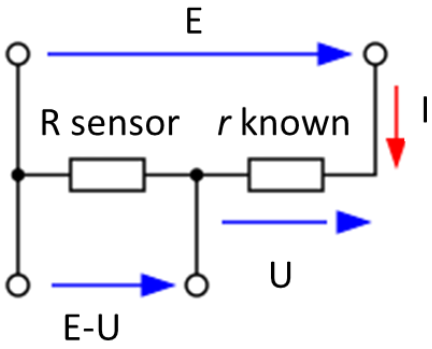

Figure 2-16. Schematic representation of voltage divider circuit. E= fixed measurement voltage, U = measured voltage, R= sensor resistor, r = fixed reference resistor.

$$I = \frac{(E - U)}{R} = \frac{U}{r} \tag{23}$$

$$R = \frac{(E - U)}{U} r \tag{24}$$

$$G = \frac{U}{(E - U) \times r} \tag{25}$$

Before injecting the target gas in the test chamber, the sensors were kept 10 h at 100 °C, and then stabilized under air flow for 5 h at 25 °C. Gas sensing properties were then measured to different concentrations of ammonia gas balanced with air with different relative humidities. The normalized conductance (G/G_0 where G_0 is the initial conductance measured under air with different RH without target gas, and G is the conductivity after 20 minutes of gas injection) is plotted to monitor the sensor response as well as to calculate the response and recovery time. In addition, the curve of relative response $(G-G_0)/G_0$ versus ammonia concentration was plotted for different sensors to compare their sensitivity. Sensors selectivity was tested versus ethanol, carbon monoxide and acetone gases.

2.4. Conclusion

We synthesized SnO_2 sensor starting from commercial SnO_2 powder. Thick film of SnO_2 was deposited by screen printing. Surface morphology, thickness and composition of the produced SnO_2 film can be characterized by SEM, ATR-FTIR, XPS etc. Unfortunately, this type of sensors previously studied in PTSI-SPIN center, has shown low selectivity to ammonia gas with respect to redox gases and has high operating temperature. Functionalization was carried out by APTES as an intermediate molecule for other modification steps to enhance the sensors performance regarding ammonia detection. Silanization was achieved in vapor and liquid phases. The effect of different liquid silanization parameters of the final APTES film will be investigated by various characterization techniques in the next chapter. Furthermore, the thermal stability of grafted APTES film on SnO_2 will be tested by XPS analysis. Finally, it will be possible to carry out the electrical characterizations under various conditions with the developed test bench.

References

[1] J.-P. Viricelle, B. Riviere, C. Pijolat, Optimization of SnO_2 screen-printing inks for gas sensor applications, Elecroceramics (2005) 2137–2140.

[2] Metal Silk Screen Company Manufacturing/Perrin Manufacturing. http://www.perrinmfg.com/metal-silk-screen-company-manufacturing.html.

[3] M. Le, C. Jimenez, E. Chainet, V. Stambouli, A Label-Free Impedimetric DNA Sensor Based on a Nanoporous SnO_2 Film: Fabrication and Detection Performance, Sensors. 15 (2015) 10686–10704.

[4] Z. Wang, Schotten-Baumann Reaction, in: Compr. Org. Name React. Reag., John Wiley & Sons, Inc., 2010.

[5] F.M. Mirabella, Principles, theory, and practice of internal reflection spectroscopy, Marcel Dekker: New York, 1993.

[6] M. Mani, Isolation and spectral characterization of the anti-viral compounds of Indian medical plant-Apium leptophyllum, (2015). http://www.tnuniv.ac.in/pdf/SMP%20-%2025%20PDF/3%20-%20M.%20Mani.pdf.

[7] K. Siegbahn, Et. Al.,Nova Acta Regiae Soc.Sci., Ser. IV, Vol. 20 (1967). 1981 Nobel Prize in Physics.

[8] H. Hertz, Phys. 31. (1887).

[9] A. Einstein, Ann. Physik 17,132 (1905). 1921 Nobel Prize in Physics.

[10] H.J. Martin, K.H. Schulz, J.D. Bumgardner, K.B. Walters, XPS Study on the Use of 3-Aminopropyltriethoxysilane to Bond Chitosan to a Titanium Surface, Langmuir. 23 (2007) 6645–6651.

Chapter 3. Physico-chemical characterization of SnO_2 before and after functionalization

3.1. Introduction

Before testing the effect of the functionalization on the sensor behavior, it is important to verify whether the functionalization is effective. The APTES silanization of thick SnO_2 film produced by screen printing is not described in the literature. It is necessary to study the effect of different synthesis parameters on final APTES film. Vapor and liquid silanization can be applied to attach APTES on SnO_2 surface. In the vapor silanization, the synthesis parameters were fixed as mentioned by Ming Hai Le et al [1]. In liquid, many parameters were investigated: water content, reaction time and APTES concentration. The presence and reactivity of grafted amine terminated film on SnO_2 were investigated using fluorescent molecules (Alexa Fluor®). In addition, APTES grafting was characterized using Attenuated Total Reflectance-Fourier Transform Infrared spectroscopy (ATR-FTIR) and X-ray Photoelectron Spectrometry (XPS) techniques. These characterizations showed how synthesis parameters affect the amount of APTES films. An XPS model was provided to calculate the APTES film thickness in addition to the concentration of grafted APTES. Optimal liquid silanization parameters were determined in order to obtain a saturated SnO_2 surface with APTES molecules. In addition, the thermal stability of APTES on SnO_2 has been investigated.

SnO_2-APTES film has been used as a substrate to attach ester, acid and alkyl functional groups. These functional groups are supposed to interact selectively with gases. The characterization of ester, acid and alkyl modified SnO_2-APTES was carried out by ATR-FTIR technique.

3.2. Characterization of pure SnO_2 sensing layer on alumina

The surface morphological analysis of SnO_2 thick films was performed by scanning electron microscopy (SEM). Figure 3-1 shows the cross section and top images of SnO_2 film deposited on alumina substrate by screen printing. Figure 3-1a illustrates the film with various thicknesses which are related to the threads of the screen printing mesh. The film has a thickness around 40 µm (Figure 3-1b). In addition, Figure 3-1c and d show that the film is very porous and contains

SnO_2 particles with spherical shape and different sizes. The porosity of the film is due to the evaporation of the organic binder and the solvent during drying and annealing steps (700 °C, 10 h). These pores are very important since the molecules in the functionalization steps can deposit inside SnO_2 film in addition to its surface. These features make SnO_2 a good substrate for molecular modification. The screen printed film exhibit SnO_2 particles with sizes between 30 to 500 nm as present in Figure 3-1d. The effect of annealing on the particle size was studied by X-ray diffraction technique (XRD). We have found that the average particle size of the initial powder and in the annealed film were almost the same, around 80 nm. Therefore, the annealing step does not affect the size of SnO_2 particles.

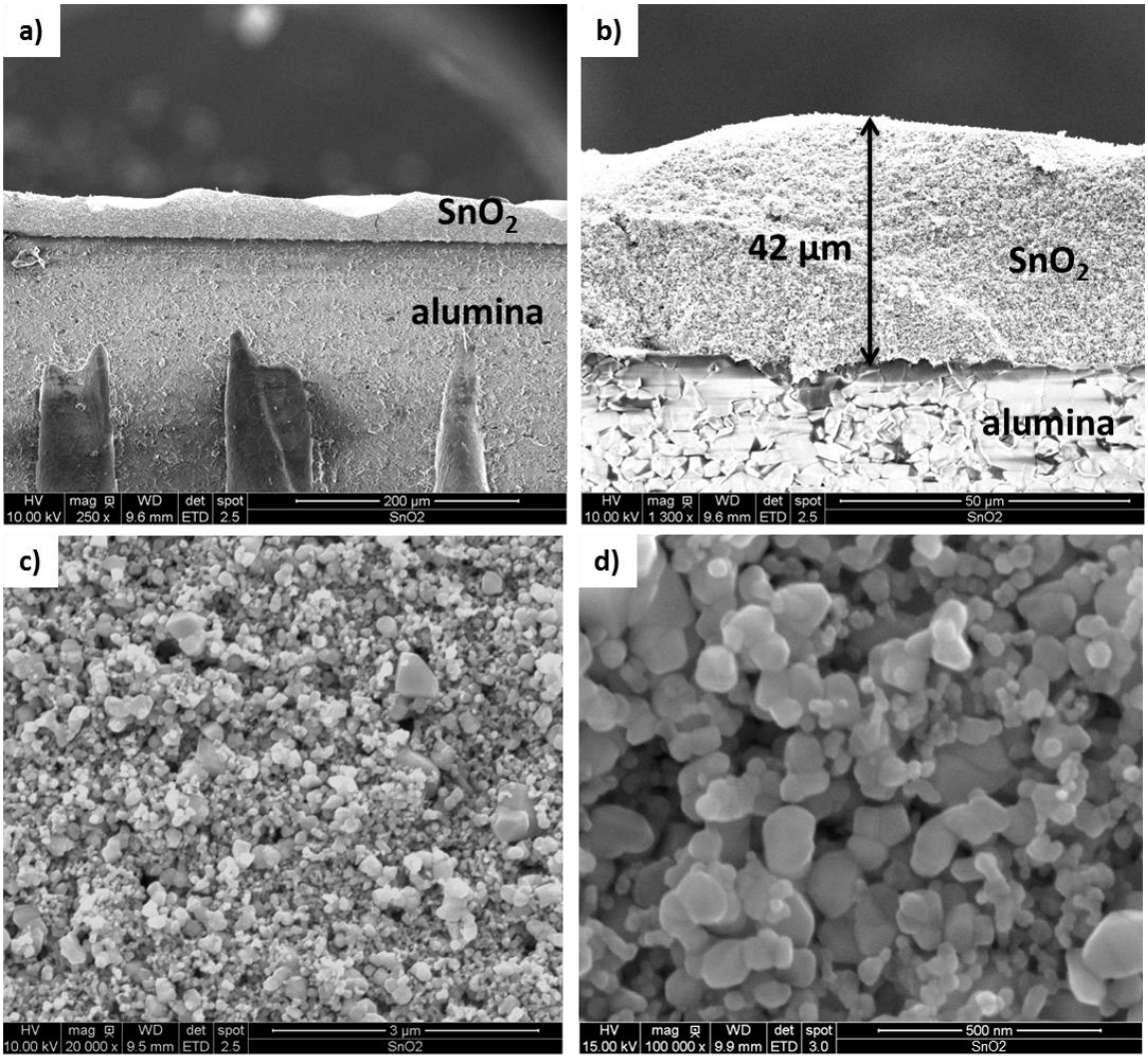

Figure 3-1. SEM images of the cross section (a and b), and top SnO_2 film (c and d) on alumina substrate.

Then, SnO_2 film acts as a substrate for molecular functionalization. As shown in chapter 1, the silanization reaction takes place between the hydroxyl groups of SnO_2 and the hydroxyl groups of silane molecule. So, hydroxyl groups on SnO_2 surface are necessary to perform functionalization by silane products like APTES. To check the present species on SnO_2 surface, ATR-FTIR was achieved.

ATR-FTIR spectrum in Figure 3-2 presents the absorption bands of SnO_2 film between 400 cm^{-1} and 4000 cm^{-1}. The most important FTIR information regarding pure SnO_2 are found as two intense broad peaks at 462 cm^{-1} and 571 cm^{-1} which correspond to Sn-OH and O-Sn-O bonds respectively. Another broad peak at 3480 cm^{-1} is related to the OH groups adsorbed on SnO_2 (Figure 3-2). In addition, the peak at 1627 cm^{-1} corresponds to the OH bond of adsorbed water molecules on SnO_2 surface. This peak confirms the presence of adsorbed water molecules at ambient temperature as shown in chapter 1. All the sensors (pure and modified) show similar features in the range between 1950 and 2380 cm^{-1} which is not exploitable as it corresponds to CO_2 gas contributions in ambient air. The spectrum of SnO_2 will be used later to identify the adventitious peaks after functionalization.

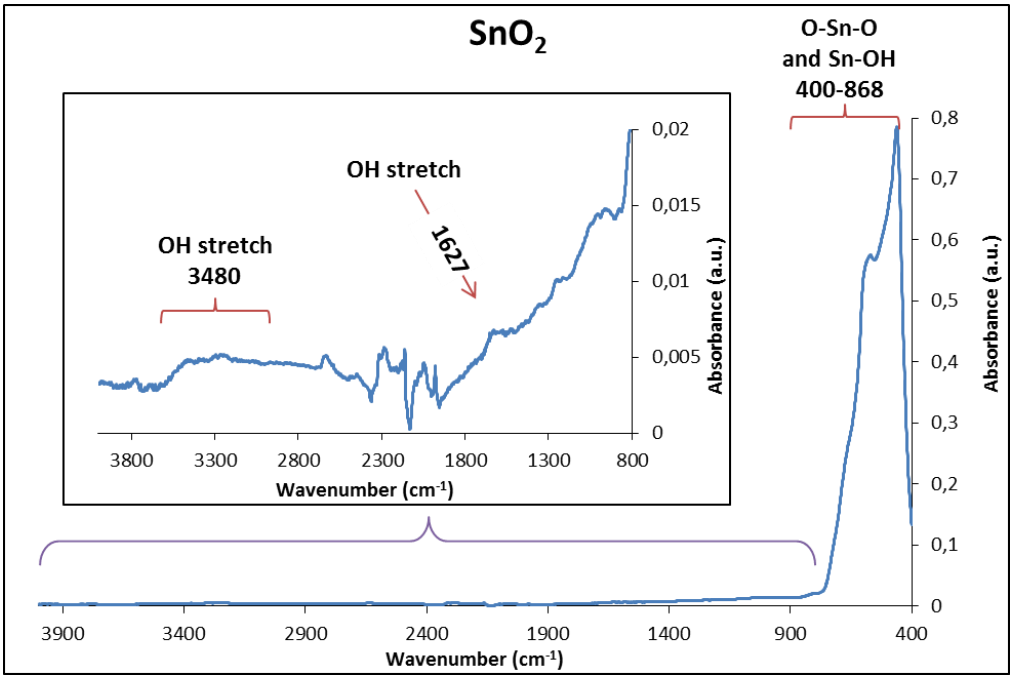

Figure 3-2. ATR-FTIR spectrum of SnO_2 film between 400 and 4000 cm^{-1} and the zoom between 800 and 4000 cm^{-1}.

SnO_2 film was also characterized by XPS in order to investigate if there are any impurities as well as the presence of hydroxyl groups. Figure 3-3 shows the XPS survey spectrum of SnO_2 film. It can be noticed that the spectrum contains only the peaks of Sn and O which are related to SnO_2 material. This means that the SnO_2 film to be functionalized has high purity. The most intense peaks related to Sn are Sn 3d3/2 and Sn 3d5/2 which are found at 495.2 and 486.8 eV respectively. These two peaks will be used later to compare their intensities before and after functionalization. The molecular layer on SnO_2 surface is supposed to reduce the intensity of Sn 3d peaks. Other peaks related to Sn such as Sn 3p1/2, Sn 3p3/2 and Sn 4d are found at 755, 713 and 23 eV respectively. The two peaks present at 976 and 1058 eV are related to Auger effect. The peak at 976 eV corresponds to KLL Auger transition of oxygen atom. The well-known Auger effect is a result of electron-electron interactions. In the relaxation state after the emission of XPS electron, the electron in the inner L level (L_1) of oxygen atom is transferred to the lower energy and releases energy. The released energy results in the emission of Auger electron from the outer L level ($L_{2,3}$). The same effect was found for Sn atom which is represented in a peak at 1058 eV. This peak is related to Sn MNN Auger transition. O1s peak is found at 530.5 eV which is assigned to the oxygen of SnO_2.

The narrow scan on O 1s zone of SnO_2 is shown in Figure 3-4. As O 1s peak is not symmetric, fitting was carried out to analyze the different contributions. The envelope represents the average of the O 1s peak (raw data). The base line was estimated for the calculation of peak area. First and second fits represent the possible comportment under the original peak. As shown in Figure 3-4, O 1s peak is composed of two components at 530.3 eV, and 531.7 eV which correspond to Sn–O, and Sn–OH bonds respectively [2]. These hydroxyl groups on the surface of APTES will be the reactive sites for the silanization process by APTES. Resulting SnO_2-APTES films will contain higher quantity of oxygen on the surface since each APTES molecule contains 3 oxygen atoms. Furthermore, functionalization by APTES introduces Sn-O-Si and Si-O-Si bonds. Therefore, the O 1s peak presented in Figure 3-4 will be compared with the peak after modification.

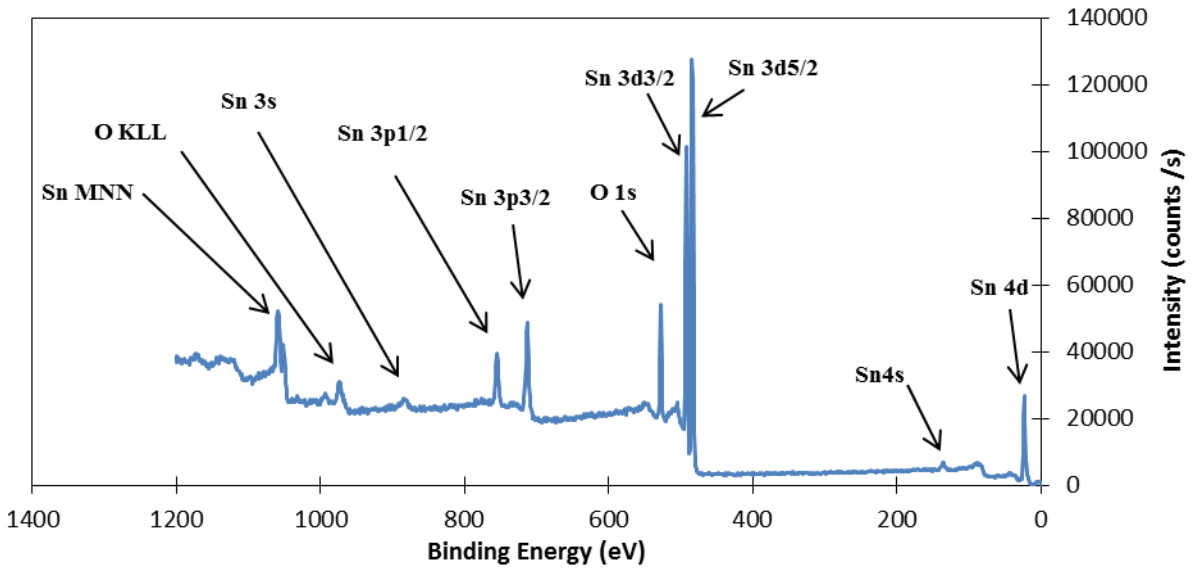

Figure 3-3. XPS survey spectrum of SnO_2 film on Al_2O_3 substrate.

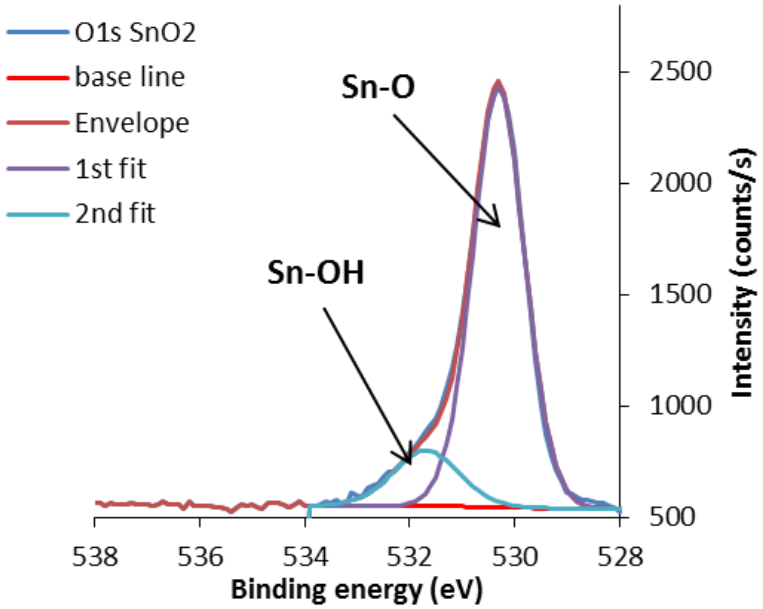

Figure 3-4. XPS narrow scan of O 1s peak for SnO_2 (X-ray incident angle is 41°).

3.3. Macroscopic checking of APTES grafting

In order to check, that silanization by APTES has occurred, wettability tests were carried out. Indeed, APTES is supposed to create a hydrophobic film on SnO_2 which should increase the

contact angle after silanization [3]. Contact angle on SnO_2 film before and after functionalization was found to be less than 5°. This low contact angle value is due to the fact that the SnO_2 film is very porous as shown by SEM images and very hydrophilic (before functionalization) because of the adsorbed water species. As reported in chapter 1, the silanization can also be established on Al_2O_3 surface. Thus, the wettability test was carried out on Al_2O_3 substrate instead of SnO_2. Figure 3-5 shows the change of the contact angle after silanization on Al_2O_3 substrate. The contact angle was changed from 35° to 80° after silanization. It results from the modification of alumina by APTES molecules.

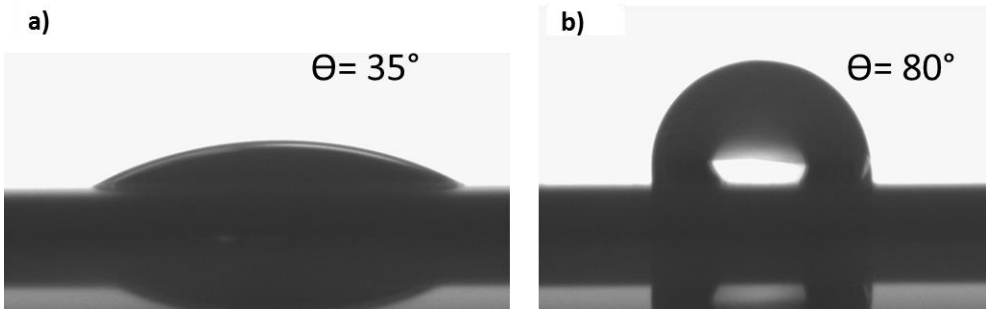

Figure 3-5. Photographs of water droplets (wettability test) on alumina substrate before (a) and after (b) silanization.

SnO_2-APTES film will be further used as a substrate to attach molecule containing acyl chloride group. For these reasons, it is important to verify the effectiveness of grafting on SnO_2. The reactivity of terminated amine groups of APTES with respect to coupling reactions was checked using fluorescent molecules such as Alexa Fluor molecules which have affinity with amine groups of APTES. Figure 3-6 shows the epifluorescence microscope images of SnO_2 (Figure 3-6a), and SnO_2-APTES after silanization in vapor (Figure 3-6b) and liquid phase (synthesis parameters: 50 mM of hydrous APTES solution, immersed for 5 h, Figure 3-6c) modified by Alexa Fluor. As expected, for SnO_2 without modification by APTES, no fluorescence was observed (Figure 3-6a). On the contrary, the obtained fluorescence of SnO_2-APTES films (Figure 3-6b and c) means that the Alexa Fluor molecules are attached to the surface by the grafted amine terminal part of APTES. The fluorescence intensity after silanization was measured by Fluorescence Spectrometer. The intensity of APTES modified SnO_2 in vapor phase was 3185 (arbitrary units), while it was 4541 in liquid silanization. Therefore, more reactive amine groups are present on the surface for the SnO_2-APTES carried out in liquid phase.

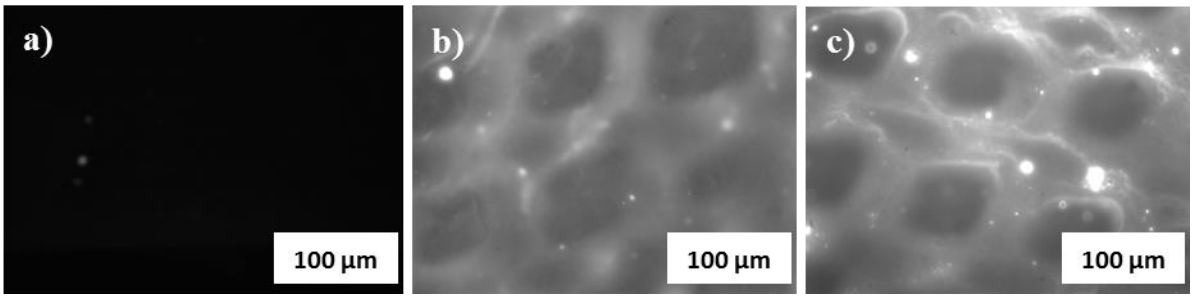

Figure 3-6. Epifluorescence images after immersion in Alexa Fluor solution: (a) SnO_2, (b) SnO_2-APTES-vapor phase and (c) SnO_2-APTES-liquid phase (5 vol% H_2O, 50 mM of APTES, 5 h).

Another method to check the presence and the reactivity of APTES film, as well as the distribution of APTES molecules on SnO_2 was carried out by using 20 nm citrated gold nanoparticles. The primary amine groups of APTES react with the citrate groups present on the surface of gold nanoparticles. This reaction leads to the physisorption of the gold nanoparticles on the surface of SnO_2. As shown in Figure 3-7, The SnO_2-APTES sample has changed to grey, while the other sample (pure SnO_2) has remained white after 1.5 h reaction. The change in color is due to the attachment of gold nanoparticles on SnO_2 as shown in Figure 3-8. Gold nanoparticles on SnO_2-APTES are clearly seen by SEM (Figure 3-8b), contrary to pure SnO_2 (Figure 3-8a). This ensured the presence of APTES on the surface of SnO_2. Furthermore, gold nanoparticles are distributed in the entire tested zone which means that APTES is homogenously distributed over SnO_2 surface.

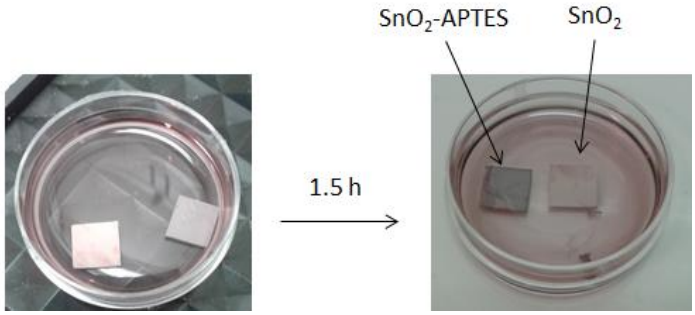

Figure 3-7. The change in color of SnO_2 and SnO_2-APTES after 1.5 h dipping in suspension of citrated gold nanoparticles.

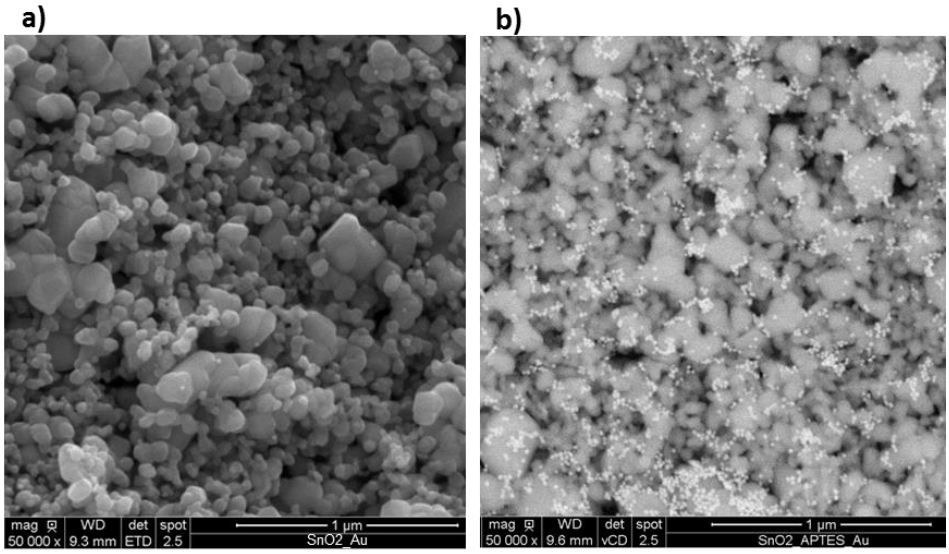

Figure 3-8. SEM images of pure and modified SnO_2 after 1.5 h dipping in suspension of citrated gold nanoparticles.

3.4. Chemical analyses of APTES grafting

The grafted APTES films on SnO_2 substrate were chemically characterized by ATR-FTIR and XPS. These techniques were used to study the structure of APTES on SnO_2 as well as the effect of different synthesis parameters.

Regarding the characterization of APTES film by Attenuated Total Reflectance-Fourier Transform Infra-Red spectroscopy (ATR-FTIR), the most important signals corresponding to APTES were found between 800 and 1800 cm^{-1} as shown in Figure 3-9. The peak at 938 cm^{-1} is attributed to Sn-O-Si stretch [4]. The peak at 1070 cm^{-1} arises from the un-hydrolyzed ethoxy groups of APTES ($–OCH_2CH_3$) [5]. The strong absorption peaks at 1029 and 1125 cm^{-1} are attributed to Si-O bond of polymerized APTES on the surface [6,7]. The vibrational mode around 1390 cm^{-1} is assigned to Si-C bond ($-Si-CH_2-$) [7]. NH_2 vibrational signal is found at 1570 cm^{-1} which confirms the presence of amine end functional group of APTES after silanization. The two peaks present at 1486 and 1643 cm^{-1} correspond respectively to the symmetric and asymmetric $–NH_3^+$ group indicating the protonation of amine group in air [8,9]. All these modes are being proportional to the quantity of the APTES on SnO_2.

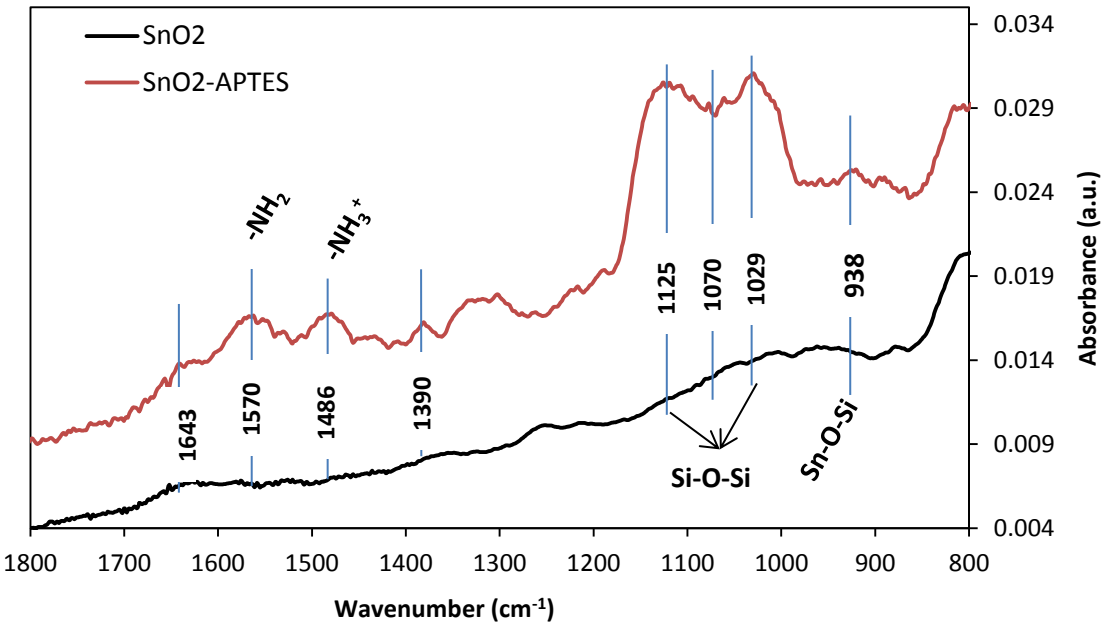

Figure 3-9. ATR-FTIR spectra of SnO_2 and SnO_2-APTES (hydrous liquid silanization, 50 mM APTES, 5 h).

XPS was carried out to show the elemental evolution after silanization process. The XPS survey scan spectrum of SnO_2-APTES film obtained by hydrous liquid synthesis presented in Figure 3-10 shows the presence of Sn and O related to the SnO_2 substrate. These two peaks have less intensity comparing with pure SnO_2 (Figure 3-3). The grafting of APTES film decreases the intensity of the peaks related to SnO_2 (Sn and O) because of the formed film. In addition, this spectrum reveals the existence of N, C and Si atoms related to APTES molecules at the surface which confirms the silanization of SnO_2. N, C, and Si peaks were found at 400, 285 and 102 eV respectively.

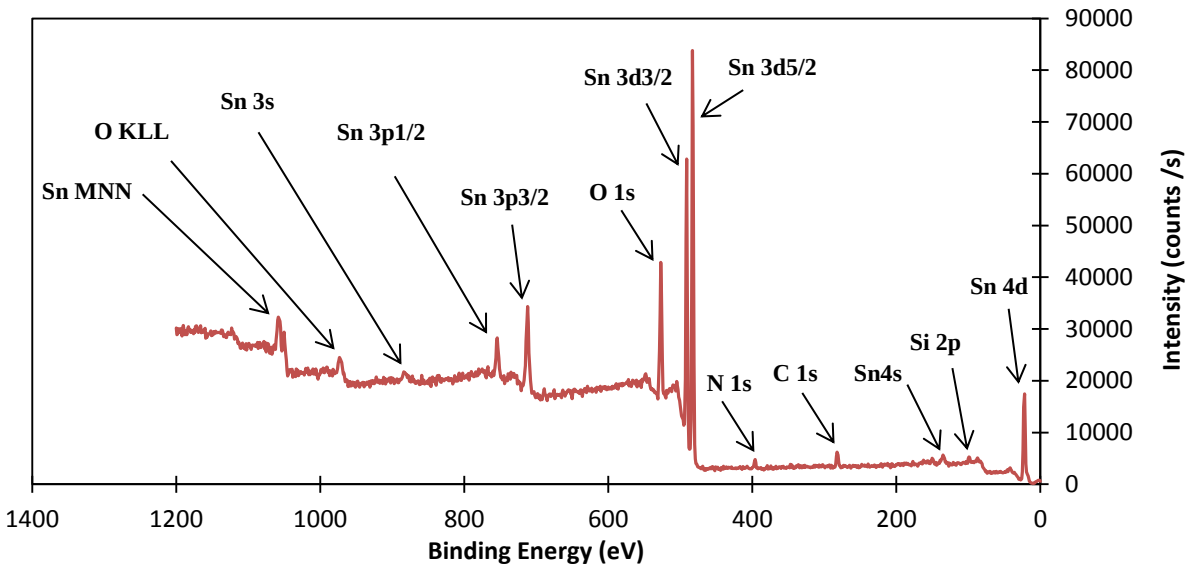

Figure 3-10. XPS survey spectra of SnO_2-APTES synthesized in hydrous liquid phases.

To identify the origin of unsymmetrical peaks, fitting of C 1s, O 1s, and N 1s peaks was performed. As shown in Figure 3-11, three components at 284.2 eV, 284.9 eV and 286.4 eV were found for C 1s peak (Figure 3-11a) which were assigned respectively to C-Si, C-C/CH and C-N chemical bonds. These chemical bonds correspond to APTES molecule. The nitrogen N 1s core level (Figure 3-11b) exhibits two contributions, one located at 399.4 eV which is related to amine group bounded to carbon C-NH_2. The second located at 401.3 eV, could be attributed to C-NH_3^+ [10]. The shape of the O 1s peak (Figure 3-11c) was adjusted using two components at 530.3 eV, and 531.8 eV according to oxygen in Sn–O, and Si–O respectively [11]. Regarding only the peak at 531.8 eV, it can be hardly differentiated with Sn-OH peak at 531.9 eV (Figure 3-4). To conclude, one have also to consider the Si 2p peak located at 101.9 eV (figure 3-11d). This peak was assigned to Si atom bonded to oxygen and carbon. So, the whole XPS spectrum allows to confirm the presence of the different chemical bonds related to APTES molecules.

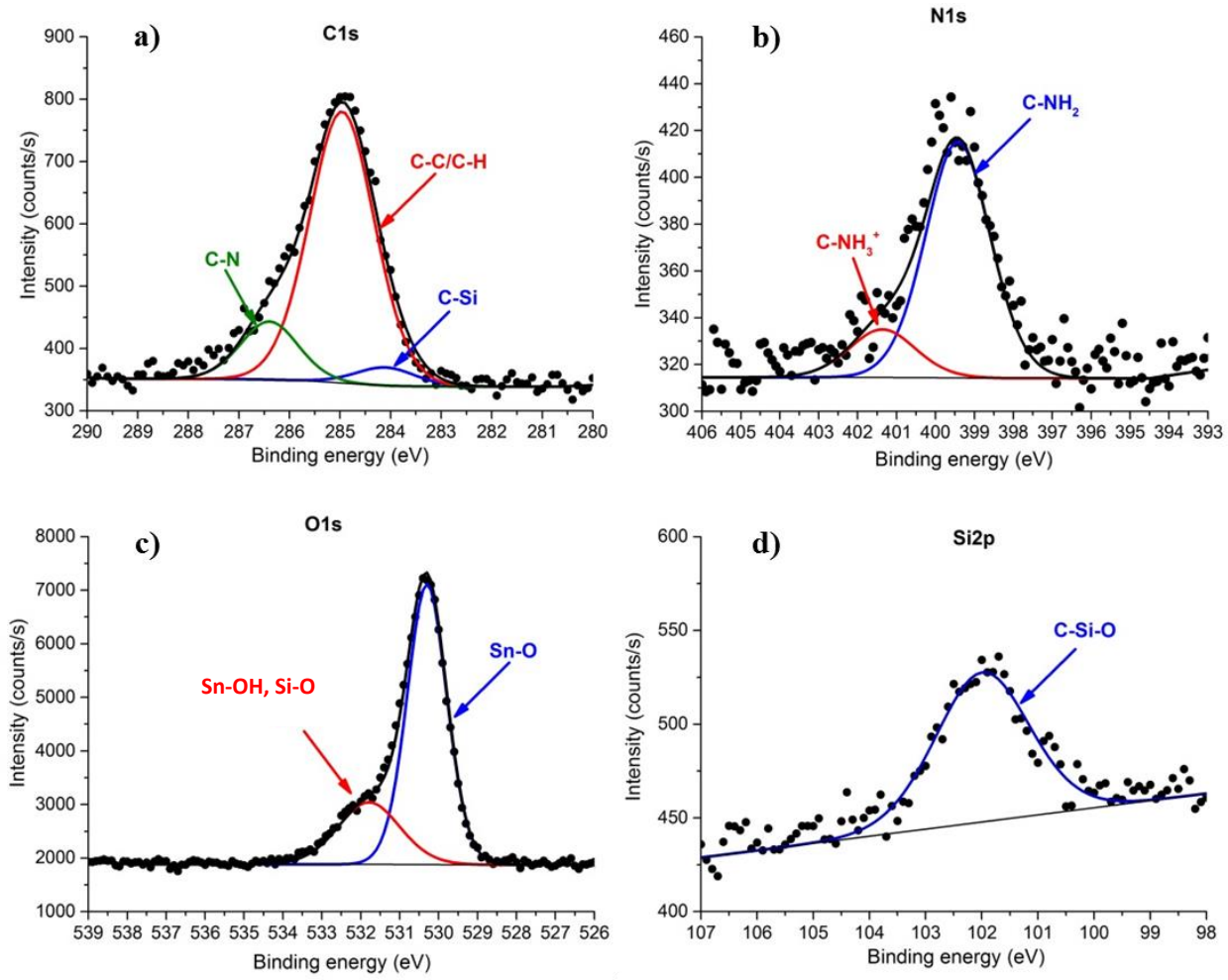

Figure 3-11. XPS peak fitting of (a) C 1s, (b) N 1s, (c) O 1s, and (d) Si 2p of SnO_2-APTES film.

Therefore, both the characterizations by ATR-FTIR and XPS confirm that the functionalization by APTES is achieved. In the next discussion, the synthesis parameters will be investigated to produce an optimum APTES modified SnO_2.

3.5. Influence of synthesis parameters in silanization

Different parameters were explored for APTES grafting: vapor and liquid silanization with or without H_2O, APTES concentrations and reaction times. Each of these parameters could affect the grafted APTES film quantitatively and qualitatively.

3.5.1. Comparison between vapor, liquid hydrous and liquid anhydrous silanization processes

The effect of different silanization ways were characterized by ATR-FTIR to check the effects on the produced SnO_2-APTES film. Generally, the peaks corresponding to APTES are more or less significant depending on the synthesis procedures. As shown in Figure 3-12, APTES liquid deposition in presence of 5 vol% H_2O (red curve) shows the most intense peaks for all the vibrational modes (938, 1029, 1125, 1390, 1496, and 1570 cm^{-1}) which implies that more APTES molecules were grafted on the surface in this synthesis. As mentioned before, the intensity of these peaks is proportional to the amount materials (APTES). Furthermore, the observed peak at 1070 cm^{-1} in the case of vapor silanization (green curve) and liquid synthesis without H_2O (blue curve) is linked to un-hydrolyzed ethoxy groups of APTES as mentioned earlier [5]. This peak has disappeared for the SnO_2-APTES film synthesized with H_2O. The water molecules initiate the silanization process by hydrolysis of ethoxy groups to create corresponding hydroxysilane ($RSi(OH)_3$) [12]. Hydrolysis of ethoxy groups of APTES pushes forward the condensation reaction between SnO_2 film and APTES [9,13]. From these results, one can notice that the presence of water in the synthesis solution increases the APTES grafting on SnO_2 with also more APTES molecules bonding with the surface and with APTES each other. Therefore, APTES is more stable on SnO_2 surface in presence of water during synthesis.

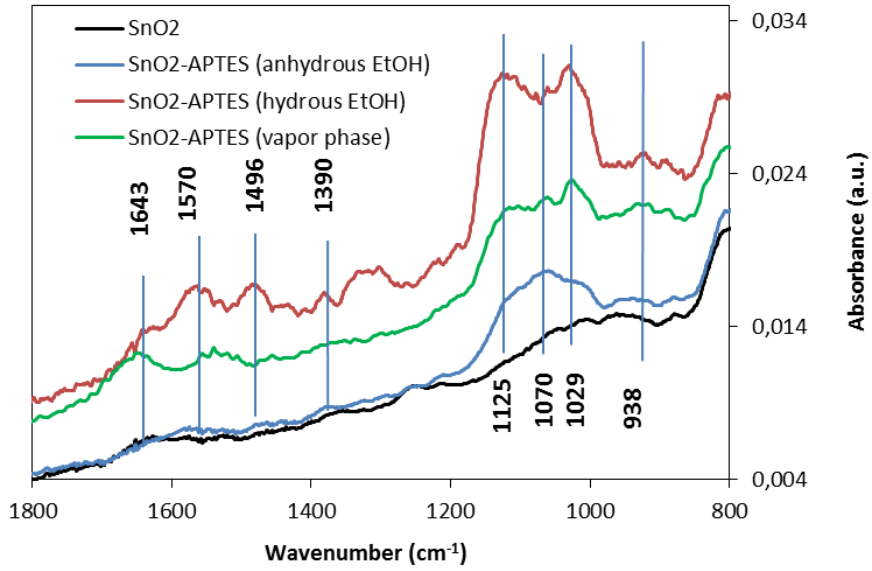

Figure 3-12. ATR-FTIR spectra of SnO_2, and SnO_2-APTES synthesized in liquid and vapor phase. Liquid phase silanization was carried in 50 mM APTES dissolved in hydrous or anhydrous ethanol for 5 h.

The effect of water in the liquid silanization was also investigated by XPS. Figure 3-13 illustrates the N 1s, Si 2p, Sn 3d and C 1s peaks of SnO_2-APTES synthetized in hydrous and anhydrous APTES solution. N 1s, Si 2p, and C 1s peaks are more intense for the film synthesized in aqueous APTES solution than in a dry one. For Sn 3d peaks, the film prepared with water has lower peak intensity than the dry one. All these results imply that more APTES molecules are grafted on the surface in solution with water that in dry one as already shown by ATR-FTIR (Figure 3-12). Indeed, the more grafted APTES there is, the higher N 1s, Si 2p and C 1s peaks are. For Sn 3d, if SnO_2 is covered by APTES, as XPS analyzes only the surface of the film, less Sn atoms can be seen.

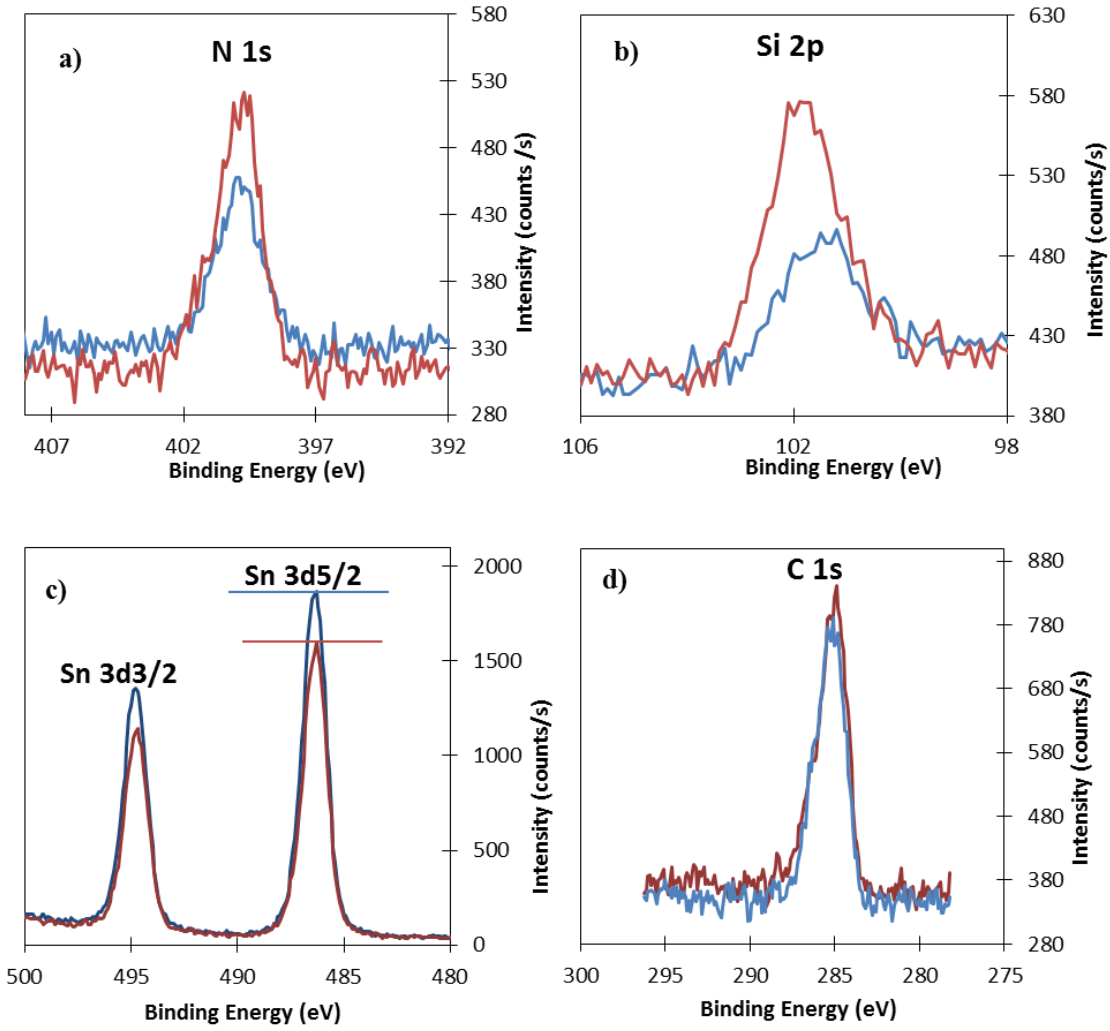

Figure 3-13. XPS peaks of a) N 1s, b) Si 2p, c) Sn 3d, and d) C 1s for SnO_2-APTES synthetized in solution with 5% by volume of H_2O (red curve) and without H_2O (blue curve) for 5 h and 50 mM of APTES.

3.5.2. Effect of APTES concentration in liquid hydrous phase

As shown in the previous discussions, more APTES molecules were grafted by hydrous liquid silanization than anhydrous liquid and vapor silanization. Thus, the synthesis parameters have been more deeply investigated for hydrous liquid silanization. In Figure 3-14, three APTES concentrations (1 mM, 50 mM, 500 mM) were tested in ethanol solution with 5 vol% H_2O for 5 h. Peaks intensities of Si-O-Si bonds at 1029 and 1125 cm^{-1} are low with 1 mM APTES solution (green curve) while they increase with 50 mM (red curve), and then almost no change is noticed when the concentration is increased up to 500 mM (purple curve). Therefore, a very little amount

of APTES was grafted on the surface with a concentration of 1 mM, while a concentration of 50 mM was sufficient to well cover SnO_2 with APTES molecules.

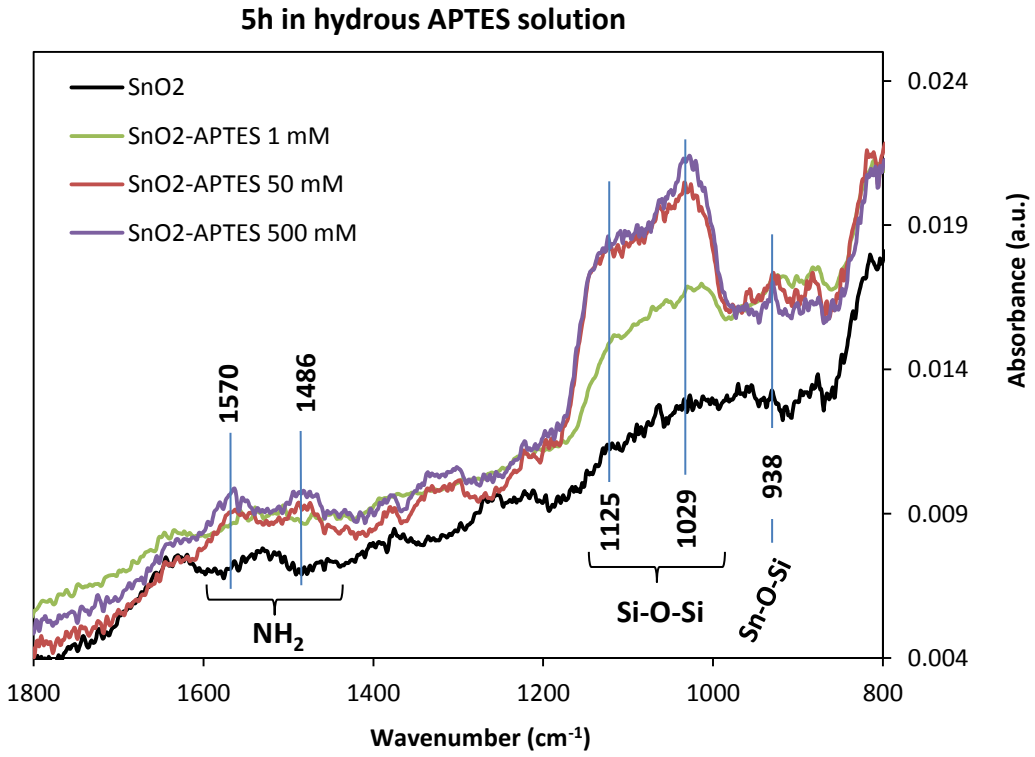

Figure 3-14. Hydrous liquid phase silanization (5 h) with different APTES concentrations of 1, 50 and 500 mM in 5 mL ethanol.

3.5.3. Effect of reaction time in liquid hydrous phase

With the same idea, to improve the synthesis parameters, reaction time was also investigated. Figure 3-15 shows different reaction times of SnO_2 film in APTES solution (ethanol with 5 vol% H_2O, 50 mM of APTES). The peak of Si-O-Si (1029 cm^{-1}) rises with the increase of reaction time. As this peak is proportional to the amount of APTES attached on the surface [6], one can note that the increase of reaction time from 5 min to 4 h attaches a larger amount to the surface. No increase in the amount of grafted APTES on the surface was observed after 4 h, since the signal intensity is the same between films immersed 4 and 5 h. Evidently, this steady state means that 4 h is sufficient to saturate the SnO_2 film with APTES.

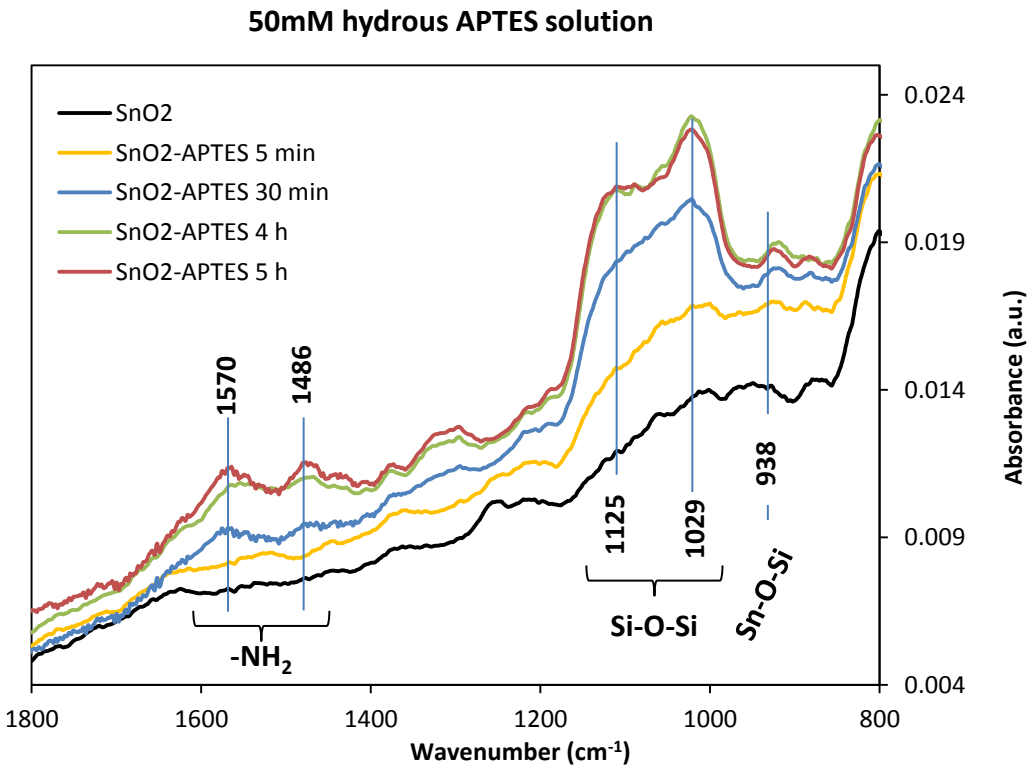

Figure 3-15. ATR-FTIR of SnO_2 and SnO_2-APTES synthesized in various reaction times.

3.6. Nanostructure of the APTES film on SnO_2

Nanostructure of the APTES film was determined from inelastic electron background analysis of the Sn 3p transition taking advantage of the weak sensitivity of this method to the roughness. "Analyze" program from QUASES software package developed by Tougaard [14] was used by means of the active substrate model, where the modelled signal originates from the SnO_2 substrate and is attenuated by an overlayer constituted of APTES molecules. The shape of the measured spectrum J(E) strongly depends on the morphology of the overlayer. A primary excitation spectrum F(E) is obtained after correction of the measured spectrum J(E) by an inelastic background calculated for a given coverage and thickness of the overlayer. These set of parameters can be adjusted using two criterions. The first one is that after background subtraction F(E) must be of zero intensity in an energy region beyond 30 eV below the primary peak energy. As a second criterion, F(E) can be compared to the one determined from the analysis of spectrum on reference sample with well-known in depth concentration profile. Reference Sn 3p spectrum was recorded on a pure SnO_2 sample. After linear background subtraction and analyzer

transmission function correction, the background of the model spectrum was adjusted to zero by analyzing the reference to the depth of 1000 Å that corresponds to the infinite thick homogeneous layer. The background was calculated using 'Universal cross section' formula [15] for the inelastic electron cross section and changing the "x-scale" parameter in the QUASES program from default value to 0.97. A value of 12.36 Å for the inelastic mean free path of Sn 3p electrons in SnO_2 was considered according to the TPP2M method [16]. The same procedure and parameters were used for analyzing SnO_2 covered with APTES molecules using "active substrate" model.

Results obtained after analysis of Sn 3p spectrum measured on SnO_2 samples with different methods of silanization are presented in the Figure 3-16. From these results, two main conclusions can be drawn. First, for the three methods of silanization (vapor, hydrous liquid, anhydrous liquid), the nanostructure of the grafted film consists in a monolayer of APTES molecules which does not cover entirely the surface. Second, the silanization procedures used can be classified as "high coverage" for the hydrous liquid method (SnO_2 surface coverage of 0.8) and "low coverage" for the two other methods for which a similar SnO_2 surface coverage around 0.5 was found.

Finally, it is worth noting that considering a theoretical length of the APTES molecule of 8 Å, the calculated overlayer thickness of 6 Å indicate a ~42° grafting angle of the APTES molecules with respect to the normal of the SnO_2 surface.

However, due to the rugous surface of SnO_2 samples, even if the proposed methodology brings corrections to XPS spectrum, one must be cautious and consider relative values and differences between the analyzed samples, rather than the absolute values.

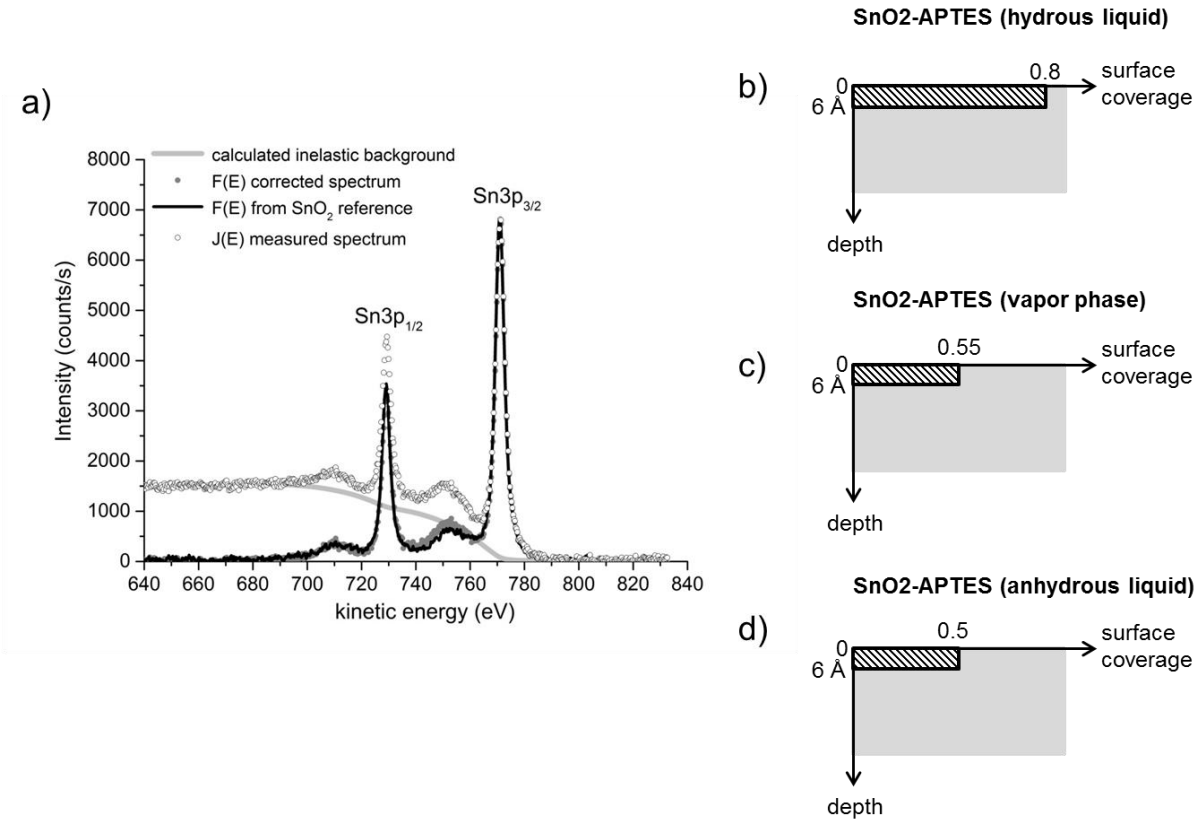

Figure 3-16. (a) Modelisation of the electron inelastic background of Sn 3p using QUASES software [14], (b) (c) (d) schematic representation of the coverage and thickness of the APTES overlayer for the three methods used for the silanization of SnO_2.

3.7. Determination of APTES concentration on SnO_2

As shown before, using electron inelastic background analysis, the silanization of SnO_2 with vapor, hydrous liquid and anhydrous liquid methods produce a monolayer film of APTES molecules which does not cover entirely SnO_2. Owing to the difference in coverage rate according to the experimental silanization protocol, it seems interesting to determine the concentration of APTES molecules grafted on SnO_2 for each method. Considering one silicon atom for each APTES molecule, these concentrations were estimated calculating the silicon concentration per unit area using the ratio of the intensities of Si 2p and Sn 4d photoelectron peaks. The choice of these peaks, especially Sn 4d which is much less intense than Sn 3d, was motivated by the fact that several assumptions can be made due to the position at high kinetic energies of these transitions as we will see below. For the purpose of this calculation, we define

three thicknesses: $d_{C_3NH_8}$, d_{Si} and d_{APTES}. These parameters are presented in the Figure 3-17 and correspond to different portions of the APTES film.

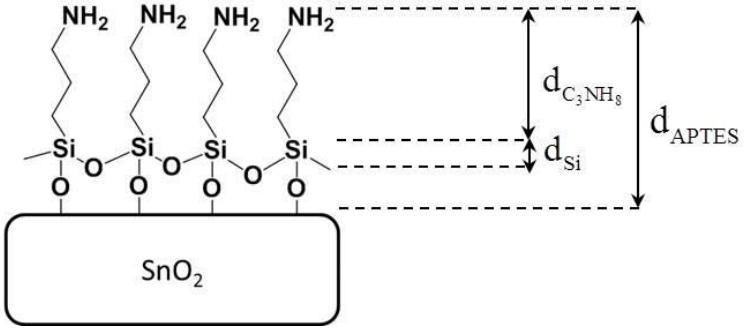

Figure 3-17. Schematic illustration of the different portions of the APTES film considered for the calculation of the APTES surface concentration using the ratio of Si 2p and Sn 4d intensities.

Using the description in Figure 3-17, the intensities of Si 2p and Sn 4d can be calculated as shown in equations (1) and (27).

$$I_{Si2p} = KT_{Si2p} N_{Si} \sigma_{Si2p} \lambda_{Si2p}^{Si} \cos\theta \left[1 - \exp\left(\frac{-d_{Si}}{\lambda_{Si2p}^{Si} \cos\theta}\right)\right] \times k_{Si2p}^{C_3NH_8} \quad (26)$$

$$I_{Sn4d} = KT_{Sn4d} N_{Sn} \sigma_{Sn4d} \lambda_{Sn4d}^{SnO_2} \cos\theta \, k_{Sn4d}^{APTES} \quad (27)$$

(see chapter 2, equation 3 for parameters definition)

Concerning the inelastic mean free path, two methods were applied. The values of λ_{Si2p}^{Si} and $\lambda_{Sn4d}^{SnO_2}$ were estimated using the TPP2M method [16] which gives respectively 30.8 Å and 24.1 Å. As regards the value of λ_{Si2p}^{Si}, one may assumes that $d_{Si} << \lambda_{Si2p}^{Si}$ which allows to modified equation (1) and express the intensity of Si 2p as a function of the silicon atomic concentration per unit area in equation (28).

$$I_{Si2p} = KT_{Si2p} n_{Si} \sigma_{Si2p} k_{Si2p}^{C_3NH_8} \quad (28)$$

With $n_{Si} = N_{Si} d_{Si}$

The silicon surface concentration can be consequently expressed as a function of the ratio of the intensities of Si 2p and Sn 4d following equation (29).

$$n_{Si} = \frac{I_{Si2p}}{I_{Sn4d}} \times \frac{T_{Sn4d} N_{Sn} \sigma_{Sn4d} \lambda_{Sn4d}^{SnO_2} \cos\theta}{T_{Si2p} \sigma_{Si2p}} \times \frac{k_{Sn4d}^{APTES}}{k_{Si2p}^{C_3NH_8}} \quad (29)$$

For k_{Si2p}^{C3NH8} and k_{Sn4d}^{APTES}, a method using quantitative structure-property relationships in organic materials [17] was used. Inelastic mean free paths were determined using expression (30).

$$\lambda(nm) = \left[\frac{3.117({}^{0}x^{V}) + 0.4207 N_{rings}}{N_{non-H}}\right] \left(E/_{keV}\right)^{0.79} \quad (30)$$

With

${}^{0}x^{V} = \sum_{non-H\ atoms} \left(\frac{1}{\sqrt{\delta^{(V)}}}\right)$ the zeroth-order valence connectivity index of the molecule,

N_{rings} the number of aromatic six-member rings in the molecule,

N_{non-H} the number of atoms in the molecule excluding hydrogen,

E the kinetic energy of the electron travelling through the molecule and

$\delta^{(V)}$ the valence connectivity index which depends on the hybridization state and number of hydrogen atoms bonded to the atom considered. Values of $\delta^{(V)}$ were taken from literature using Bicerano work [18].

The values of inelastic mean free path (λ) and associated attenuation factors (k), assuming a collecting angle θ of 50°, are presented in the Table 3-1.

Table 3-1. Values of inelastic mean free path λ and associated attenuation factor k calculated using the Cumpson [17] method for an electron with kinetic energy E travelling through a given matrix with thickness d.

Matrix	Peak, E Kinetic (eV)	d^{Matrix}(Å)	λ_{peak}^{Matrix} (nm)	k_{peak}^{Matrix}
APTES	Sn 4d, 1461	8	6.01	0.81
C_3NH_8	Si 2p, 1384	~6	4.83	0.82

According to Table 3-1, equation 4 can be simplified due to a ratio of the attenuation factors k_{Sn4d}^{APTES} and k_{Si2p}^{C3NH8} close to unity. Moreover, the kinetic energies of Si 2p and Sn 4d are closed together and in range where the variation of the transmission function is weak. Following these assumptions, the silicon surface concentration n_{Si} corresponding to the surface concentration of APTES molecules n_{APTES} can be described in equation (31).

$$n_{APTES} = n_{Si} = \frac{I_{Si2p}}{I_{Sn4d}} \times \frac{N_{Sn}\sigma_{Sn4d}\lambda_{Sn4d}^{SnO_2}\cos\theta}{\sigma_{Si2p}} \quad (31)$$

It is worth noting that the main uncertainty on the estimation of APTES surface concentration comes from the electron collecting angle θ due to the roughness of the SnO_2 substrates. However, results of atomic force microscopy measurement, not presented here, have shown comparable roughness for the three substrates used which allows comparing the three processes of silanization in terms of surface concentrations of grafted APTES molecules.

Calculations were carried out with Scofield cross section (relative sensitivity factor) of 0.817 for σ_{Si2p}, 2.7 for σ_{Sn4d} and using an atomic concentration per unit volume of Sn in SnO_2 of 2.77 x 10^{22} atoms/cm^3. Table 3-2 reports the calculated concentrations after the different synthesis ways of SnO_2-APTES (anhydrous and hydrous liquid versus vapor silanization).

Table 3-2. Calculated concentrations of APTES grafted on SnO_2 obtained by different synthesis ways.

SnO_2-APTES	n_{APTES} $(molecules/cm^2)$
vapor phase	4.7×10^{14}
hydrous liquid phase	9×10^{14}
anhydrous liquid phase	4.24×10^{14}

The SnO_2-APTES carried out by liquid silanization in presence of 5 vol% H_2O processes the highest grafted APTES concentration (n_{APTEs}). The presence of H_2O hydrolyzes ethoxy groups of the APTES to silanol groups which enhances the condensation reaction with hydroxyl groups of SnO_2 and polymerization of APTES [7]. With vapor deposition and with liquid synthesis without water, the condensation is less favored due to the absence of water (n_{APTES} =4.7×10^{14}

and n_{APTES} =4.24×10^{14}, respectively). In addition, the liquid silanization without water shows lower APTES concentrations than the one in vapor, both are in the same range. As a conclusion, hydrous solution synthesis gives the higher silanization rate, superior to vapor or anhydrous synthesis.

3.8. Thermal stability of APTES on SnO_2

To study the thermal stability of APTES, samples were in-situ annealed at 110 °C (synthesis annealing temperature), 200 °C, 300 °C, and 400 °C for 4 h at a pressure of 5.10^{-9} mbar in XPS device. The evolution of the intensities of N 1s, C 1s, Si 2p, and Sn 3d are presented in Figure 3-18. The decrease of the N 1s peak intensity with temperature can be explained by the partial thermal degradation of amine group between 110 °C and 400 °C, while at 500 °C no more amine groups are present on the surface. The evolution of the intensity of C 1s peak also suggests a decrease in the amount of carbon on the surface upon thermal treatment which is related to the degradation of different carbon bonds. After 4 h treatment at 500 °C, a presence of carbon at the surface was still detected. This residual carbon was assigned to Si-CH_2 bonds as the annealing treatments show no effects on the intensity of the Si 2p peak. The intensity of Sn 3d peak depends on the attenuating APTES overlayer. The increase of the intensity of Sn 3d peak with temperature is consequently in accordance with the progressive degradation of the APTES film as the temperature increases. However, Sn 3d is still less intense for SnO_2-APTES heated at 500 °C than for pure SnO_2. This could be related to the remaining silicon layer on SnO_2 metal oxide surface. Therefore, grafted APTES started to degrade at temperature above 110 °C.

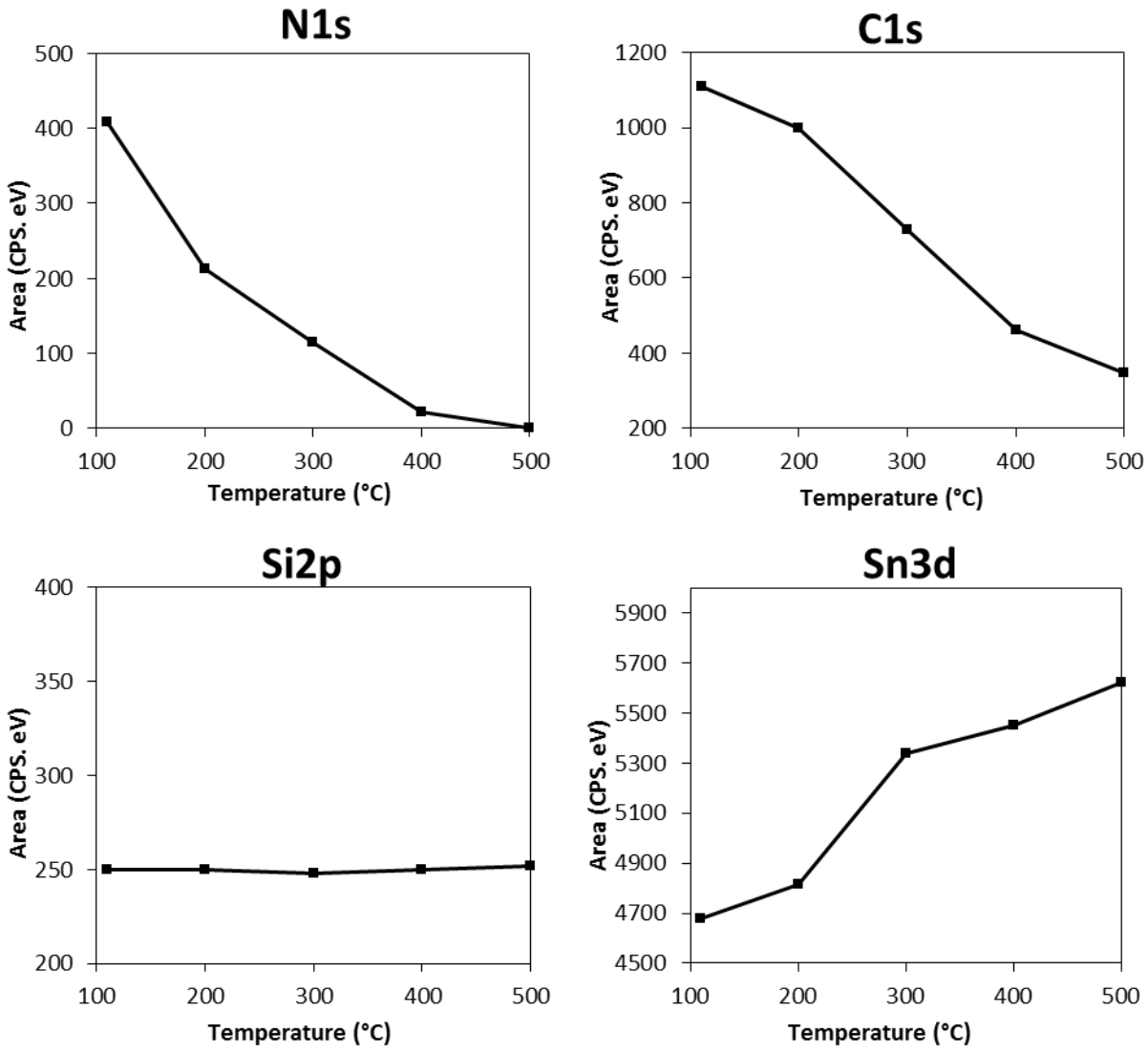

Figure 3-18. Evolution of N 1s, C 1s, Si 2p and Sn 3d intensities as a function of temperature for 4 h annealing treatment of SnO_2-APTES synthetized in vapor phase.

3.9. Characterization of SnO_2-APTES modified by different functional groups

Among the above reported synthesis parameters of APTES modified SnO_2, the modified film obtained by liquid silanization in presence of 5 vol% H_2O (4 h, 50 mM of APTES) was the most efficiently functionalized. Thus, this film was used for the second step of functionalization. APTES modified SnO_2 offers an amine terminated substrate for further modification as reported before by Bin Wang et al [19]. The second step of sensors modification is the attachment of a chemical function on SnO_2-APTES, ended with alkyl, acid or ester groups. Furthermore, the

reaction of APTES amine group with acyl chloride leads to the formation of amide bond and add more carbon on the surface of SnO_2 (CH_2, CH_3). Thus, each modified SnO_2-APTES is supposed to have amide and alkyl, acid or ester functional groups. Molecular characterization of the attached films on SnO_2-APTES was carried out by ATR-FTIR. Spectra of SnO_2 (black curve), SnO_2-APTES (blue curve), SnO_2-APTES-alkyl (red curve), SnO_2-APTES-acid (orange curve) and SnO_2-APTES-ester (green curve) are presented in Figure 3-19. The IR scan was carried out between 800 and 4000 cm^{-1}.

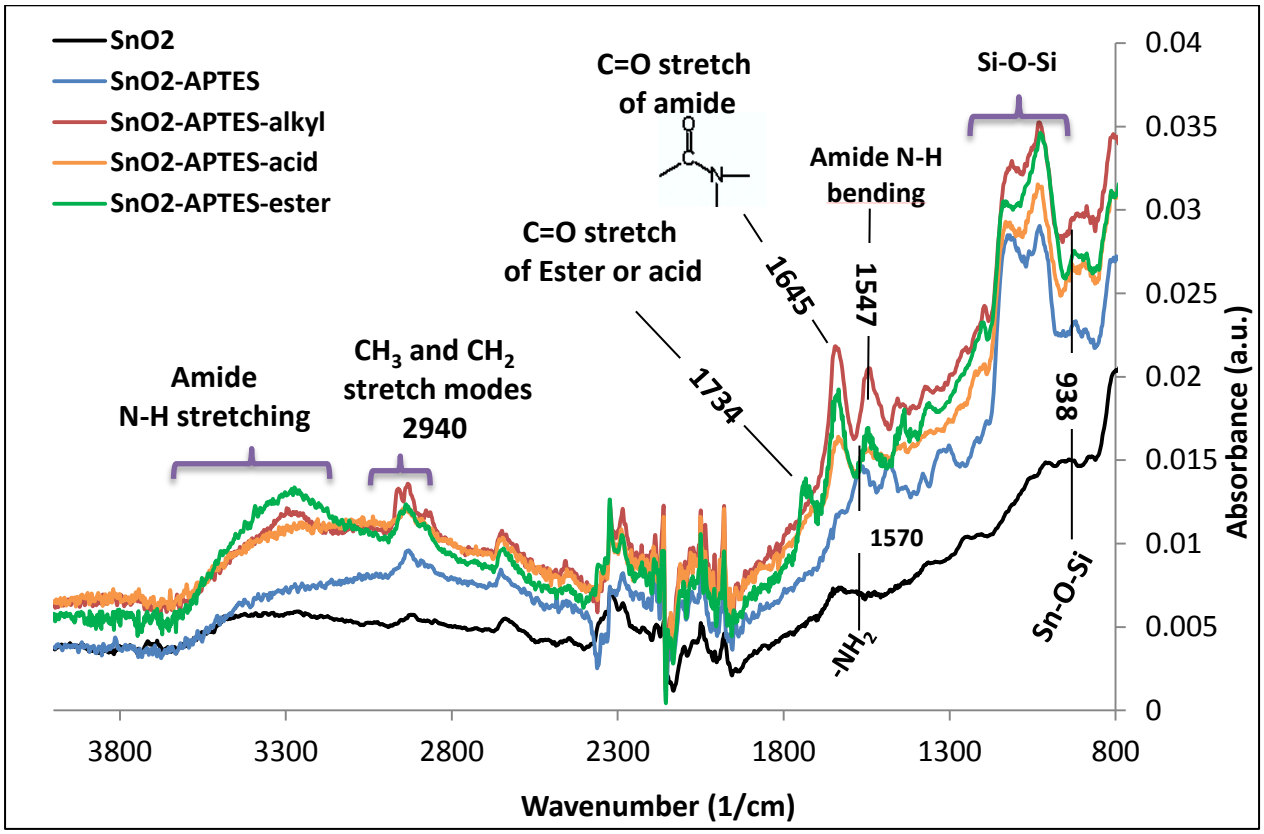

Figure 3-19. ATR-FTIR spectra of SnO_2 (black curve), SnO_2-APTES (blue curve), SnO_2-APTES-alkyl (red curve), SnO_2-APTES-acid (orange curve), and SnO_2-APTES-ester (green curve) films.

Alkyl, acid and ester modified SnO_2 (red, orange and green curves respectively) FTIR spectra exhibit two peaks at 1547 cm^{-1} and 1645 cm^{-1} which correspond to N-H bending mode and carbonyl stretch mode of amide respectively. An additional broad peak between ~ 3000 and ~ 3600 cm^{-1} corresponds to N-H stretch of amide. These peaks confirm the success of the reaction between amine group of APTES and acyl chloride group. In addition, the peak at 1570 cm^{-1} of SnO_2-APTES (blue curve) which relates to amine groups has totally disappeared. This confirms the formation of amide bond in place of amine. Asymmetrical C-H stretching mode of CH_3 for

SnO_2-APTES-alkyl and for SnO_2-APTES-ester appears at around 2940 cm^{-1}. The stretching peak of carbon double bounded to oxygen of ester group of SnO_2-APTES-ester is found at 1734 cm^{-1} (Figure 3-19, green curve).

The characterization of second modification step was also achieved by XPS analysis. These modifications increase the quantity of carbon on the surface and add carbon-based functional groups such as alkyl, acid and ester. Therefore, it is possible to detect these modifications by analyzing the changes in C 1s XPS peak. Figure 3-20 shows C 1s and Sn 3d peaks of SnO_2-APTES before and after modification by alkyl, acid and ester functional groups. As shown before (Figure 3-11a), the peaks present for SnO_2-APTES (Figure 3-20a) at 282.2, 284.9 eV and 286.4 eV were assigned respectively to C-Si, C-C/CH and C-N chemical bonds. The peak intensities may be different from previous test because the experiment was conducted in different incident angle (41°). These three peaks were found also for alkyl, acid and ester modified SnO_2-APTES at almost the same binding energy (Figure 3-20b, c, and d).

The areas under the peaks of C-Si and C-N after the second step of functionalization are the same as for SnO_2-APTES. This indicates that the APTES molecules were not dissociated during the second step. However, the area under the peak related to C-C/CH was 222 counts.eV.s^{-1} this increased after functionalization by alkyl, acid and ester as shown in Table 3-3. The increase in area is proportional to the increase in the quantity of C-C and C-H bond after the second step of functionalization. In addition to these peaks, alkyl, acid and ester modified SnO_2-APTES present a peak at around 288 eV which correspond to the formed amide bond (-N-COR; where R is the other part of molecule containing alkyl, acid or ester) by coupling reaction. Moreover, SnO_2-APTES-ester exhibits a peak at 289.1 eV which is related to the oxygen double bounded to the carbon of ester group (-$COOCH_3$, Figure 3-20d). Furthermore, Sn 3d peaks decrease after functionalization by APTES, APTES-alkyl, APTES-acid and APTES-ester (Figure 3-20e) compared to pure SnO_2, because it is covered by an organic film, as shown previously for the first step resulting in SnO_2-APTES formation. In addition, as the thickness of the organic film on SnO_2 increases, the intensity of Sn 3d peak decreases. Taking into account that XPS analyzes only 10 nm depth. For this reason, Sn 3d peak of APTES modified SnO_2 film was found with intermediate intensity between pure and alkyl, acid, and ester modified SnO_2 (Figure 3-20e, blue curve).

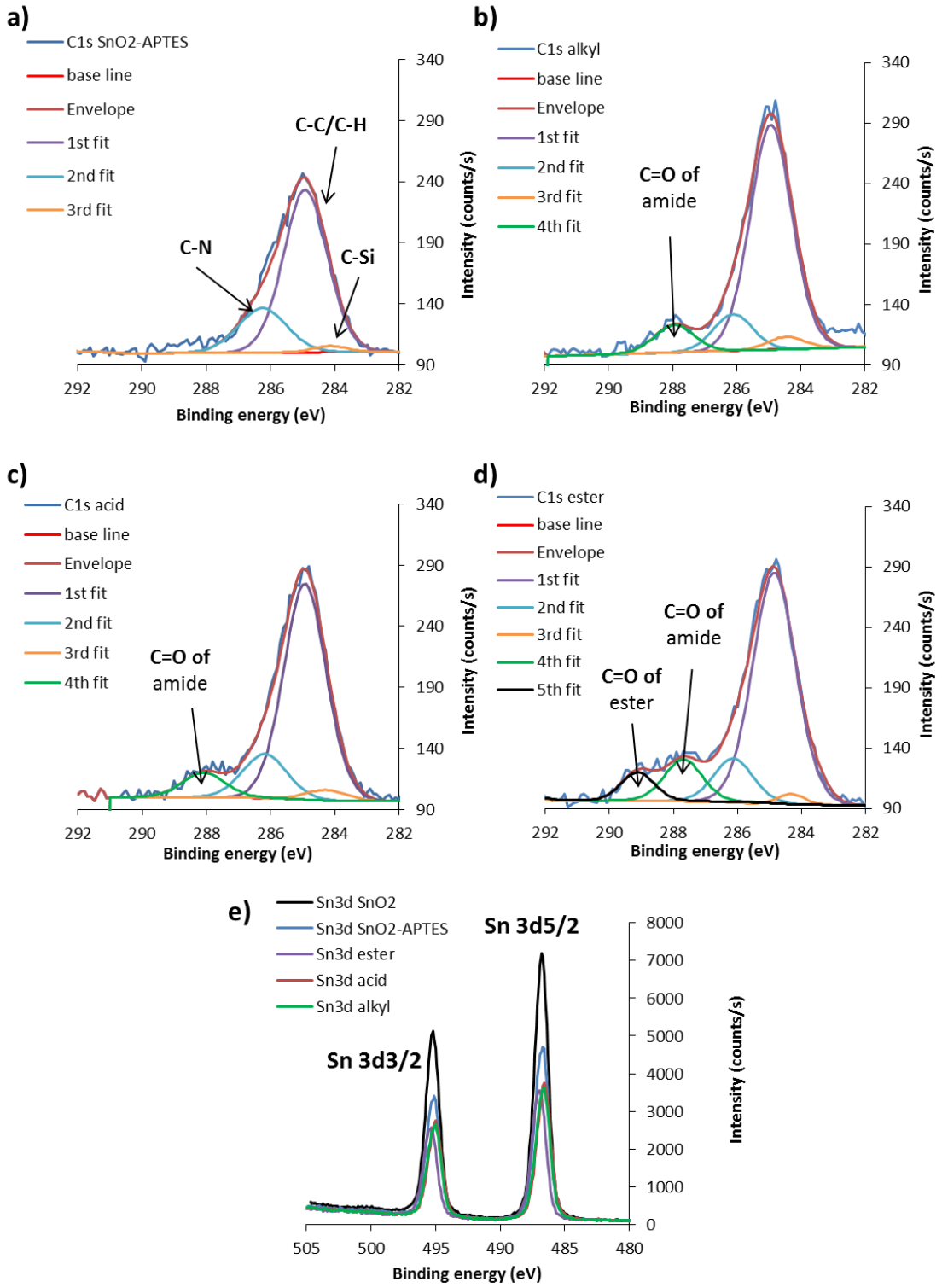

Figure 3-20. C 1s XPS spectra of SnO_2-APTES (a), SnO_2-APTES-alkyl (b), SnO_2-APTES-acid (c), SnO_2-APTES-ester (d). Sn 3d peaks of pure and modified SnO_2 by APTES, APTES-alkyl, APTES-acid and APTES-ester (e).

Table 3-3. The area under C-C/C-H component of C 1s peak found at 284.9 eV for the different functionalized SnO_2 sensors.

Sensor	Area of C-C/C-H peak (counts.eV.s^{-1})
SnO_2-APTES	222
SnO_2-APTES-alkyl	309
SnO_2-APTES-acid	296
SnO_2-APTES-ester	325

As a conclusion, FTIR and XPS analyses confirm that functionalization is effectively achieved on SnO_2-APTES after reaction with acyl chloride products by showing the presence of ester, acid and alkyl molecules.

3.10. Conclusion

Screen printed SnO_2 films exhibit particles size about 80 nm with random shapes and about 40 µm films thickness. These films were successfully functionalized by APTES via vapor and liquid phases. A comparison between the synthesis conditions was achieved. Liquid phase silanization with water clearly demonstrates more APTES grafting than vapor and liquid phase silanizations without water. Water during the liquid phase silanization enhances the polymerization of APTES on the surface. Interestingly, 4 h reaction and 50 mM were found to be sufficient to well cover SnO_2 film by APTES molecules. No larger APTES amounts or longer times are necessary. Furthermore, thermal treatment of APTES film on SnO_2-APTES shows that the APTES start to degrade at temperature above 100 °C, while no notable change in the amount of silicon between 100 °C and 500 °C is observed. Amine groups have totally disappeared after heating the film at 500 °C. We have calculated the concentration of APTES by calculating the amount of Si on the surface. The number of Si atoms of SnO_2-APTES synthesized by liquid without water and vapor silanization is respectively 4.24×10^{14} atoms.cm^{-2} and 4.7×10^{14} atoms.cm^{-2}, while it is 9×10^{14} atoms.cm^{-2} with the addition of 5 vol% H_2O. In addition, the concentrations of grafted APTES determined by XPS analyses are in good agreement with ATR-FTIR results which confirm that the liquid route in the presence of water leads to more APTES grafting onto SnO_2 with an almost 50% improvement. The optimum SnO_2-APTES film was used to attach the desired end

functional groups on it. ATR-FTIR and XPS prove that SnO_2-APTES is well modified by ester, acid and alkyl end functional groups. The change in sensitivity and selectivity of these sensors to gases will be investigated in the next chapter.

References

[1] M. Le, C. Jimenez, E. Chainet, V. Stambouli, A Label-Free Impedimetric DNA Sensor Based on a Nanoporous SnO_2 Film: Fabrication and Detection Performance, Sensors. 15 (2015) 10686–10704.

[2] V. Bukauskas, Effect of thickness of ultra-thin tin oxide film based gas sensors, Lith. J. Phys. 47 (2007) 475–483.

[3] S. Fiorilli, P. Rivolo, E. Descrovi, C. Ricciardi, L. Pasquardini, L. Lunelli, L. Vanzetti, C. Pederzolli, B. Onida, E. Garrone, Vapor-phase self-assembled monolayers of aminosilane on plasma-activated silicon substrates, J. Colloid Interface Sci. 321 (2008) 235–241.

[4] I. Matsubara, K. Hosono, N. Murayama, W. Shin, N. Izu, Organically hybridized SnO_2 gas sensors, Sens. Actuators B Chem. 108 (2005) 143–147.

[5] G. Tan, L. Zhang, C. Ning, X. Liu, J. Liao, Preparation and characterization of APTES films on modification titanium by SAMs, Thin Solid Films. 519 (2011) 4997–5001.

[6] C.-H. Chiang, H. Ishida, J.L. Koenig, The structure of γ-aminopropyltriethoxysilane on glass surfaces, J. Colloid Interface Sci. 74 (1980) 396–404.

[7] J. Kim, P. Seidler, L.S. Wan, C. Fill, Formation, structure, and reactivity of amino-terminated organic films on silicon substrates, J. Colloid Interface Sci. 329 (2009) 114–119.

[8] K. Wen, R. Maoz, H. Cohen, J. Sagiv, A. Gibaud, A. Desert, B.M. Ocko, Postassembly Chemical Modification of a Highly Ordered Organosilane Multilayer: New Insights into the Structure, Bonding, and Dynamics of Self-Assembling Silane Monolayers, ACS Nano. 2 (2008) 579–599.

[9] N. Rozlosnik, M.C. Gerstenberg, N.B. Larsen, Effect of solvents and concentration on the formation of a self-assembled monolayer of octadecylsiloxane on silicon (001), Langmuir. 19 (2003) 1182–1188.

[10] B. Wang, J.C. Cancilla, J.S. Torrecilla, H. Haick, Artificial Sensing Intelligence with Silicon Nanowires for Ultraselective Detection in the Gas Phase, Nano Lett. 14 (2014) 933–938.

[11] V. Stambouli, M. Labeau, I. Matko, B. Chenevier, O. Renault, C. Guiducci, P. Chaudouët, H. Roussel, D. Nibkin, E. Dupuis, Development and functionalisation of Sb doped SnO_2 thin films for DNA biochip applications, Sens. Actuators B Chem. 113 (2006) 1025–1033.

[12] S.P. Pujari, L. Scheres, A.T.M. Marcelis, H. Zuilhof, Covalent Surface Modification of Oxide Surfaces, Angew. Chem. Int. Ed. 53 (2014) 6322–6356.

[13] R.M. Pasternack, S. Rivillon Amy, Y.J. Chabal, Attachment of 3-(Aminopropyl)triethoxysilane on Silicon Oxide Surfaces: Dependence on Solution Temperature, Langmuir. 24 (2008) 12963–12971.

[14] S. Tougaard, QUASES: Software for Quantitative XPS/AES of Surface Nano-structures by Analysis of the Peak Shape and Background (version 5.0), QUASES-Tougaard Inc Odense Den. www.quases.com. (2003).

[15] S. Tougaard, Universality Classes of Inelastic Electron Scattering Cross-sections, Surf. Interface Anal. 25 (1997) 137–154.

[16] S. Tanuma, C.J. Powell, D.R. Penn, Calculations of electron inelastic mean free paths (IMFPS). IV. Evaluation of calculated IMFPs and of the predictive IMFP formula TPP-2 for electron energies between 50 and 2000 eV, Surf. Interface Anal. 20 (1993) 77–89.

[17] P.J. Cumpson, Estimation of inelastic mean free paths for polymers and other organic materials: use of quantitative structure–property relationships, Surf. Interface Anal. 31 (2001) 23–34.

[18] J. Bicerano, "Prediction of polymer Properties", (2nd edn), Marcel Dekker: New York, 1996.

[19] B. Wang, H. Haick, Effect of Functional Groups on the Sensing Properties of Silicon Nanowires toward Volatile Compounds, ACS Appl. Mater. Interfaces. 5 (2013) 2289–2299.

Chapter 4. Electrical characterization of pure and functionalized SnO_2 sensors

4.1. Introduction

As mentioned before, tin dioxide material allows the detection of many gaseous compounds. Nevertheless, the SnO_2-based sensors suffer from two major drawbacks which constitute an obstacle to their development:

- Lack of selectivity because SnO_2 sensitive material has a high affinity with many gases.
- High operating temperature between 250 °C and 600 °C.

The aim of the molecular functionalization performed in this work was to cover these blocking points by elaboration of a sensitive and selective sensor operating at low temperature. Functionalization was performed to optimize the interactions of sensors with ammonia gas. Molecular modification passivates the surface states on SnO_2 sensors by molecular layer containing a specific functional group. These functional groups can interact specifically with gases depending on their polarities as shown by Hossam Haick et al. [1]. They reported a silicon nanowire sensor functionalized with nonpolar end functional group to improve the detection of nonpolar gas. Other silicon nanowire sensors were modified by polar end functional groups to improve the detection of polar gases.

In the present work, we focus on the change in sensitivity and selectivity of SnO_2 sensors to ammonia after functionalization. Three SnO_2 sensors were coated with molecules having mostly polar (functional) side groups which are amine (APTES), acid (COOH), and ester ($COOCH_3$) and one SnO_2 sensor was coated with molecules having mostly nonpolar side group which is alkyl (CH_3). The sensors are firstly functionalized by APTES followed by covalent attachment of alkyl, acid or ester end functional groups molecule. The detection performances of resulting sensors are investigated in regards of ammonia detection. The changes in the response of the modified sensors were compared with pure SnO_2. Such sensor will be used for the detection of ammonia in the human breath which contains high amount of water vapor. For this reason, the effect of water vapor on the sensors performance was investigated. In addition, the selectivity was tested with respect to ethanol, acetone and carbon monoxide gases. Another objective is to reduce the power

consumption by decreasing the operating temperature, since the sensor will be used later for smart devices and portable applications.

4.2. Conditioning of the sensor

Ester modified SnO_2-APTES sensor has showed the best performance among all the functionalized sensors regarding the detection of ammonia as we will show later in this chapter. This sensor is operated preferentially at 25 °C in air with 5%RH to be a tool for breath analysis.
The modification by ester end functional groups was carried out on SnO_2-APTES synthesized by hydrous liquid (5 vol% H_2O) silanization. This silanization produces a denser APTES film than the others (vapor and anhydrous liquid silanization) as shown in chapter 3. After this process, the films were annealed in the oven to desorb the unreacted molecules (not fixed) as well as the water from the film. The next step was the reaction of APTES film with acyl chloride products. Here, the annealing after the reaction was performed in-situ to control its effect on the response to ammonia. In addition, the needed time to clean the film from unreacted molecules and other physisorbed species in the film can be estimated. Annealing was carried out in-situ at 100 °C for different times. The effect of annealing was noticed on the stability of response to ammonia at 25 °C. Figure 4-1 shows the normalized response of SnO_2-APTES-ester (a) and SnO_2 (b) to ammonia at 25 °C, pre-heated at 100 °C under air with 5%RH for different times. SnO_2-APTES-ester presents different responses to 50 ppm of ammonia depending of the time of pre-heating. For SnO_2-APTES-ester without heating and heated for 5 min, decrease in conductance was observed. However, after heating 30 min, increase in conductance was noticed. In addition, the response value increases with increase of pre-heating time until 9.5 h. At this level, stable response and base line were remarked. In contrast, SnO_2 shows no changes in the response to 50 ppm of ammonia gas after heating for different times. SnO_2 shows decrease in conductance upon exposure to ammonia with and without pre-heating. Noise in the curve can be due to the limit of the electrical measurements. These results indicate that SnO_2 and SnO_2-APTES-ester without or with short-pre-heating (5 min) give a negative response (conductance decrease) to ammonia. The fact that the response becomes positive (conductance increase) for SnO_2-APTES-ester with longer heat treatment, but remain unchanged for SnO_2, reveals that the treatment affects SnO_2-APTES-ester surface by modifying reactive species.

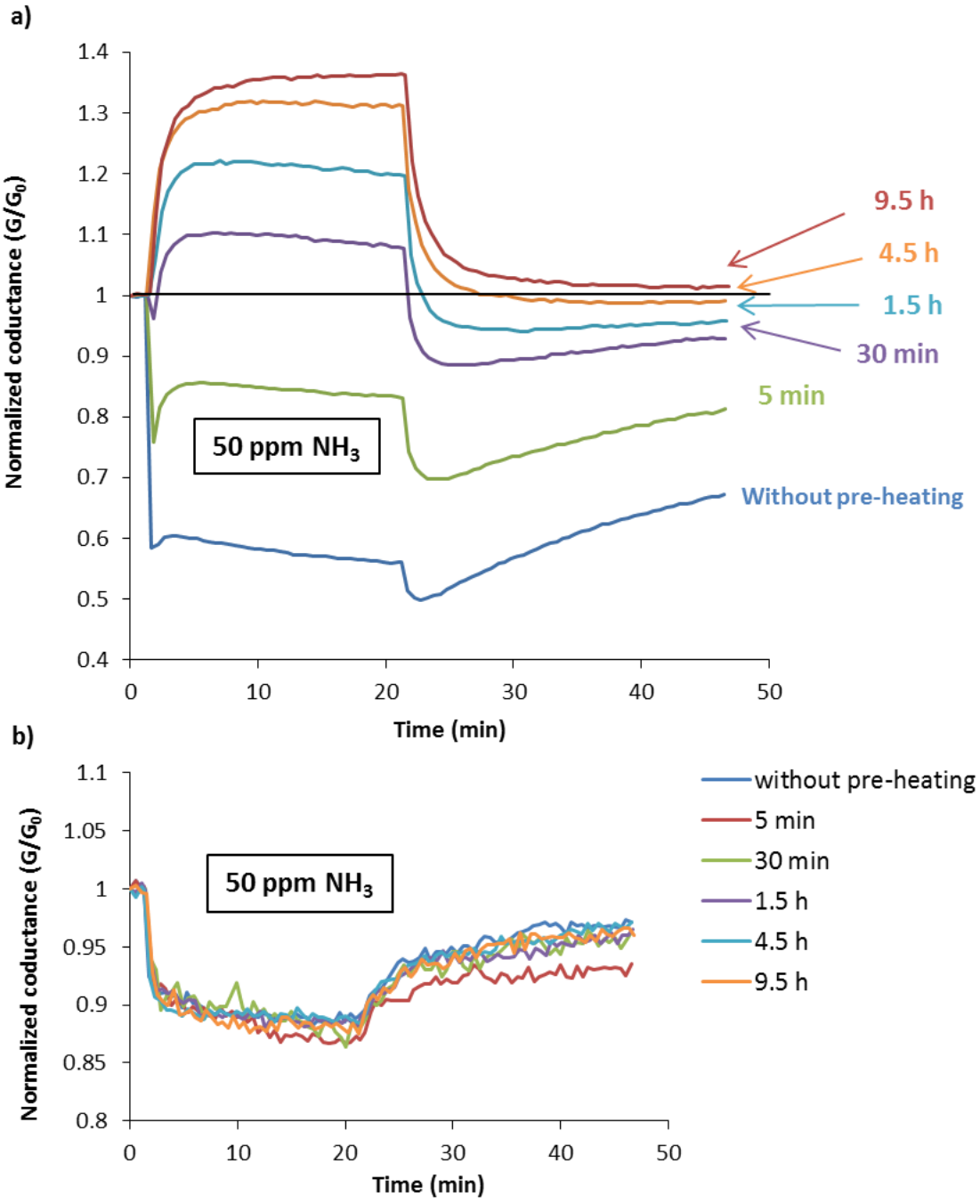

Figure 4-1. Normalized conductance of SnO_2-APTES-ester (a) and SnO_2 (b) sensor upon exposure to 50 ppm of ammonia at 25 °C just after the synthesis (without pre-heating) and after heating at 100 °C for 5 min, 30 min, 1.5 h, 4.5 h, and 9.5h. The test was carried out in air with 5 %RH.

This process adjusts the polarity of the ester film on SnO_2 and changes the dipole moment as well as the response to ammonia. This indicates that the sensors should be heated at least 9.5 h to remove the adsorbed species from SnO_2-APTES-ester surface and to obtain stable response. The interaction mechanism of ammonia with SnO_2 and SnO_2-APTES-ester sensors will be studied in the following discussion.

The desorption of the trapped species including water, unreacted APTES or acyl chloride in the organic film was checked by ATR-FTIR. Figure 4-2 shows the ATR-FTIR spectra of SnO_2-APTES-ester sensor before and after heating 10 h at 100 °C. With respect to APTES, the peaks related to Si-O-Sn and Si-O-Si bonds still exist after the thermal treatment with almost the same intensities. The little change in intensity after heating of the peak at 1029 cm^{-1} is due to the polymerization of unreacted hydroxysilane groups of APTES film. The other groups which are related to the second step of molecularly modifications such as amide, ester, CH_2, and CH_3 are retained after thermal treatment. However, the intensity of these peaks are less than that without heating at 100 °C because of the desorption of unreacted molecules (acyl chloride). Therefore, the thermal treatment of the sensors does not affect the safety of the grafted organic film.

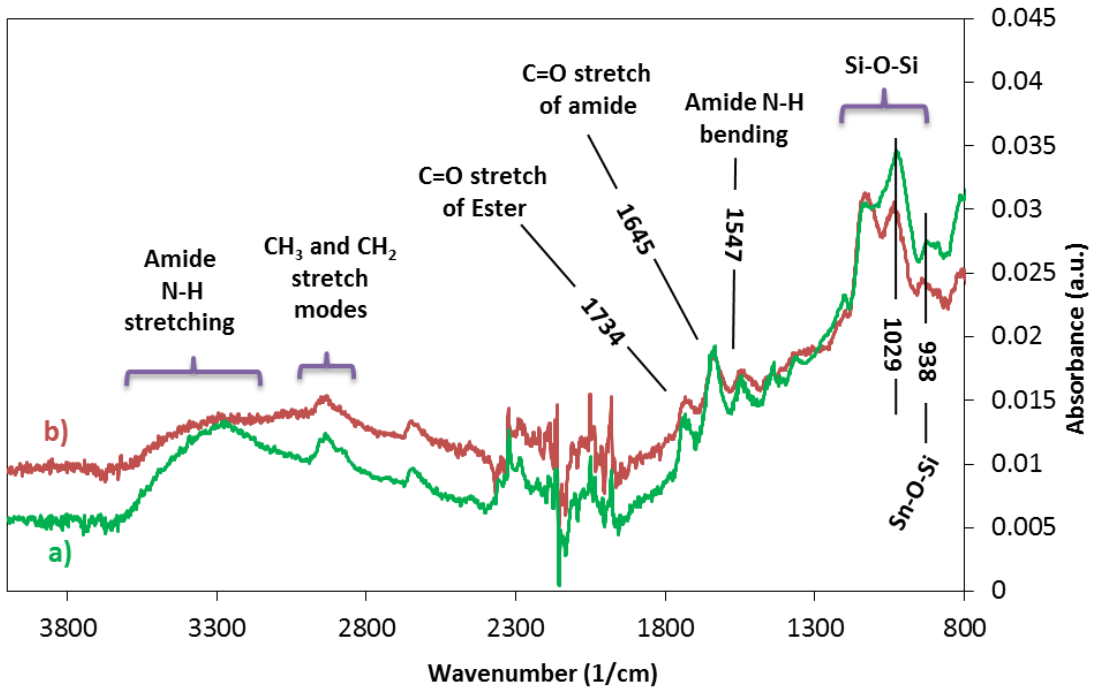

Figure 4-2. ATR-FTIR spectra of SnO_2-APTES-ester before (a) and after heating in-situ (in test bench) for 10 h in air with 5%RH (b).

4.3. Sensing measurements of the different functionalized SnO_2 sensors

The previous discussions have shown that SnO_2 sensors are well functionalized by APTES, APTES-alkyl, APTES-acid and APTES-ester. In addition, we have shown that the conditioning of functionalized sensor at 100 °C does not damage the grafted film. Now the test under gases can be achieved. For the entire test under gas shown in this section, the sensors were heated in-situ for 10 h at 100 °C. The sensors operated at 25 °C in air with 5 %RH.

4.3.1. Response of the different sensors towards ammonia

The first part of the test under gases was to show the characteristic of the response of different sensors to ammonia gas. As shown in Figure 4-3, the sensors were tested to 100 ppm of ammonia balanced with 5% RH air at 25 °C. Figure 4-3 (red curve) shows that the conductance of pure SnO_2 decreases upon exposure to ammonia gas. This type of response has been found before by Kamalpreet Khun Khun et al. [2] at temperature between 25 to 200 °C. They have supposed that ammonia reacts with molecular adsorbed oxygen ion (O_2^-, created as shown in equation (32)) producing nitrogen monoxide gas (NO) according to equation (33). In presence of oxygen, NO can be easily transformed into NO_2 especially at low temperature (equation (34)). The reaction of NO_2 with SnO_2 at ambient temperature causes the decrease of sensor conductance because NO_2 is a good oxidizing agent. NO_2 adsorbs on SnO_2 surface adsorption sites (s) and bring out electrons from the conduction band (equation (35)) [3]. Thus, the overall reaction of ammonia with SnO_2 at room temperature can be written as in equation (36). Therefore, this reaction confirms the obtained results because the conductance was actually decreased when SnO_2 sensor is exposed to ammonia. In addition, the abundant species adsorbed on SnO_2 surface at room temperature are the hydroxyl groups. This explains the measurable conductance base line under air balanced with 5%RH of pure SnO_2 [4].

$$O_2 + s + e^- \rightarrow s\text{-}O_2^- \quad (32)$$

$$4NH_3 + 5s\text{-}O_2^- \rightarrow 4NO + 6H_2O + 5s + 5e^- \quad (33)$$

$$2NO + O_2 \leftrightarrow 2NO_2 \quad \text{(equilibrium in air)} \tag{34}$$

$$NO_2 + s + e^- \rightarrow s\text{-}NO_2^- \tag{35}$$

$$4NH_3 + 4s + 7O_2 + 4e^- \rightarrow 4s\text{-}NO_2^- + 6H_2O \tag{36}$$

Where s is an adsorption site.

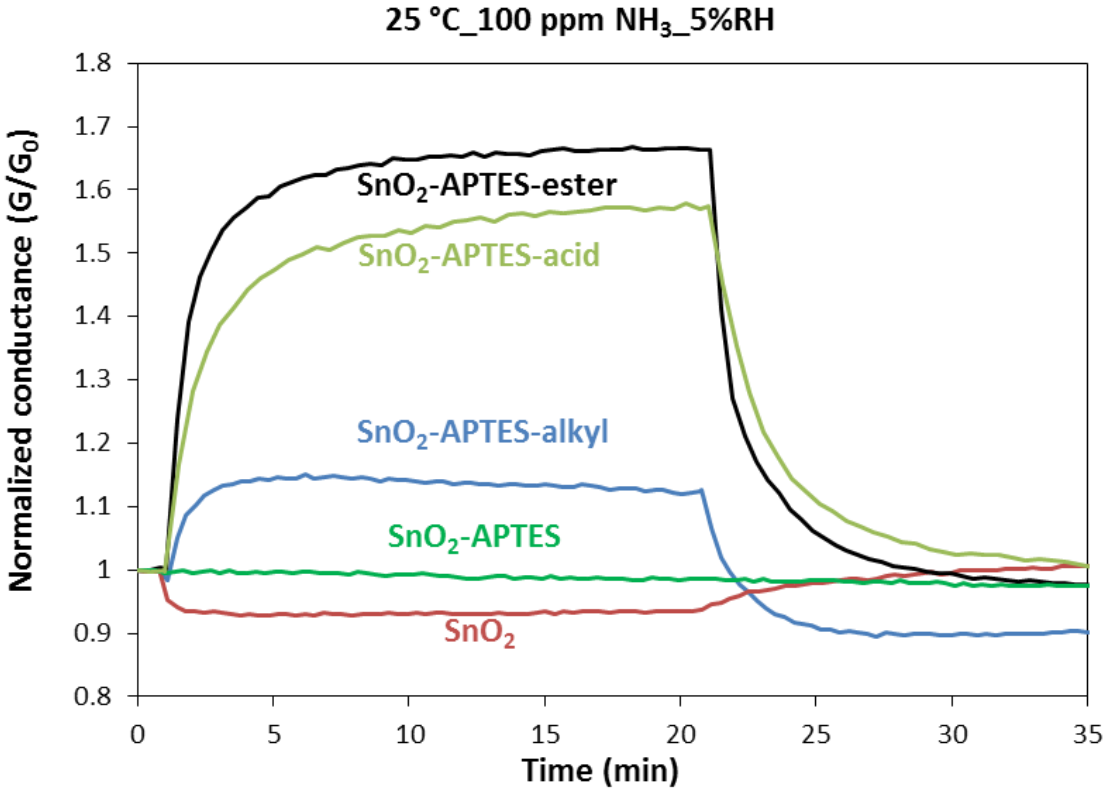

Figure 4-3. The sensor response of SnO_2 (G_0=1.4×10^{-5}), SnO_2-APTES (G_0=7.9×10^{-6}), SnO_2-APTES-alkyl (G_0=1.5×10^{-5}), and SnO_2-APTES-ester (G_0=9.5×10^{-6}) to 100 ppm ammonia gas balanced with humid air (5%RH) at 25 °C.

From Figure 4-3, it is observed that functionalized SnO_2 sensors do not respond in the same direction as pure SnO_2. The next discussion is focused on explanations of the sensing mechanism of functionalized sensors to ammonia.

APTES modified SnO_2 sensor present no change in conductance upon exposure to 100 ppm of ammonia (Figure 4-3, dark green curve). Formation of APTES film on SnO_2 prevents the water

molecules to adsorb on the surface because the active sites of SnO_2 are occupied by O-Si bond of APTES, and because of the hydrophobic nature of APTES film. Therefore, in the following discussion, the conventional mechanism of interaction of SnO_2 with gases cannot be taken in consideration. For example, the interactions with adsorbed oxygen species and the production of NO_x cannot take place in this case. SnO_2-APTES shows no response to ammonia (Figure 4-3). This implies that no significant interactions occur between the grafted APTES and ammonia gas. In term of polarity and other chemical properties like acidity, the amine and ammonia groups are almost the same, since amine is one of the derivatives of ammonia. In addition, this behavior indicates that the SnO_2 surface is well covered by APTES molecules because the negative response observed on pure SnO_2 is totally inhibited.

SnO_2-APTES-alkyl, SnO_2-APTES-acid and SnO_2-APTES-ester exhibit increase in conductance upon exposure to 100 ppm of ammonia gas as shown in Figure 4-3. However, the response of SnO_2-APTES-ester and SnO_2-APTES-acid are more important than for SnO_2-APTES-alkyl. These responses could be related to the different polarities of the attached end functional groups. Ester and acid are electron withdrawing groups, while alkyl is mostly considered as nonpolar. Ammonia molecule is a nucleophilic molecule (donating). Regarding the interactions between electron withdrawing groups from one side (ester and acid) and electron donating group (ammonia) in from the other side, dipole-dipole interaction is taking place. On the contrary, in the case of SnO_2-APTES-alkyl, the interaction is of induced dipole type because ammonia is a polar molecule and alkyl end group is mostly nonpolar as presented in Figure 4-4. It was reported before by B. Wang et al. [5], that the dipole-dipole interaction is always stronger than induced dipole interaction. This can explain the difference in the response between SnO_2-APTES-ester, SnO_2-APTES-acid and SnO_2-APTES-alkyl sensors to ammonia gas. These two types of interactions (i.e. dipole-dipole and induced-dipole) result in a modification in the dipole moment of the whole film. The variation in the molecular layer's dipole moment affects the electron mobility in SnO_2 film which modifies the conductance [6,7]. The exposure to ammonia leads to increase in electron mobility (proportional to conductance). The same behavior was found for a selection of polar and non-polar gases but on alkyl, acid and ester silicon oxide functionalized substrate [5]. Since the dipole-dipole interaction is stronger than the induced dipole interaction, adsorption of ammonia on ester and acid end groups lead to larger change in conductance than on alkyl one. But we can also mention that the interaction can also result from diffusion of the gas in

the molecular layer. This type of interaction is favorable only for SnO_2-APTES-alkyl. It is difficult for ammonia molecules to diffuse in the molecular layer of SnO_2-APTES-ester as well as SnO_2-APTES-acid, because of the steric hindrance induced by ester and acid end groups. This phenomenon can explain the response of SnO_2-APTES-alkyl to ammonia in addition to the induced dipole interaction.

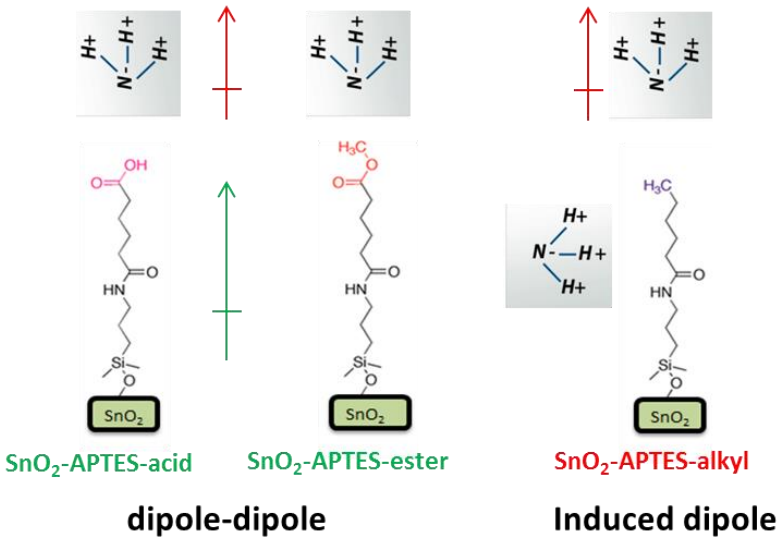

Figure 4-4. Schematic illustration of the interaction between ammonia and alkyl, acid and ester functionalized SnO_2-APTES sensors.

According to the above discussion, the response of the molecular modified sensors does not obey the conventional mechanism of direct interaction with SnO_2. The response comes mainly from the interaction of ammonia molecules with end function group of the attached layer. The response of SnO_2-APTES-ester and SnO_2-APTES-acid is generated from dipole-dipole interaction, while the response of SnO_2-APTES-alkyl is produced from induced dipole interaction which has less significant effect (Figure 4-4).

4.3.2. Sensitivity

Regarding the different sensors sensitivity against ammonia concentrations, Figure 4-5 shows the relative responses versus ammonia concentrations of SnO_2-APTES-ester and SnO_2-APTES-acid in comparison with pure SnO_2, SnO_2-APTES and SnO_2-APTES-alkyl sensors. Sensitivity is defined as the slope of the relative response curve versus ammonia concentrations, i.e., how large

is the change in the sensor signal upon a certain change in ammonia concentration. Pure SnO_2 and SnO_2-APTES sensors have almost no sensitivity to different ammonia concentrations. In addition, SnO_2-APTES-alkyl gives no significant response between 0.2 ppm and 30 ppm, but its sensitivity starts to increase from 30 ppm of ammonia. It can be noticed that SnO_2-APTES-ester and SnO_2-APTES-acid exhibit constant sensitivity between 0.2 ppm and 10 ppm, around 0.023 ppm^{-1}. For higher concentration, the response is no more linear and the sensitivity continuously decreases down to nearly zero at 100 ppm of ammonia. This means that the sensors reach a saturation state. The saturation state can be interpreted as the state where attached layer reaches a maximum value of dipole moment. However, the sensitivity of SnO_2-APTES-ester and SnO_2-APTES-acid at concentrations higher than 30 ppm is still more significant than the sensitivity of SnO_2-APTES-alkyl. These results confirm the above discussion which assumes that SnO_2-APTES-ester and SnO_2-APTES-acid have the strongest interactions among the functionalized sensors toward ammonia. The response at low concentrations and the standard deviation of the base line over 10 min were used to calculate the limit of detection (LOD) of the ester and acid modified SnO_2 sensors to ammonia gas which is around 80 ppb. This value confirms the potentiality of ammonia detection for breath analysis application, as concentrations to detect are in the range of ppb.

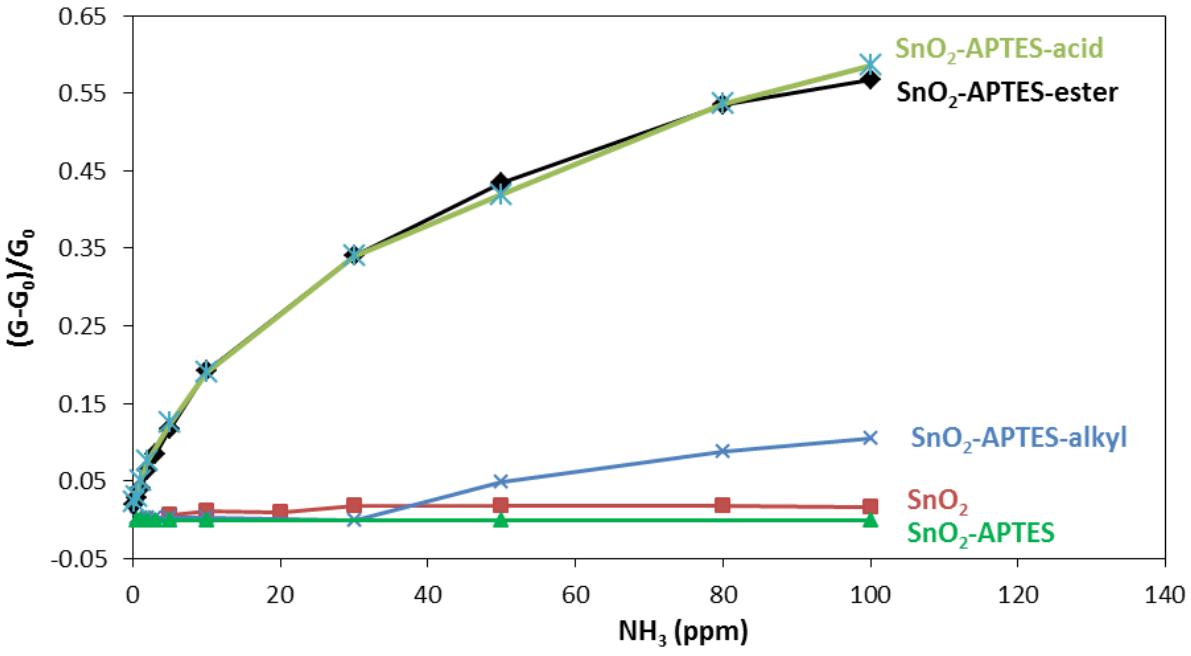

Figure 4-5. Relative response of pure SnO_2, SnO_2-APTES, SnO_2-APTES-alkyl, SnO_2-APTES-acid, and SnO_2-APTES-ester sensors versus ammonia concentrations balanced with 5% RH air at 25 °C.

To summarize this section, SnO_2-APTES-ester and SnO_2-APTES-acid sensors showed good sensitivity to ammonia gas in a range of concentration compatible with breath analysis applications (sub-ppm). These two sensors are studied in more details in the following parts.

4.4. Focus on SnO_2-APTES-ester and SnO_2-APTES-acid sensors

4.4.1. Effect of humidity

As known, human breath contains high amount of humidity (100 %RH at 37 °C). Water molecule presents high polarity, hence it can affect the response to ammonia gas. In order to check this effect, SnO_2-APTES-ester and SnO_2-APTES-acid were tested to ammonia gas under different amount of relative humidity ranging from 5 to 50% RH. Figure 4-6 shows the sensor responses of SnO_2-APTES-ester and SnO_2-APTES-acid to 50 and 100 ppm in dry and humid air at 25 °C. Upon exposure to ammonia gas the sensors conductance increases in the all cases (the two sensors, dry air, 5%RH, 26%RH, and 50%RH). As shown in Figure 4-6a and b, the response and recovery times decrease with the increase of the relative humidity percentage for the two sensors. In dry air and 5%RH, SnO_2-APTES-ester (Figure 4-6a) shows almost the same response magnitude, 1.3 for 50 ppm of ammonia, which decreases to 1.14 and 1.04 in 26%RH and 50%RH respectively. Decrease in response was also observed for SnO_2-APTES-acid (Figure 4-6b) to 50 ppm ammonia by addition of 5%RH (decrease from 1.68 to 1.59).This means that a small quantity of relative humidity does not affect the sensor response, while at elevated amount the response starts decrease significantly. A potential explanation is that the attached ester or acid films are saturated by water molecules or adsorbed hydroxyl groups at high RH. Hence, during exposure to ammonia, there is a limitation of response due to adsorption competition between water and ammonia.

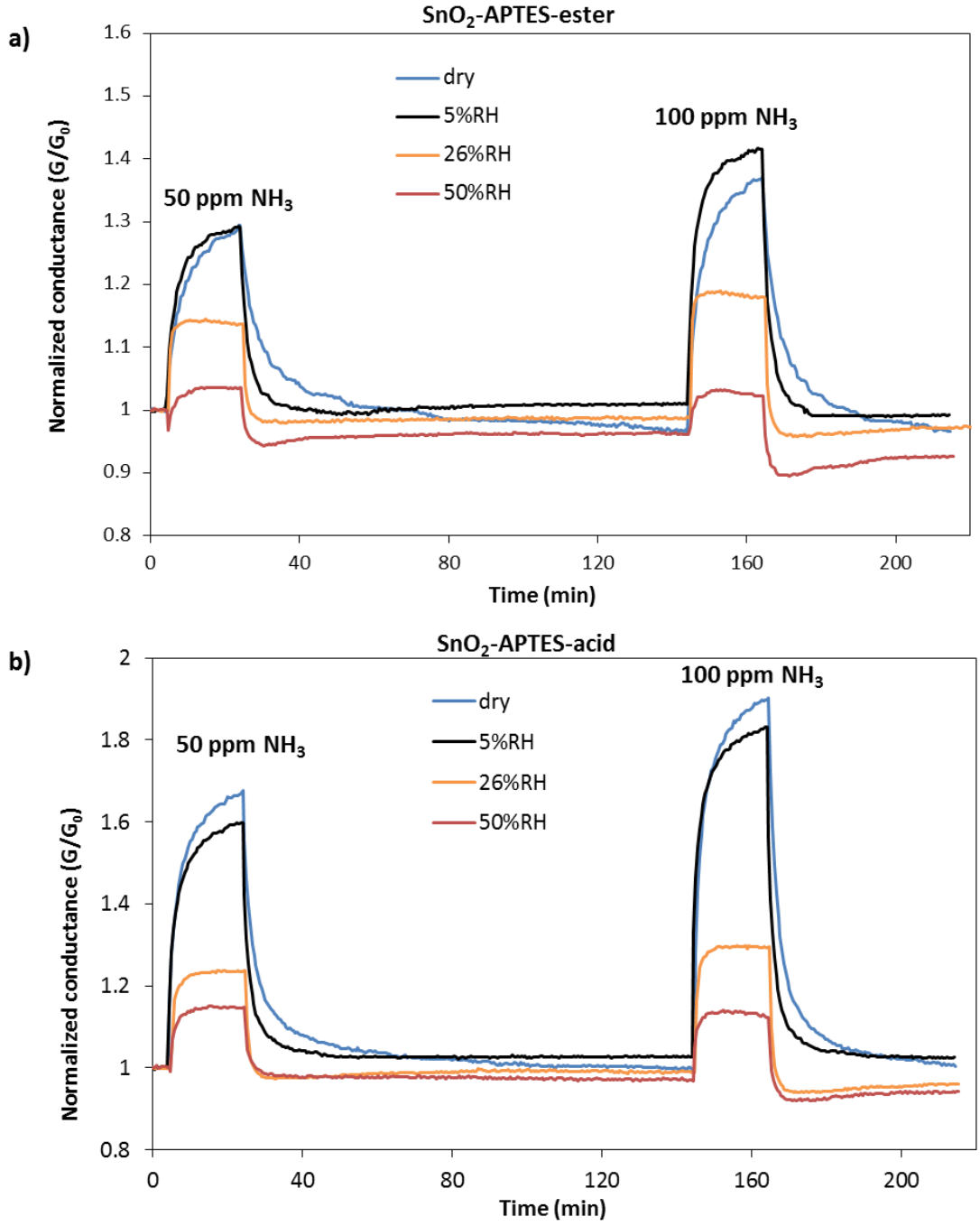

Figure 4-6. The sensor response curves of a) SnO_2-APTES-ester and b) SnO_2-APTES-acid sensors to 50 and 100 ppm of ammonia gas balanced with dry air, 5%RH, 26%RH, and 50%RH at 25 °C.

To better understand the effect of water, Figure 4-7a and b show the response of SnO_2-APTES-ester and SnO_2-APTES-acid sensors respectively to different relative humidity percentage at 25 °C in dry air. SnO_2-APTES-ester exhibits almost no change in conductance to 5%RH while SnO_2-APTES-acid shows increase in conductance. These responses explain the fact that SnO_2-

APTES-ester has the same response to ammonia in dry or 5%RH in contrast to SnO_2-APTES-acid. In addition, the conductance of the two sensors increases with the increase of the relative humidity percentage starting from 5%RH as shown for 26 and 50%RH responses. Water causes variation in the dipole moment in the same sense of ammonia, since water molecule is polar. As for ammonia, the injection of water cause increase in conductance. Thus, the presence of water in air increases the base line of the sensor which can hide the response to ammonia.

As mentioned, ester and acid modified SnO_2 start to attain a saturation level at 100 ppm of ammonia as shown in Figure 4-5. Water molecules assist the sensors to reach the saturation by increasing the dipole moment of the attached molecular layer. For this reason the response to ammonia decreases with the increase of relative humidity.

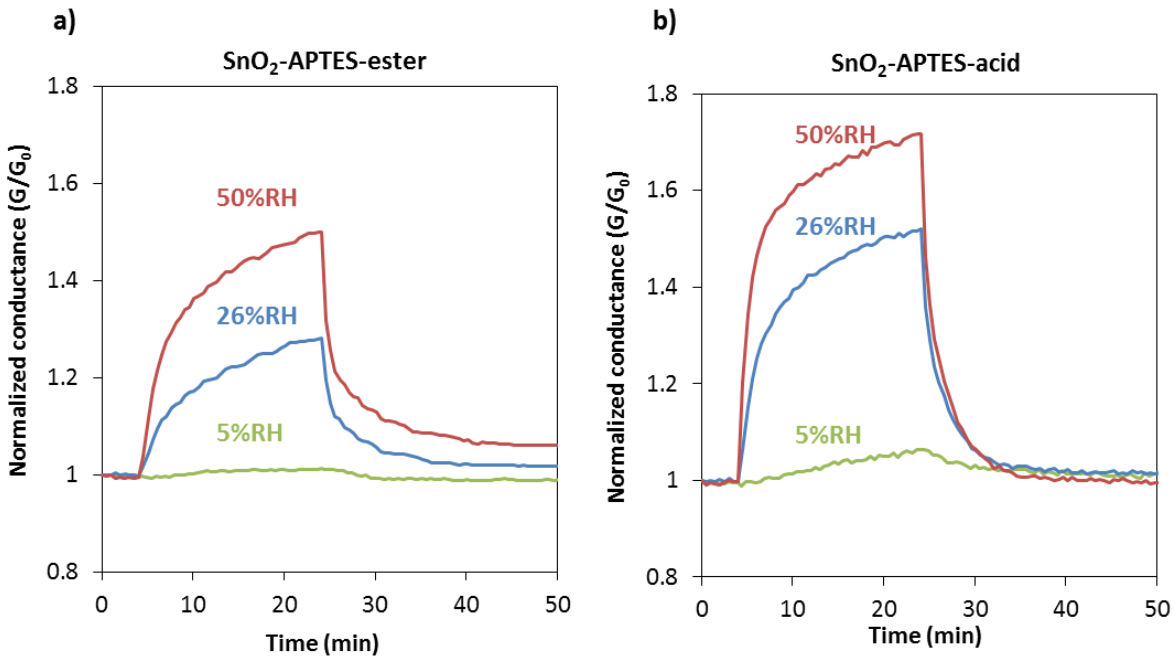

Figure 4-7. The response of a) SnO_2-APTES-ester and b) SnO_2-APTES-acid to different percentage of relative humidities at 25 °C in dry air.

In these conditions, 5%RH at 25 °C, the response and recovery times (as defined in chapter 1) are around 98 s and 130 s respectively for the two sensors, which is quite noticeable for a tin oxide based sensors working at room temperature. For the future tests, the humidity will be kept at 5%RH.

4.4.2. Effect of operating temperature

In the most cases, the increase of the operating temperature of SnO_2 sensors increases the sensitivity to gases. In order to evaluate the influence of the temperature on functionalized sensors performance, acid and ester modified SnO_2-APTES sensors were operated at different temperature (25 °C, 50 °C and 100 °C) and the response to ammonia was recorded. As shown in Figure 4-8, the response of SnO_2-APTES-ester to ammonia decreases from 1.47 (25 °C) to 1.18 and 1.06 when the operating temperature is increased to 50 °C and 100 °C respectively (Figure 4-8a). The same behavior was found for SnO_2-APTES-acid, the response to ammonia decreases from 1.42 (25 °C) to 1.17 and 1.02 when the operating temperature is increased to 50 °C and 100 °C respectively (Figure 4-8b). Therefore, the interaction of ammonia with ester or acid attached to SnO_2 is more significant at low temperature (25 °C) than at higher one (50 and 100 °C).

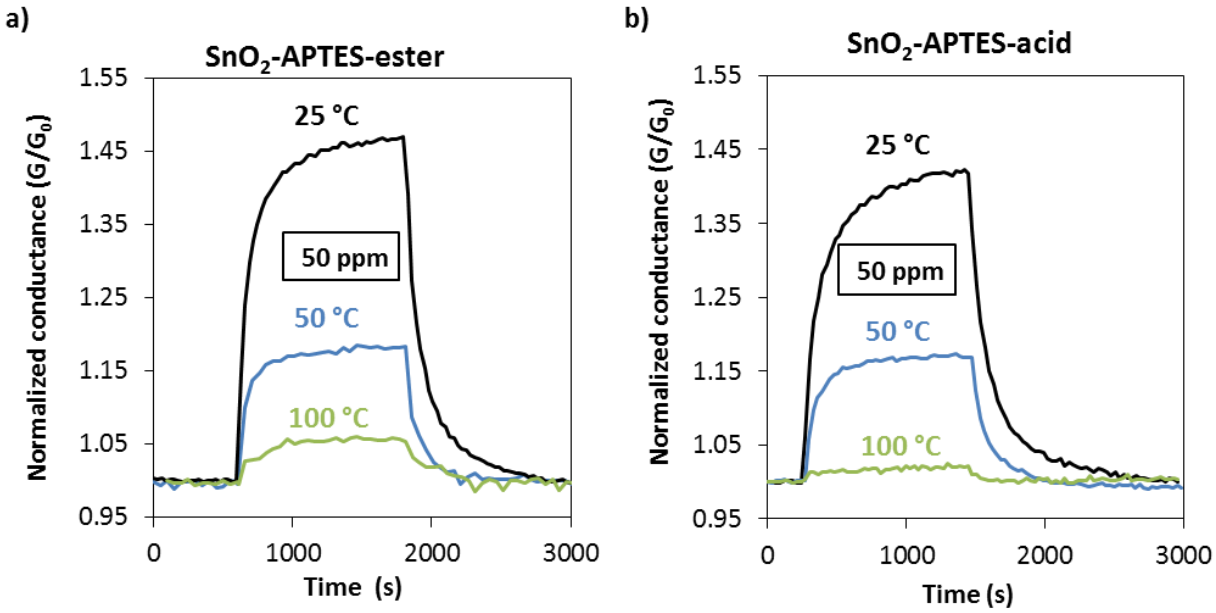

Figure 4-8. The sensor response of SnO_2-APTES-ester (a) and SnO_2-APTES-acid (b) to 50 ppm of ammonia gas balanced with humid air (5%RH) at 25 °C, 50 °C, and 100 °C.

These changes in the response to ammonia at different operating temperature are generated from the effect of temperature on the dipole moment as reported by Vera Doron et al [8]. The increase in temperature changes the dipole moment value in the same sense as the effect of ammonia (increase in conductance, showed experimentally). A hypothesis can be drawn to explain the

decrease in the response to ammonia when the sensor operating temperature increases as demonstrated in Figure 4-9. The dipole moment, illustrated as a vector in green, increases with the increase of operating temperature. The molecular layer reaches almost maximum dipole moment value at 100 °C (Figure 4-9a). This increase in the dipole moment increases the conductance base line of the sensor. At 100 °C, the dipole moment reaches a maximum value due to temperature, before the injection of ammonia (Figure 4-9). Hence, the dipole moment cannot change any more. Thus, very little response was observed to 50 ppm of ammonia at 100 °C. The same explanations can be applied on acid modified SnO_2-APTES sensor concerning the effect of temperature on the response to ammonia. At 50 °C, the response to ammonia is less important that at 25 °C as shown in Figure 4-8, because the dipole moment is already increased by the temperature.

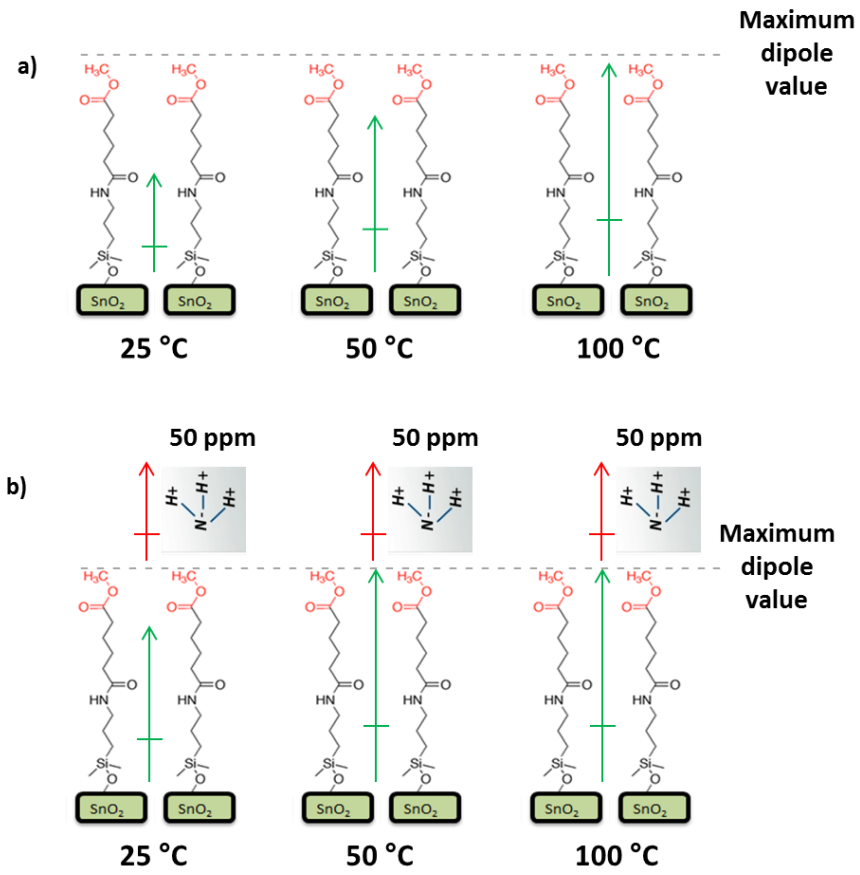

Figure 4-9. Schematics demonstration of SnO_2-APTES-ester a) at different temperatures b) upon exposure to 50 ppm of ammonia at different operating temperatures.

In contrast to most of sensors, in the case of SnO_2-APTES-ester and SnO_2-APTES-acid, the increase of temperature generates decrease of ammonia sensor response. So, interesting conclusion is that SnO_2-APTES-ester and SnO_2-APTES-acid sensors have to be operated close to room temperature (25 °C), without any power consumption for the sensitive detection of low ammonia concentrations.

4.4.3. Selectivity

Human breath contains a wide variety of volatile organic compounds which are polar or non-polar, oxidant or reductant. It is well known that SnO_2 sensor which usually operates at temperature between 350-500 °C can give a response to most of these types of gases, unfortunately without distinction (selectivity) or even with compensating effect for oxidant/reducing gases [9]. Field effect transistors functionalized with ester end group have shown responses to a wide variety of volatile organic compounds like alcohols and alkanes [10]. This implies that these sensors also have a lack of selectivity. To check the selectivity to ammonia of the developed SnO_2-APTES-ester and SnO_2-APTES-acid, such sensors were tested with respect to ethanol, carbon monoxide and acetone gases.

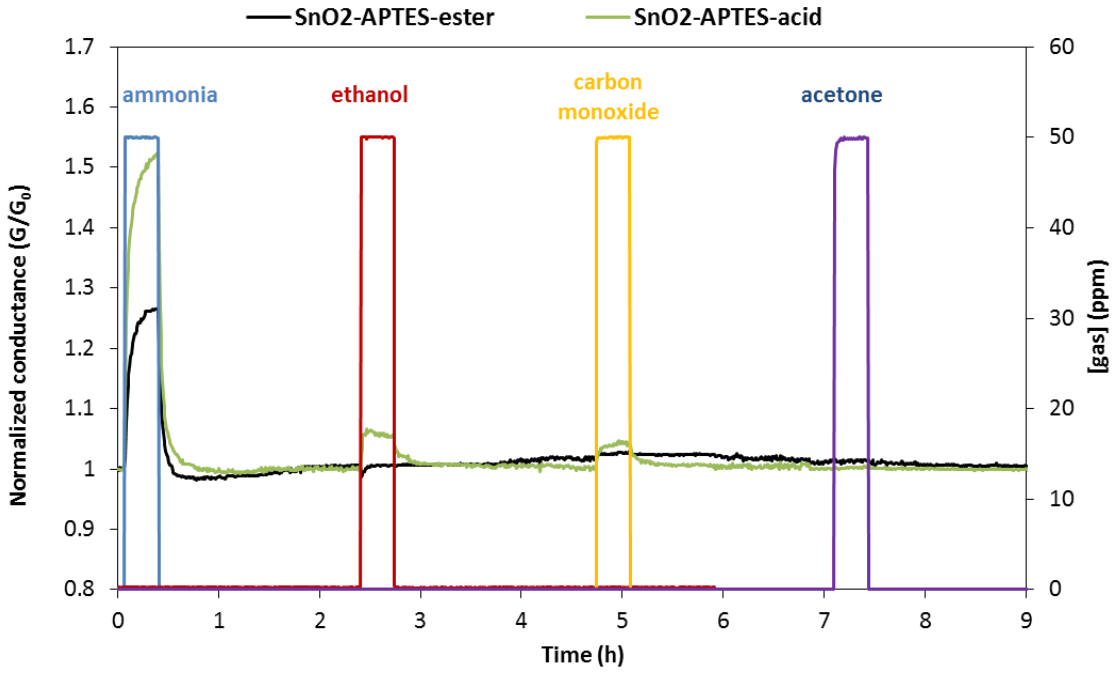

Figure 4-10. The sensor response of SnO_2-APTES-ester and SnO_2-APTES-acid upon exposure to 50 ppm of ammonia, ethanol, and acetone gases in humid air (5%RH) at 25 °C.

Figure 4-10 shows that the SnO_2-APTES-ester sensor has almost no change in conductance upon exposure to 50 ppm of ethanol, carbon monoxide and acetone at 25 °C. This means that ester modified sensor is selective to ammonia, at least in regards of the three tested gases. This particular selectivity derives from the unique interactions of the grafted layer on SnO_2 with ammonia gas. As mentioned previously, interactions occur between the ester end group which is strongly electron withdrawing, and the ammonia molecule which is electron donnating. Hence, electrons are withdrawed by the attached ester end group from the ammonia molecules adsorbed on it during exposure. These interactions lead to the significant change in the dipole moment which in turn leads to the presented response of SnO_2-APTES-ester sensor to ammonia. Others molecules like ethanol, carbon monoxide and acetone do not have this high affinity to donate the electrons to SnO_2-APTES-ester, explaining negligable changes in conductance upon exposure to these gases.

Concerning SnO_2-APTES-acid, it is less selective to ammonia than SnO_2-APTES-ester with respect to ethanol and carbon monoxide. SnO_2-APTES-acid gives response to ethanol and carbon monoxide which are 1.05 and 1.04 respectively. SnO_2-APTES-acid shows no response to acetone gas.

Polar molecule such as ammonia might selectively attach to the functional group of the molecular layer. It is likely that the adsorption process occurs through interaction between the nitrogen of ammonia and the end functional group of the molecular layer (alkyl, acid and ester). The difference in response of ester and acid modified SnO_2-APTES sensors to ethanol and carbon monoxide gases is due to the fact that carboxylic acid is more polar than ester group. The increase in the polarity of the attached film increases the response to gases. In addition to the reaction with acid end functional group, these gas molecules can penetrate into the organic layer and interact with the amide group which is polar. But this is not the case for SnO_2-APTES-ester because of the steric hindrance generated by the CH_3 group of ester. Regarding the response of acetone gas, the steric hindrance is generated by the CH_3 of acetone molecule. For this reason, no response to acetone gas was found for the two sensors as shown in Figure 4-10.

4.4.4. Stability and reproducibility

A common challenge in organically modified sensors is how to elaborate many sensors with good stability and reproducibility. The main parameter that can affect these properties is the amount of grafted molecule on each sensor, since the interactions occur with these molecules.

The influence of ammonia concentrations on sensor response of SnO_2-APTES-ester and SnO_2-APTES-acid was studied at the optimum conditions defined previously, 5%RH at 25 °C. Figure 4-11 shows the change in conductance of SnO_2-APTES-ester (Figure 4-11a and b) and SnO_2-APTES-acid (Figure 4-11c and d) upon exposure to different concentrations of ammonia gas (0.2-100 ppm). Curves a) and c) present the response to low ammonia concentrations (0.2-5 ppm). These two curves were used to draw the sensitivity curve at low concentration presented in Figure 4-3.

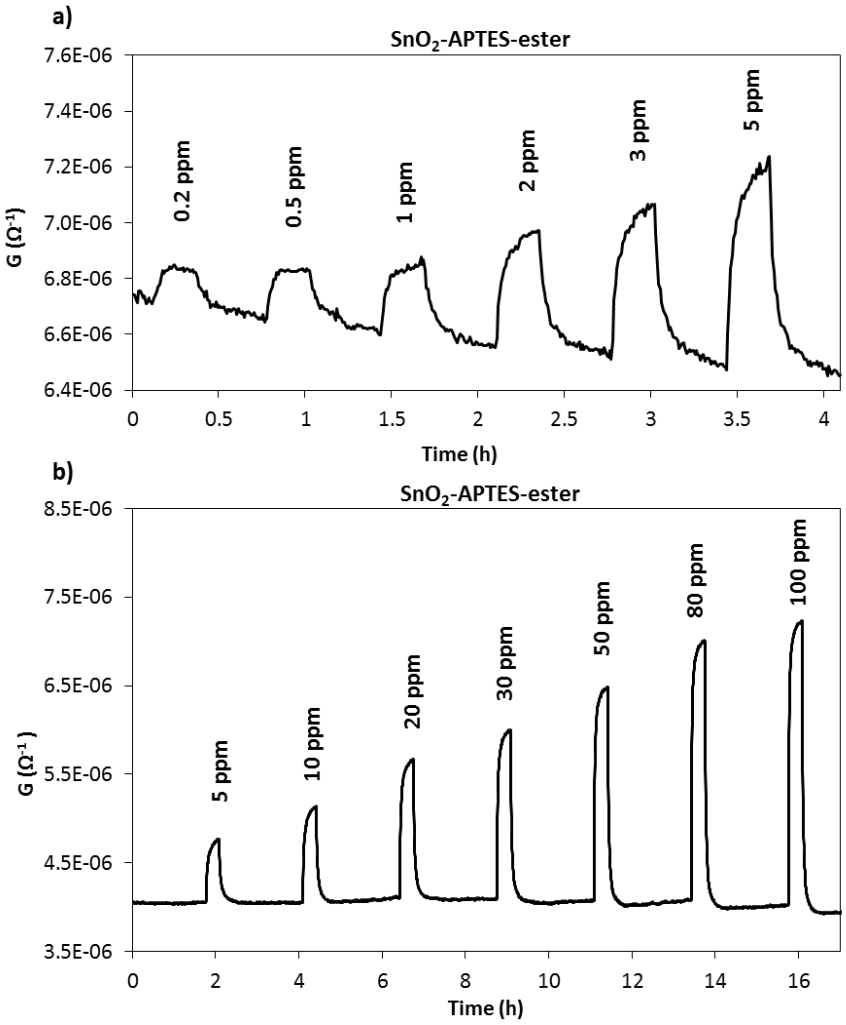

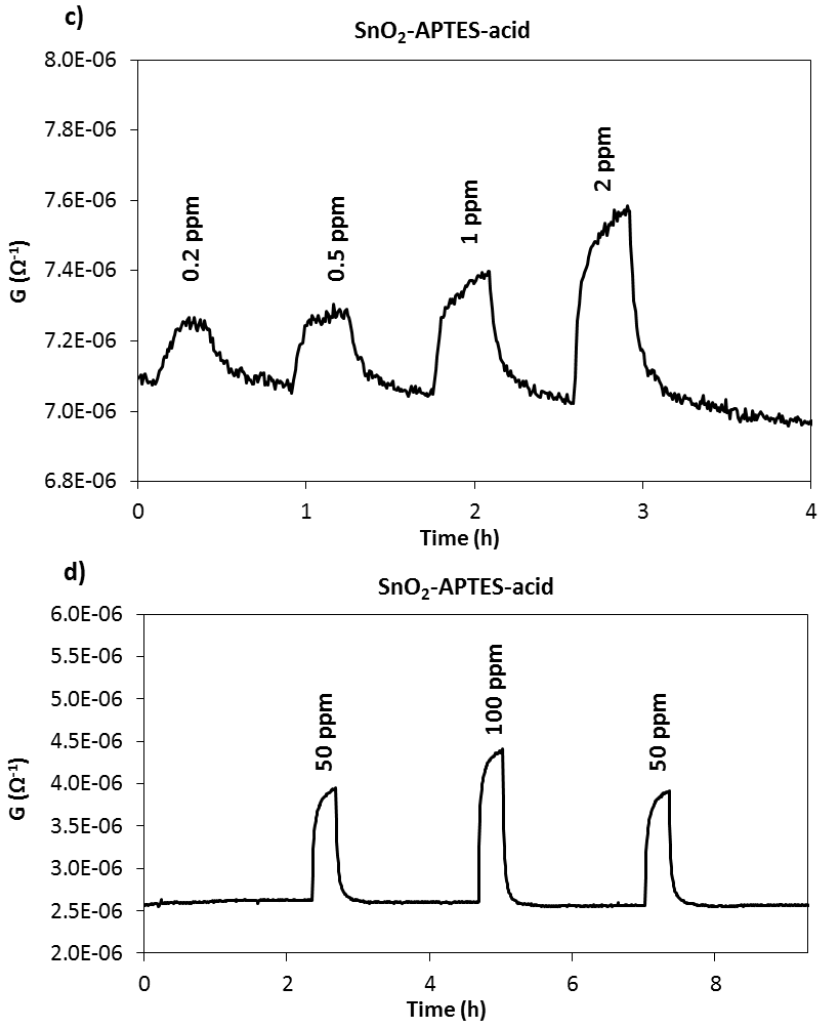

Figure 4-11. The change in conductance of SnO_2-APTES-ester and SnO_2-APTES-acid upon exposure to different concentrations of ammonia gas in humid air (5%RH) at 25 °C. a) and c) [NH_3] ranging from 0.2 to 5 ppm. b) and d) [NH_3] ranging from 5 to 100 ppm.

The other curves (concentration higher than 5 ppm, Figure 4-11b, and d) show the stability of the sensors with time even with different injections of ammonia. The stability of metal oxide is a challenge mostly for room temperature gas sensors. Present results also show the baseline stability with time. The drift is around 0.98% over 10 hours for the two sensors.

The reproducibility test was carried out on two sensors of SnO_2-APTES-ester and two of SnO_2-APTES-acid. Figure 4-12 shows the response of ester and acid modified SnO_2-APTES sensors to different ammonia concentrations (0.2-100 ppm) at 25 °C. All the sensors exhibit the same sensitivity between 0.2 and 10 ppm of ammonia (Figure 4-12b). This is the interesting

concentration zone for the detection of the liver disease as mentioned in chapter 1. Above 10 ppm, the sensitivity becomes a bit different between the tested sensors.

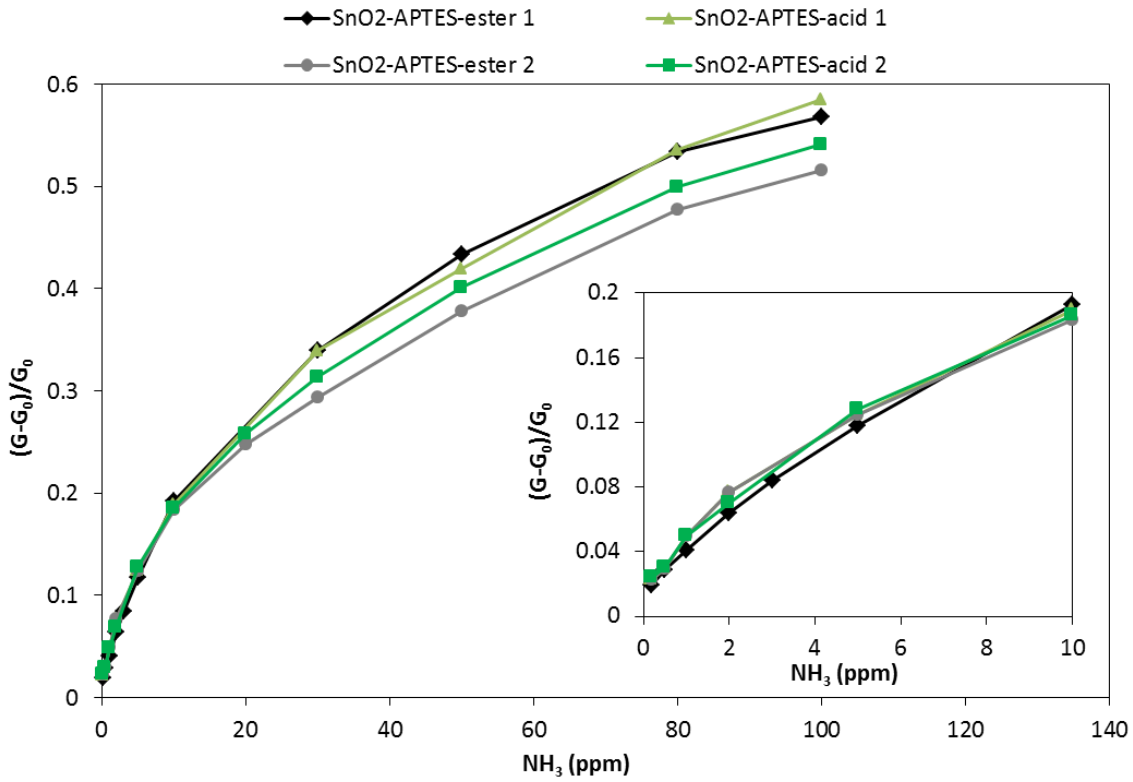

Figure 4-12. Sensors response versus ammonia concentrations of SnO_2-APTES-ester and SnO_2-APTES-acid at 25 °C under 5%RH (magnification shows 0.2-10 ppm ammonia concentration range).

4.4.5. Effect of oxygen

As said in chapter 1, the metal oxide gas sensors are highly affected by the amount of oxygen. In addition, the exhaled breath of human has not always the same amount of oxygen because it depends on many reasons like the time of breath holding. This is a blocking point which limits the use of such sensors in breath analysis in addition to other factors (selectivity and operating temperature). As the interaction is not any more with adsorbed oxygen ions of the molecularly modified sensors, the oxygen quantity is expected to have no influence on the response to ammonia gas. Figure 4-13 shows the response to different ammonia concentrations at 25 °C either in 20% of oxygen or in inert gas (N_2). It can be clearly noticed that no significant change occur in the response to ammonia in presence and in absence of oxygen, at least for the duration of the experiment (20 min). These results confirm the above discussion regarding the sensing

mechanism, which is based on the interaction of ammonia with attached molecular layer. These interactions modify the dipole moment of the molecular layer [5]. The mobility of electrons is affected by the change in dipole moment. By modifying the dipole moment, the conductance of the whole film variates. Thus, oxygen does not participate in the detection mechanism of ammonia by ester modified SnO_2 sensor. Therefore, oxygen has no impacts on the detection of ammonia in the exhaled breath by this sensor.

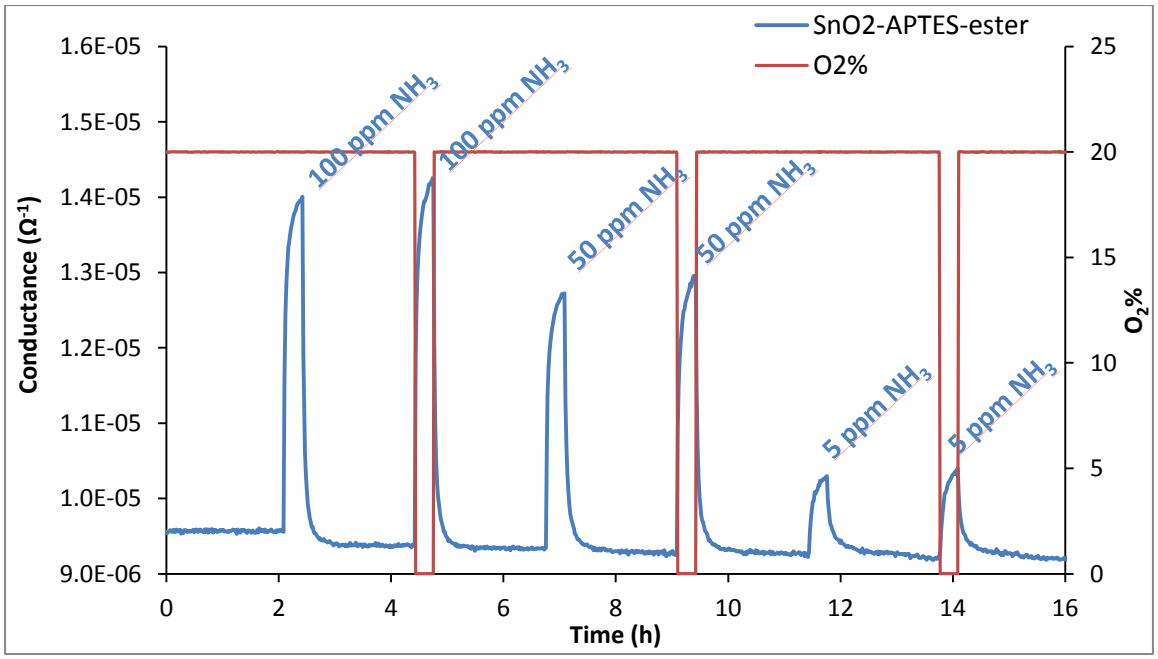

Figure 4-13. The response of SnO_2-APTES-ester sensor to ammonia in air or nitrogen at 25 °C with 5%RH.

4.5. Conclusion

Molecularly modified SnO_2 thick films were produced by screen printing followed by functionalization using solution chemical processes. The functionalization processes were carried out first by grafting of 3-aminopropyltriethoxysilane followed by reaction with hexanoyl chloride, 1,4-butanedicarbonyl chloride, or methyl adiapoyl chloride. Then, tests under gases were performed. APTES modified SnO_2 did not show any significant sensitivity to ammonia between 0.2-100 ppm under 5%RH at 25 °C. The sensitivity to ammonia becomes significant from 30 ppm for alkyl modified sensor. For ester and acid modified sensors, fast response and recovery time to ammonia with a limit of detection estimated to 80 ppb at 5%RH, 25 °C is observed. In addition, these sensors show constant sensitivity between 0.2 and 10 ppm to

ammonia (0.023 ppm^{-1}). Ester and acid modified SnO_2-APTES sensors have also shown increase of sensor response to ammonia with the decrease of operating temperature in presence of 5 %RH. These interesting responses to ammonia gas are generated mostly from the interactions of gas with the end functional groups. Ester and acid functional groups interact with ammonia by dipole-dipole interactions. These interactions change the dipole moment of the film which produces an increase in the conductance of the whole film. Moreover, ester modified SnO_2-APTES sensor is more selective to ammonia gas with respect to reducing gases like ethanol, carbon monoxide and acetone than the acid modified one. 5%RH does not affect the response of SnO_2-APTES-ester to ammonia in contrast to SnO_2-APTES-acid. However, relative humidity higher than 5% decreases the response to ammonia for the ester and acid modified SnO_2-APTES. These sensors are reproducible regarding the sensitivity tests from one sensor to another and are not affected by the oxygen content in the gas. By working at room temperature, ester modified sensor is a good candidate for breath analysis applications for the diagnosis of diseases related to ammonia gas biomarker.

References

[1] N. Shehada, J.C. Cancilla, J.S. Torrecilla, E.S. Pariente, G. Brönstrup, S. Christiansen, D.W. Johnson, M. Leja, M.P.A. Davies, O. Liran, N. Peled, H. Haick, Silicon Nanowire Sensors Enable Diagnosis of Patients via Exhaled Breath, ACS Nano. 10 (2016) 7047–7057.

[2] K. Khun Khun, A. Mahajan, R.K. Bedi, SnO_2 thick films for room temperature gas sensing applications, J. Appl. Phys. 106 (2009) 124509.

[3] S. Maeng, S.-W. Kim, D.-H. Lee, S.-E. Moon, K.-C. Kim, A. Maiti, SnO_2 Nanoslab as NO_2 Sensor: Identification of the NO_2 Sensing Mechanism on a SnO_2 Surface, ACS Appl. Mater. Interfaces. 6 (2014) 357–363.

[4] J.H. Yu, G.M. Choi, Selective CO gas detection of CuO-and ZnO-doped SnO_2 gas sensor, Sens. Actuators B Chem. 75 (2001) 56–61.

[5] B. Wang, H. Haick, Effect of Functional Groups on the Sensing Properties of Silicon Nanowires toward Volatile Compounds, ACS Appl. Mater. Interfaces. 5 (2013) 2289–2299.

[6] R.C. Hoft, M.J. Ford, M.B. Cortie, Effect of dipole moment on current-voltage characteristics of single molecules, in: Nanosci. Nanotechnol. 2006 ICONN06 Int. Conf. On, IEEE, 2006.

[7] R.H. Young, T.-M. Kung, J.A. Sinicropi, N.G. Rule, J.J. Fitzgerald, J.E. Eilers, C.H. Chen, N.W. Boaz, Effect of group and net dipole moments on electron transport in molecularly doped polymers, J. Phys. Chem. 100 (1996) 17923–17930.

[8] V. Doron, C. Fischer, Temperature dependence of the dipole moment of dichlorobis(acetylacetonato)tin(IV), Inorg. Chem. 6 (1967) 1917–1918.

[9] C. Pijolat, J.P. Viricelle, G. Tournier, P. Montmeat, Application of membranes and filtering films for gas sensors improvements, Proc. 4th Int. Workshop Semicond. Gas Sens. SGS 2004. SGS 2004. 490 (2005) 7–16.

[10] B. Wang, J.C. Cancilla, J.S. Torrecilla, H. Haick, Artificial Sensing Intelligence with Silicon Nanowires for Ultraselective Detection in the Gas Phase, Nano Lett. 14 (2014) 933–938.

General conclusions and perspectives

The objective of this thesis was to elaborate a sensitive and selective ammonia gas sensors based on organically modified SnO_2 thick film. In this contribution, a first step of functionalization by organic functional groups was the attachment of APTES on SnO_2 which acts as a substrate in the second step. This step was achieved in vapor and liquid phases. Thus, a part of this work was devoted to the investigation and improvement of APTES grafting on SnO_2 film by studying the effect of different APTES synthesis parameters. The second step of functionalization was to attach alkyl, acid and ester functional groups on the fixed APTES. After physico-chemical characterizations of all the synthesized sensors, tests under different gases were carried out to investigate the effect of functionalization on SnO_2 sensor behavior. Ammonia was the target gas since the elaborated sensors are expected to be used later in the detection of liver diseases in the exhaled breath. The selectivity was tested regarding ethanol, carbon monoxide and acetone gases. Furthermore, a sensing mechanism between ammonia and the different sensors was proposed in this study.

Major conclusions are reported thereafter.

Thick film of SnO_2 was deposited by screen printing. The deposited film exhibit a particle size of about 80 nm with random shapes and about 40 µm films thickness. APTES was deposited via liquid and vapor phases on SnO_2 films. The synthesis parameters in liquid phase silanization such as water content, reaction time and APTES concentration were investigated. Liquid phase silanization with water clearly demonstrates more APTES grafting than vapor and liquid phase silanization without water. Water during the liquid phase silanization enhances the polymerization of APTES on the surface. Interestingly, keeping SnO_2 film for 4 h under stirring in 50 mM APTES solution was found to be sufficient to efficiently cover it by APTES molecules. Furthermore, thermal treatment of APTES film on SnO_2-APTES shows that the APTES start to degrade at temperature above 110 °C, while no notable change in the amount of silicon between 110 °C and 500 °C was observed. Amine groups had totally disappeared after heating the film at 500 °C. A model to calculate the concentration of APTES grafted after silanization was proposed. This model shows that the silanization leads to attach APTES in form of self-assembled monolayer with different densities depending on the synthesis procedures. The concentrations of

APTES grafted by liquid without water and vapor silanization were respectively 4.24×10^{14} molecules.cm^{-2} and 4.7×10^{14} molecules.cm^{-2}, while it is 9×10^{14} molecules.cm^{-2} with the addition of 5 vol% H_2O. In addition, the obtained results from this model were in good agreement with the ATR-FTIR characterization results. Therefore, all the used characterization techniques confirm that the liquid silanization in the presence of water leads to more APTES grafting onto SnO_2 indicating an almost 50% improvement. This film was used to attach the desired end functional groups on it. In this step, molecules containing acyl chloride group from one side and alkyl, acid or ester functional groups from the other side were used. For the second step functionalization, ATR-FTIR and XPS demonstrate that SnO_2-APTES is well modified by ester, acid and alkyl end functional groups.

The tests under gases have reaveled that pure SnO_2 sensor and APTES modified SnO_2 do not display any significant sensitivity to ammonia between 0.2-100 ppm under 5%RH at 25 °C. However, the sensitivity to ammonia begins to increase starting from 30 ppm for alkyl modified SnO_2-APTES sensor. On the contrary, ester and acid modified SnO_2-APTES sensors show constant sensitivity (0.023 ppm^{-1}) to ammonia in the range of interest between 0.2 and 10 ppm. In addition, these sensors exhibit fast response and recovery time to ammonia with a limit of detection estimated to 80 ppb at 25 °C in air with 5%RH. These interesting responses to ammonia gas could be generated mostly from the dipole-dipole interactions of gas with the end functional groups. These interactions change the dipole moment of the film which produces an increase in the conductance of the whole film. Concerning the effect of water vapor, 5%RH does not affect the response of SnO_2-APTES-ester to ammonia in contrast to SnO_2-APTES-acid. The test under different operating temperatures (25, 50 and 100 °C) demonstrates that the ester and acid modified sensors work better at 25 °C. Moreover, ester modified SnO_2-APTES sensor has shown better selectivity to ammonia gas with respect to reducing gases like ethanol, carbon monoxide and acetone than the acid modified one. The repetition of test on several ester and acid modified sensors have proved that these sensors are reproducible regarding the sensitivity to ammonia. Furthermore, ester modified sensors were not affected by the oxygen content in the mixture of gases. The presented results show that ester modified sensor is a good candidate for the detection of liver diseases from the exhaled breath. The working at room temperature makes this sensor convenient for smart portable applications.

Regarding the obtained results, the following perspectives could be investigated:

- Confirm the proposed sensing mechanism by in-situ Raman, AFM and DRIFT. These characterization techniques can be carried out in special cell under gas flow. Thus, the type of ammonia interactions with the functionalized sensor can be checked. Ammonia changes the polarity of the attached layer that can variate the intensity of Raman and IR peaks. In addition, adsorbed ammonia on the attached layer can be characterized. The change of dipole moment caused by ammonia could be detected by AFM.
- Test the effect of other gases present in human exhaled breath (amines and other gases) on ester modified SnO_2 sensor to simulate the performance of this sensor in real conditions. After this step, the sensors can be tested under real conditions for the detection of liver diseases.
- Develop a method for sampling of exhaled breath because the breath contains high amount of water vapor which can condense on the sensor since it is operated at room temperature. Thus, the sampling should include a way to reduce the amount of humidity in the sample to less than 5%RH. In addition, the sensor response to ammonia is affected by relative humidity superior to 5%.
- Integrate the functionalized sensor on plastic substrates because they are flexible and less expensive than alumina and silicon supports and in growing interest for portable device applications.

Scientific production

Publications in international journals with reviewing committee

1. M. Hijazi, M. Rieu, V. Stambouli, G. Tournier, J.-P. Viricelle, and C. Pijolat, "Selective Ammonia Gas Sensor based on SnO_2-APTES Modification", *Procedia Eng.*, 168, 280–283, 2016.

2. M. Hijazi, V. Stambouli, M. Rieu, G. Tournier, C. Pijolat, and J.-P. Viricelle, "Sensitive and Selective Ammonia Gas Sensor Based on Molecularly Modified SnO_2," Proceedings, 1, 4, 2017.

3. M. Hijazi, V. Stambouli, M. Rieu, V. Barnier, G. Tournier, T. Demes, J.-P. Viricelle, C. Pijolat, Synthesis and characterization of tin dioxide thick film modified by APTES in vapor and liquid phases, J. Mater. Sci. 2017.

4. M. Hijazi, M. Rieu, V. Stambouli, G. Tournier, J.-P Viricelle, and C. Pijolat. "Ambient temperature selective ammonia gas sensor based on SnO_2-APTES modifications." Sensors and Actuators B: Chemical 2017.

Article submitted to scientific journal

M. Hijazi, M. Rieu, V. Stambouli, G. Tournier, J-P. Viricelle, C. Pijolat, "Modified SnO_2-APTES gas sensor for selective ammonia detection at room temperature" to Materialstoday (accepted).

International Conferences

1. M. Hijazi, M. Rieu, V. Stambouli, G. Tournier, J.-P. Viricelle, and C. Pijolat, "Selective Ammonia Gas Sensor based on SnO_2-APTES Modification", the 30th anniversary conference Eurosensors (2016), Budapest, Hungary (Poster).

2. M. Hijazi, V. Stambouli, M. Rieu, G. Tournier, J.-P. Viricelle, and C. Pijolat, "Functionalization of APTES modified tin dioxide gas sensor", The 16th International Meeting on Chemical Sensors (2016), Jeju Island, Korea (Oral).

3. M. Hijazi, M. Rieu, V. Stambouli, G. Tournier, J-P. Viricelle, C. Pijolat, "Modified SnO_2-APTES gas sensor for selective ammonia detection at room temperature" Surfocap workshop (2017), Besancon, France (oral).

4. M. Hijazi, M. Rieu, V. Stambouli, G. Tournier, J.-P. Viricelle, and C. Pijolat, "Selective Ammonia Gas Sensor based on SnO_2-APTES Modification", the 31th anniversary conference Eurosensors (2017), Paris, France (Oral).

École Nationale Supérieure des Mines
de Saint-Étienne

NNT : 2017LYSEM030

Mohamad HIJAZI

Thesis title: Sensitive and selective ammonia gas sensor based on molecularly functionalized tin dioxide working at room temperature

Speciality: Chemical and process engineering

Keywords: SnO_2, Screen printing, Molecular functionalization, APTES, Acid, Ester, Ammonia, Selectivity, Room temperature detection, Exhaled breath analysis

Abstract:

One of the major challenges in the modern era is how we can detect the disease when we are still feeling healthy via noninvasive methods. Exhaled breath analysis is offering a simple and noninvasive tool for early diagnosis of diseases. Molecularly modified SnO_2 sensors seem to be promising devices for sensing polar gases such as ammonia. In this study, SnO_2 surface functionalization was performed in order to obtain sensitive and selective ammonia gas sensor that operates at room temperature. The first step of functionalization is the covalently attachment of 3-aminopropyltriethoxysilane (APTES) film on SnO_2 in vapor or liquid phases. Liquid phase silanization was achieved in hydrous or anhydrous APTES solution. The characterization performed by the Attenuated Total Reflectance-Fourier Transform Infrared Spectroscopy (ATR-FTIR), X-ray Photoelectron Spectroscopy (XPS), show that more APTES were grafted by hydrous liquid phase silanization. This film was used as a substrate for further modifications. The second step was the functionalization of APTES modified SnO_2 with molecules having acyl chloride of different end functional groups molecules such as alkyl, acid and ester groups. Pure SnO_2 and APTES modified SnO_2 sensors did not show any significant sensitivity to ammonia (0.2-100 ppm) at 25 °C, while the sensitivity to ammonia gas started to increase from 30 ppm for alkyl modified sensor. On the contrary, acid and ester modified sensors are sensitive to ammonia between 0.2 and 10 ppm at room temperature. However, ester modified SnO_2 was more selective than acid modified sensor regarding the ethanol and carbon monoxide gases. These results imply that the response is generated by the attached acid and ester functional groups. Ammonia variates the attached molecular layer's dipole moment which leads to change in SnO_2 conductance. Working at ambient temperature is also one of the advantages of these sensors in addition to the selectivity to ammonia regarding other gases such as ethanol, carbon monoxide and acetone.

École Nationale Supérieure des Mines
de Saint-Étienne

NNT : 2017LYSEM030

Mohamad HIJAZI

TITRE DE LA THÈSE : Capteur de gaz SnO_2 fonctionnalisé fonctionnant à température ambiante, sensible et sélectif pour la détection d'ammoniac

Spécialité : Génie des procédés

Mots clefs : SnO_2, Sérigraphie, Fonctionnalisation moléculaire, APTES, Acide, Ester, Ammoniac, Sélectivité, Détection à température ambiante, Analyse d'haleine

Résumé :

Dans le domaine de la santé, l'un des défis actuel est de détecter une maladie de façon non invasive alors que nous nous sentons en «bonne santé». L'analyse de l'haleine expirée offre un outil simple et non invasif pour le diagnostic précoce des maladies. Les capteurs de gaz à base de SnO_2 modifiés de manière moléculaire semblent être des dispositifs prometteurs pour détecter les gaz polaires tels que l'ammoniac. Dans cette étude, la fonctionnalisation de la surface de SnO_2 a été réalisée afin d'obtenir un capteur de gaz sensible et sélectif à l'ammoniac, qui puisse fonctionner à température ambiante. La première étape de la fonctionnalisation est la fixation covalente d'un film de 3-aminopropyltriéthoxysilane (APTES) sur SnO_2 en phase vapeur ou liquide. La silanisation en phase liquide a été réalisée dans une solution APTES hydratée ou anhydre. Les caractérisations effectuées par Spectroscopie Infrarouge à Réflectance Totale Atténuée (ATR-FTIR) et Spectrométrie Photoélectronique X (XPS) montrent qu'une quantité plus importante d'APTES a été greffée par une silanisation en phase liquide hydratée. Ce film a donc été utilisé comme substrat pour la deuxième étape qui consiste à fonctionnaliser le SnO_2 modifié par APTES avec des molécules contenant du chlorure d'acyle avec différents groupes fonctionnels finaux, tel que des groupes alkyle, acide et ester. Les capteurs SnO_2 et SnO_2-APTES n'ont pas montré de sensibilité significative à l'ammoniac (0,2-100 ppm) à 25 °C, tandis que la sensibilité à l'ammoniac a commencé à augmenter à partir de 30 ppm pour le capteur SnO_2-APTES modifié par un alkyle. Au contraire, les capteurs modifiés par des acides et des esters sont sensibles à l'ammoniac entre 0,2 et 10 ppm à température ambiante. Cependant, le SnO_2-APTES modifié par l'ester s'est révélé être plus sélectif que le capteur modifié par l'acide pour l'éthanol et le monoxyde de carbone. Ces résultats impliquent que la réponse est générée par les groupes fonctionnels acide et ester. L'ammoniac modifie le moment dipolaire de la couche moléculaire greffée, ce qui entraîne une modification de la conductance de SnO_2. Le fonctionnement à température ambiante est l'un des avantages de ces capteurs, tout comme leur sélectivité à l'ammoniac en regard d'autres gaz tels que l'éthanol, le monoxyde de carbone et l'acétone.